Review Article

Head and Neck Diseases Conflux

Gene Therapy for Non-Syndromic Hearing Loss

Authors

Yu Qi, Fangzhi Tan, Maoli Duan, Ling Lu

Correspondence

entluling60@126.com (L. Lu), maoli.duan@ki.se (M. Duan), 101013491@seu.edu.cn (F. Tan)

Graphical Abstract

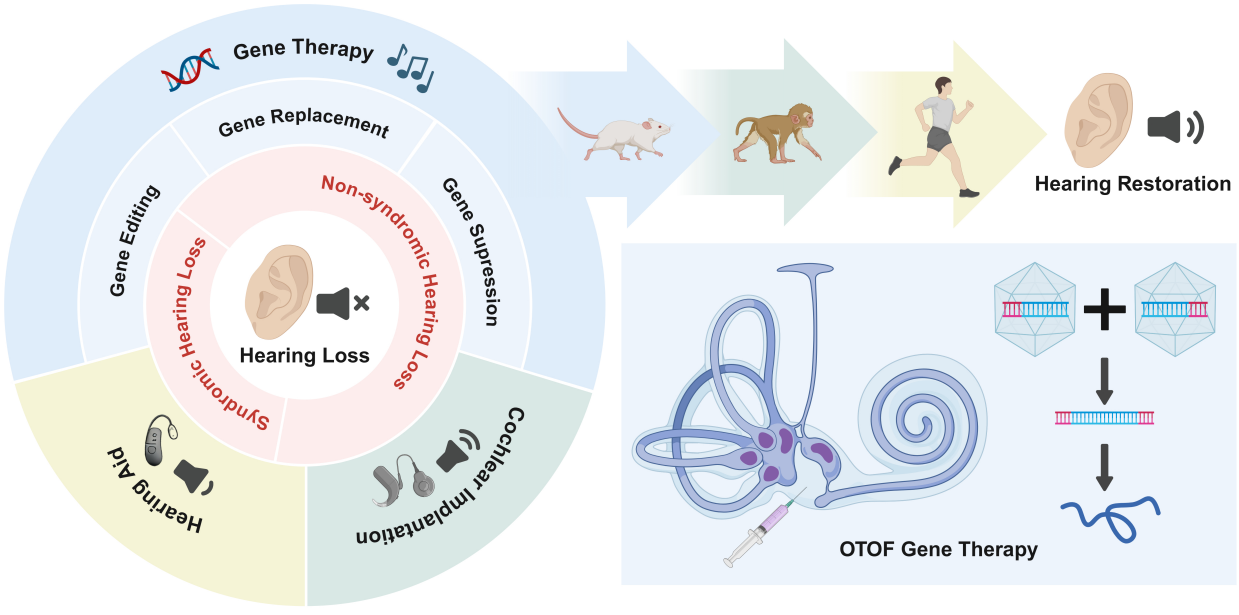

https://doi.org/10.71321/703b4949

Review Article

Head and Neck Diseases Conflux

Gene Therapy for Non-Syndromic Hearing Loss

Yu Qi [1], Fangzhi Tan [1*], Maoli Duan [2,3*], Ling Lu [1*]

Received: 2025-12-28 | Accepted: 2026-02-10 | Published online: 2026-03-11

Abstract

Hereditary hearing loss accounts for over 60% of congenital deafness cases, with non-syndromic hearing loss (NSHL) representing the most common subtype. Typically caused by monogenic mutations, NSHL presents a promising candidate for gene therapy. Recent advances in deciphering the genetic underpinnings of deafness and developing gene delivery systems have greatly accelerated the progress of inner ear gene therapy, leading to a number of breakthrough achievements. This review provides an overview of the latest developments in gene therapy for NSHL. After outlining the genetic basis of NSHL, we summarize the preclinical progress made during the first decade of hereditary deafness gene therapy. Special emphasis is placed on gene replacement strategies for DFNB9, an autosomal recessive form of hearing loss caused by mutations in the OTOF gene. We highlight the remarkable journey of OTOF gene therapy and discuss future directions in this transformative field.

Keywords: non-syndromic hearing loss; gene therapy; OTOF; DFNB9

Introduction

Hearing loss is projected to affect 2.45 billion individuals by 2050, with consequences extending far beyond health impairments [1-2]. Over 60% of congenital and childhood hearing loss cases are hereditary, which is further categorized into syndromic hearing loss and non-syndromic hearing loss (NSHL) [3-4]. Accounting for approximately 70% of hereditary hearing loss cases, NSHL represents a major clinical entity. It primarily involves the auditory system and is predominantly monogenic, with well-characterized genetic mechanisms [5]. To date, 156 genes associated with NSHL have been identified, yet no pharmacotherapeutic options are commercially available.

Currently, cochlear implantation remains the clinical gold standard for hearing loss intervention. This device bypasses damaged hair cells by directly stimulating the auditory nerve with electrical pulses to transmit sound signals to the brain [6]. However, it does not correct the underlying genetic defects in target cells, nor does it restore natural physiological hearing [7-8].

Gene therapy, a concept first proposed nearly six decades ago, is now recognized as a promising treatment for a wide range of genetic disorders [9]. It involves the manipulation of gene presence or expression and is generally implemented through three main strategies: gene replacement, gene suppression, and gene editing [10]. More than 3,000 clinical trials targeting genetic diseases across multiple organ systems are currently underway [11]. Patients with various conditions, including blindness, neuromuscular disorders, hemophilia, primary immunodeficiencies, and certain cancers, have already derived clinical benefits from gene therapy interventions. Given its typically monogenic etiology and confined anatomical focus, NSHL is considered an ideal candidate for inner ear gene therapy. Combined with next-generation sequencing based diagnostics that enable precise genetic characterization, this approach holds the potential to directly restore auditory cell function, offering a curative solution.

This rapidly evolving field has generated substantial progress. Successful translation from animal studies to clinical trials has also brought hope to patients with hereditary deafness [12-16]. Notably, a comparative study suggests that gene therapy may present several advantages over cochlear implants, including faster recovery of auditory function, improved speech perception in noisy environments, and better music discrimination [17]. Given limitations such as short follow-up periods and small sample sizes, it would be premature to conclude which

1 Department of Otolaryngology-Head and Neck Surgery, Zhongda Hospital, Southeast University, Nanjing, Jiangsu 210009, China

2 Department of Clinical Science, Intervention and Technology, Karolinska Institutet, Stockholm 171 77, Sweden

3 Department of Otolaryngology Head and Neck Surgery & Audiology and Neurotology, Karolinska University Hospital, Stockholm 171 76, Sweden

* Corresponding Author.

approach is superior. However, these findings indicate that gene therapy may provide a novel effective treatment for genetically driven congenital deafness.

In light of the remarkable advances in deafness gene therapy in recent years, a timely synthesis of these developments is essential to consolidate knowledge and guide future research. This review summarizes the latest progress in gene therapy for NSHL and discusses its clinical implications. We place particular emphasis on gene replacement strategies for DFNB9, an area that has attracted extensive research interest and exhibits strong translational potential.

The Genetic Basis of Non-syndromic Hereditary Hearing Loss

NSHL exhibits heterogeneous inheritance patterns, predominantly autosomal recessive (75–80%) and autosomal dominant (about 20%), with minor contributions from sex-linked (about 2%) and mitochondrial (less than 1%) patterns[18-19]. To date, 156 causative genes have been identified in major databases such as ClinVar, OMIM, and the Hereditary Hearing Loss database [5, 20], providing a foundational framework for the understanding of NSHL pathogenesis. Among these, GJB2 and SLC26A4 are the most frequently implicated pathogenic genes, with other significant contributors including MT-RNR1, OTOF, MYO15A, MYO7A, and TMC1, among others [21-24]. Allelic heterogeneity further compounds this genetic complexity, wherein multiple distinct deafness-causing mutations can occur within a single gene [25].

Autosomal recessive NSHL

Currently, 88 genes have been identified to cause autosomal recessive NSHL, the most prevalent subtype of NSHL [5]. Over 90% of autosomal recessive NSHL cases manifest as prelingual, severe-to-profound sensorineural hearing impairment, which typically affects all frequencies. This clinical presentation can be attributed to the critical roles played by the corresponding proteins in the development, structural integrity, and physiological function of various inner ear structures, including stereocilia bundles, the mechanoelectrical transduction (MET) channel complex, and the stria vascularis (Table 1).

Among these causative genes, GJB2 is the most prevalent, accounting for approximately half of congenital sensorineural hearing loss worldwide [26]. It encodes connexin 26, a gap junction protein essential for intercellular permeability [27]. SLC26A4 represents another common deafness gene, which is involved in anion transport, and mutations in this gene are associated with an enlarged vestibular aqueduct [28]. Another significant gene is OTOF, which has emerged as a promising target for gene therapy. It encodes otoferlin, a calcium sensor believed to regulate exocytosis and highly expressed in inner hair cells [29].

Autosomal dominant NSHL

To date, 64 genes have been identified as causative for autosomal dominant NSHL [5]. The products of these genes are primarily involved in the maintenance and homeostatic regulation of inner ear structures, including cellular activity, functional stability, and transcriptional control (Table 2). Consequently, the associated clinical phenotype is typically less profound than that of autosomal recessive NSHL. It is generally characterized by post-lingual onset, emerging from late childhood to early adulthood, and featuring progressive deterioration. This form of hearing loss is usually bilateral, predominantly affects high frequencies (resulting in a sloping audiometric configuration), and varies in severity from mild to profound [19, 30].

Common forms of autosomal dominant NSHL involve genes such as KCNQ4, TECTA, POU4F3, WFS1, EYA4, and ACTG1 [30-32]. Notably, some cases exhibit gene-specific frequency impairments. For example, mutations in DIAPH1 (DFNA1) and WFS1 (DFNA6/14/38) typically affect low frequencies, while DFNA16 (for which the causative gene remains unidentified) is characterized by fluctuating hearing loss [30].

Sex-linked and mitochondrial NSHL

Only a negligible proportion of NSHL cases are attributed to mutations in sex chromosomes or mitochondrial DNA [18]. Sex-linked hereditary hearing loss demonstrates a distinct gender bias in its inheritance pattern, characterized by a higher prevalence, earlier onset, and more severe impairment in males than in females [33], [5, 34]. To date, seven DFNX and two DFNY loci have been identified as contributors to this form of hearing impairment. The Clinical Genome Resource (ClinGen) has established definitive gene-disease relationships for NSHL involving POU3F4, PRPS1, SMPX, and AIFM1 [35]. Among these, POU3F4 (DFNX3) is the most frequently implicated X-linked locus [34].

Mitochondrial NSHL is a maternally inherited condition resulting from mutations in mitochondrial DNA, and affected fathers do not transmit the hearing loss to their offspring. Nine loci have been reported to contribute to mitochondrial NSHL. The m.1555A>G and m.1494C>T mutations in the MT-RNR1 gene (encoding 12S rRNA) represent the most common forms of mitochondrial hearing loss, with the former being more prevalent than the latter [36]. These variants alter the secondary structure of the 12S rRNA, creating a potential binding site for aminoglycosides and thereby conferring heightened susceptibility to their ototoxic effects [36-37]. Exposure to aminoglycosides, even at standard therapeutic doses, has been reported to induce profound, bilateral sensorineural hearing loss that may continue to progress for years after drug discontinuation [38]. Therefore, genetic screening to identify carriers, coupled with the subsequent avoidance of aminoglycosides, is crucial for preventing this form of deafness [38-39].

Gene Therapy for NSHL

Nonsyndromic hearing impairments exhibit unparalleled heterogeneity, yet they can be generally categorized into three functional effects: loss-of-function (LOF), gain-of-function (GOF) and dominant-negative (DN) [40]. LOF variants can result in either recessive, or dominant inheritance (haploinsufficiency), where a single LOF allele is insufficient to maintain normal function. Meanwhile, GOF and DN mutations typically cause dominant disorders [41]. To counteract these mechanisms, three primary gene therapy strategies are designed: gene replacement, gene suppression, and gene editing. Accordingly, different strategies provide solutions for different pathogenic mechanisms. Gene replacement compensates for LOF through functional protein supplement, while gene suppression aims

to silence or counteract the deleterious effects of GOF and DN [26]. Since gene editing enables direct intervention of DNA sequences, it holds the potential to address all variant types [41]. Advances in understanding the genetic basis of deafness, combined with improved gene delivery systems, have greatly propelled these strategies into therapy for congenital hearing loss. The first successful hearing recovery in deaf mammals was reported in 2005, using adenovirus-mediated delivery of the ATOH1 gene into the scala media of guinea pigs [42]. This approach induced hair cell regeneration and led to significant, sustained hearing recovery, particularly in high-frequency regions, despite some localized hair cell loss at the injection site

Table 1. Autosomal recessive NSHL .

Locus name	Gene symbol	Role in the inner ear
DFNB1A	GJB2	Physiological ion balances
DFNB3	MYO15A	Stereocilia elongation
DFNB4	SLC26A4	Anion and bases transmembrane transport
DFNB6	TMIE	MET complex component
DFNB7/11	TMC1	MET complex component
DFNB8/10	TMPRSS3	Signaling regulation through proteolytic activation
DFNB9	OTOF	$Ca2^{+}$ sensor for exocytosis in hair cells
DFNB12	CDH23	Adhesion protein assisting stereocilia organization
DFNB15/72/95	GIPC3	Vesicle trafficking protein complex component
DFNB16	STRC	Stereocilia cohesion, apical tip positioning
DFNB18B	OTOG	Sensory epithelial patches component
DFNB21	TECTA	Hardesty's membrane component
DFNB22	OTOA	Anchoring protein of tectorial membrane
DFNB24	RDX	Cross-linkers between integral membrane proteins and actin of cytoskeleton
DFNB25	GRXCR1	Modulator of actin cytoskeleton in stereocilia development
DFNB28	TRIOBP	Actin-binding Protein
DFNB29	CLDN14	Selective paracellular permeability
DFNB30	MYO3A	Stereocilia component
DFNB31	WHRN	Stereocilia elongation
DFNB32/105	CDC14A	Mitosis assistance
DFNB35	ESRRB	Development of marginal cells and stria vascularis
DFNB36	ESPN	Myosin III cargo protein
DFNB39	HGF	Regulation of epithelial cell development and motility
DFNB42	ILDR1	Integral protein of the tricellular tight junction complex
DFNB48	CIB2	Intracellular calcium signaling mediation
DFNB49	MARVELD2	Integral membrane protein in tight junction strand
DFNB53	COL11A2	Tectorial membrane component
DFNB57	PDZD7	Hair-cell stereocilia ankle-link complex composition
DFNB59	PJVK	Stereocilia maintenance, pexophagy against the oxidative stress
DFNB63	LRTOMT	TMC1/2 localization to the MET complex
DFNB67	LHFPL5	MET complex component
DFNB68	S1PR2	S1P-mediated cellular response and calcium signaling assistance
DFNB73	BSND	Accessory subunit of chloride channels
DFNB74	MSRB3	Oxidatively damaged protein repairment
DFNB76	SYNE4	Intracellular organelle positioning
DFNB77	LOXHD1	Stereociliary bundle stabilization
DFNB79	TPRN	Stereocilia taper composition
DFNB84A	PTPRQ	Phosphoinositide-mediated cellular regulation
DFNB84B	OTOGL	Acellular structures production or function
DFNB86	TBC1D24	Proper intracellular vesicle trafficking maintenance
DFNB91	SERPINB6	Cochlear homeostasis preservation
DFNB93	CABP2	Calcium signaling pathway modulation
DFNB101	GRXCR2	Cochlear stereocilia bundle integrity maintenance
DFNB102	EPS8	Stereocilia elongation, EGFR signaling and trafficking
DFNB104	RIPOR2	Circumferential ring near basal tapers of stereocilia
DFNB106	EPS8L2	Actin remodeling in response to EGF stimulation
DFNB111	MPZL2	Homophilic intercellular adhesion promotion
DFNB113	CEACAM16	Connection between stereocilia and Hardesty's membrane

[42-43].

In 2012, VGLUT3 became the first NSHL locus successfully treated via gene replacement in mice [44]. Since then, proof-of-concept studies have been achieved for more hereditary hearing loss loci, largely focusing on recessive forms. Among the most promising therapeutic targets, such as OTOF, GJB2, USH3A, USH1C, and TMC1, the latter is the most extensively studied. Since many previous reviews have thoroughly documented the studies of deafness gene therapy during its first decade, we will not elaborate further here [26, 41, 45-47].

Gene replacement is the most widely applied strategy, frequently employing viral vectors, especially adeno-associated viruses (AAVs), due to their high transduction efficiency and sustained expression. Novel engineered AAV variants, including AAV2/Anc80L65 and AAV2/9-PHP.eB, show enhanced transduction in cochlear hair cells and are widely used in preclinical studies [48-49].

Surgical delivery methods have also evolved (Figure 1). Techniques such as round window membrane (RWM) injection, oval window delivery, utricle injection, cochleostomy, and canalostomy enable perilymphatic or endolymphatic targeting [26]. RWM injection, adapted from clinical cochlear implantation, is used in over 60% of successful cases due to its reliability and its minimal invasiveness [41]. In the landmark VGLUT3$^{-/-}$ mouse study, RWM delivery achieved 100% treatment efficacy, far surpassing cochleostomy [44]; further refinements like RWM injection with canal fenestration have improved vector distribution and reduced trauma, though their safety and stability require further validation [50].

Figure 1. Overview of surgical delivery routes to the inner ear. (**A**) Anatomical locations of round window membrane injection, oval window delivery, utricle injection, cochleostomy, and canalostomy. (**B**) Corresponding drug distributions in perilymphatic and endolymphatic spaces of different surgical delivery routes. Created with BioRender.com.

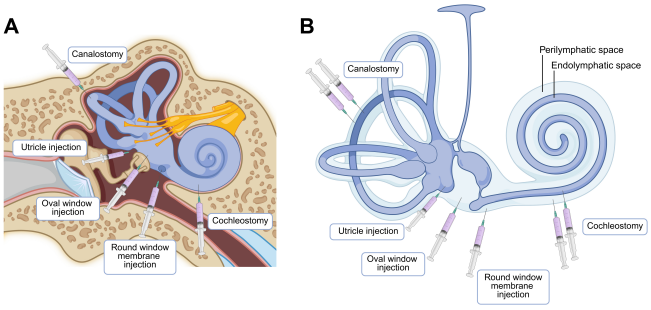

Treatment timing is another crucial factor. While interventions in mice have been applied from embryonic stages to adulthood, most studies focus on the early postnatal period (P0–P10). Early intervention (P0–P2) generally yields more robust and durable hearing recovery [26, 51-53]. However, the murine auditory system at P10 is approximately equivalent to that of a human fetus at 20 weeks of gestation [54]. Consequently, the optimal therapeutic period identified in mouse models corresponds to the human fetal stage theoretically, which presents significant challenges for clinical translation.

Moreover, substantial anatomical and developmental differences between rodent and human inner ears limit direct clini-

Table 2. Autosomal dominant NSHL

Locus name	Gene symbol	Role in the inner ear
DFNA1	DIAPH1	Cytoskeletal organization regulation
DFNA2A	KCNQ4	Cellular repolarization
DFNA4A	MYH14	Actin-cytoskeleton interactions, cytokinesis, motility and polarity regulation
DFNA4B	CEACAM16	Connection between stereocilia and Hardesty's membrane
DFNA5	GSDME	Pyroptosis assistance
DFNA6/14/38	WFS1	ER calcium channel or ER calcium channel regulator
DFNA7	LMX1A	Neural progenitor specification and dopamine neurogenesis promotion
DFNA8/12	TECTA	Tectorial membrane component
DFNA9	COCH	Innate immunity
DFNA10	EYA4	Innate immune response cotranscription factor
DFNA11	MYO7A	MET complex component
DFNA13	COL11A2	Tectorial membrane component
DFNA15	POU4F3	Transcription factor related to hair cells maintenance
DFNA17	MYH9	Actin-cytoskeleton interactions, cytokinesis, motility and polarity regulation
DFNA20/26	ACTG1	Structural and functional maintenance of hair cells
DFNA22	MYO6	Intracellular vesicle and organelle transport
DFNA25	SLC17A8	Glutamate synaptic vesicle transport
DFNA28	GRHL2	Epithelial morphogenesis and epidermal development promoter
DFNA36	TMC1	MET complex component
DFNA37	COL11A1	Tectorial membrane component
DFNA41	P2RX2	Temporary threshold shift for cochlea protection
DFNA50	MIR96	mRNAs translation and stability assistance
DFNA66	CD164	Cell adhesion receptor
DFNA67	OSBPL2	Lipid metabolism (possibly)
DFNA68	HOMER2	Stereociliary scaffolding protein
DFNA82	ATP2B2	Stereociliary calcium remove
DFNA84	ATP11A	Phospholipid transport and uphill ion transport across membranes execution

cal extrapolation [54-55]. Non-human primate (NHP) models, with cochleae closely resembling those of humans, offer a critical translational bridge. Studies in rhesus and cynomolgus monkeys have established safe injection volumes (30–90 μL, a range relevant for human application) and demonstrated feasible AAV transduction via RWM injection, albeit with notable individual variability and dose dependency [55]. In 2022, a refined NHP RWM injection protocol, which incorporated oval window venting and transmastoid facial recess exposure, was shown to enhance delivery precision and distribution while minimizing trauma, offering a more clinically relevant approach [56].

These cumulative advances set the stage for clinical translation. A decade after the inception of inner-ear gene therapy, the first clinical trial was registered, and its first patient was enrolled at the end of 2022.

Preclinical Advances in OTOF Gene Therapy

Biallelic mutations in the OTOF gene cause DFNB9, a recessive form of profound prelingual deafness classified as auditory neuropathy. The gene encodes otoferlin, a calcium-sensing protein localized in inner hair cells (IHCs) that is essential for synaptic vesicle exocytosis [29]. While structural integrity of the cochlea is preserved in DFNB9, synaptic transmission is severely impaired, leading to abnormal auditory brainstem responses but preserved otoacoustic emissions. These characteristics, combined with the relatively high prevalence of DFNB9, make OTOF an attractive target for gene therapy.

A major challenge in OTOF therapy is the gene's large coding sequence, which exceeds the packaging capacity of a single AAV vector. In early 2019, two independent studies demonstrated that dual-AAV systems could deliver full-length otoferlin cDNA into IHCs of OTOF knockout mice [57-58].

Currently, dual-AAV gene replacement remains the dominant strategy. A team developed a dual AAV-PHP.eB system using intein-mediated trans-splicing, identifying an efficient split site that enabled stable expression of human OTOF (hOTOF) in mice and restored hearing for over 6 months [59]. Another team led by Renjie Chai developed a humanized OTOF mouse model [60]. Using an Anc80L65 vector with a hair cell–specific Myo15 promoter, they achieved full-frequency hearing recovery for at least two months in adult mice, with partial restoration lasting over 150 days. Safety and efficacy were further confirmed in cynomolgus monkeys.

Beyond auditory brainstem response (ABR) recovery, recent work by Benamer et al. demonstrated that dual AAV8-OTOF therapy also restored central auditory processing, such as frequency discrimination, in a DFNB9 mouse model, supporting the functional relevance of treatment [61]. Separately, Decibel Therapeutics (a Regeneron affiliate) characterized the expression kinetics of their candidate DB-OTO, an AAV1-based therapy using a Myo15 promoter to drive hOTOF expression [62]. In OTOF-deficient mice, OTOF mRNA and protein emerged within days and plateaued by 2–3 weeks, correlating with robust mid-frequency hearing recovery sustained for at least 3 months.

Together, these studies underscore the translational progress of OTOF gene therapy, establishing dual-AAV delivery as a viable strategy and paving the way from preclinical proof-of-concept toward clinical application.

Clinical Trials of OTOF Gene Therapy

Following promising preclinical results, a wave of clinical trials for OTOF-mediated hearing loss has commenced. To date, seven such trials are underway worldwide: four in China (ChiCTR2200063181, NCT05901480, ChiCTR2400091517, NCT06722170) and three in the USA and Europe (NCT05821959, NCT05788536, NCT06370351) (Table 3).

In early 2024, the Southeast University/Otovia Therapeutics team reported initial results for their dual-vector drug OTOV101N+OTOV101C [13]. Following unilateral RWM injection via a transmastoid facial recess approach, a 5-year-old child with a contralateral cochlear implant showed rapid hearing recovery. ABR thresholds returned to normal, and pure-tone average (PTA) improved from 70–95 dB HL to 30–35 dB HL within one month, reaching near-normal levels across speech frequencies by three months. By contrast, an 8-year-old receiving bilateral injection at a higher dose exhibited more modest improvement (PTA 30–50 dB HL at 40 days), suggesting that age, dose, and individual factors may influence outcomes.

Two months later, preliminary results from the single-arm RRG-003 trial were disclosed [12]. Children aged 1–6 years showed improved auditory function and speech perception after unilateral injection, with hearing recovery emerging 4–6 weeks post-treatment. Average ABR thresholds dropped by 40–57 dB across five children. Although one 5-year-old with pre-existing AAV neutralizing antibodies showed no benefit, the overall safety profile was favorable, with no dose-limiting toxicity or serious adverse events over 26 weeks.

In 2025, the Southeast University/Otovia Therapeutics team reported updated results from a multicenter trial involving ten DFNB9 patients aged 1.5 to 23.9 years [15]. All participants showed hearing improvement over 6–12 months of follow-up, with a favorable safety profile. However, efficacy varied with age: three children aged 1–2 years responded less robustly than those aged 5–8, despite higher systemic AAV exposure. Similarly, a 14.5 year old and a 23.9 year old achieved only 30–45 dB PTA improvement over six months, whereas the best-responding individual improved by 87 dB. One poorly responding patient safely received a second injection in the same ear, indicating that redosing may be a viable option. These findings suggest an age-dependent therapeutic window, possibly aligned with the period of auditory cortical plasticity. Auditory deprivation during this period would perturb neural circuit maturation, whereas later intervention may fail to achieve satisfactory restoration [26, 63], explaining limited benefits in older children. In children aged 1–2 years, elevated serum neutralizing antibodies suggest a stronger immune response, potentially due to the immature blood-labyrinth barrier. The immature synaptic architecture may also inadequately support newly expressed otoferlin, resulting in decreased therapeutic efficacy. Nevertheless, the postnatal developmental trajectory of the human inner ear is not fully mapped [64], rendering such explanations hypothetical.

Most recently, Regeneron's CHORD trial evaluated DB-OTO, a dual AAV1-based gene therapy, in twelve profoundly deaf patients aged 0.9 to 16 years [16]. Participants received DB-OTO via RWM injection combined with lateral semicircular canal fenestration to facilitate perilymph drainage. By week 24, six participants could perceive soft speech and three could hear

whispers. Two 16-year-olds showed partial hearing recovery, with PTA thresholds improving to 60–80 dB, consistent with earlier observations in adolescents [15]. Transient high-frequency hearing loss occurred in two patients, possibly related to injection-associated mechanical stress or perioperative infection, underscoring the need for surgical refinement and careful postoperative care.

Beyond formally published results, other gene therapies, including AK-OTOF and SENS-501, have also been reported to improve hearing safely and effectively in preliminary releases. Together, these results mark the rapid maturation of OTOF gene therapy from concept to clinically meaningful treatment for DFNB9 within just a few years.

Conclusions and Prospects

Gene therapy for NSHL is advancing rapidly, with treatment of OTOF-related DFNB9 emerging as a prominent focus. The successful translation from murine models to human trials marks a historic milestone, demonstrating that congenital deafness in children can be functionally reversed. This breakthrough holds promise for improving life satisfaction and quality of life in individuals with DFNB9, while also offering a valuable framework for gene therapy targeting other forms of genetic deafness.

Nevertheless, several limitations in current findings must be addressed to achieve robust clinical translation. Although auditory function assessed via auditory brainstem response, distortion product otoacoustic emissions, and pure-tone audiometry has been consistently restored in trials, evidence remains scarce regarding recovery of higher-order auditory capacities. These include speech-in-noise understanding, music perception, and long-term language development. Furthermore, clinical research on DFNB9 is still in early stages, constrained by small patient cohorts and considerable interindividual variability, which limit statistical power. Key variables such as vector biodistribution, surgical precision, and baseline patient characteristics require further elucidation. A clearer understanding of the relationship between these factors and clinical outcomes will be essential for predicting therapeutic efficacy. Long-term safety profile of OTOF gene therapy also requires more exploration. Current studies involve only two patients with a one-year follow-up, which is inadequate to evaluate long-time risks. Therefore, larger clinical trials with extended follow-up are necessary to assess the stability of transgene expression, the durability of therapeutic benefits, and the potential immune risks associated with redosing or AAV diffusion. Finally, comparative evaluation of gene therapy versus cochlear implants awaits additional data from ongoing trials.

Despite the encouraging efficacy of OTOF-directed therapy, its overall impact may be constrained by the relatively small proportion of OTOF mutations among all hereditary hearing loss cases. Expanding the reach of deafness gene therapy will

Table 3. OTOF gene therapies in clinical trials.

Registration date	Identifier	Drug	Serotype	dosing strategies (per cochlear)	Injection route	Participant age	Ref.
Sep 1, 2022	ChiC-TR2200063181	RRG-003	AAV1	30/50/70/140/210μl dose-escalation groups at 2.8×10^{11} vg/μl	Transcanal, RWM injection, OW fenestration	6 Months and older	[12, 14, 65]
Feb 8, 2023	NCT05821959	AK-OTOF	Anc80L65	Volume unkonwn Low (Up to 4.1×10^{11} vg) dose group High (Up to 8.1×10^{11} vg) dose group	Unknown	Any age	[66]
Mar 15, 2023	NCT05788536	DB-OTO	AAV1	240μl (7.2×10^{12} vg)	Transmastoid facial recess, RWM injection, lateral semicircular canal fenestration	Up to 17 Years	[16, 67]
May 9, 2023	NCT05901480	OTOV101N +OTOV101C	Anc80L65	30μl (8.4×10^{11} vg) to 60μl (1.68×10^{12} vg)	Transmastoid facial recess, RWM injection	1 Year and older	[13, 15, 68]
Apr 9, 2024	NCT06370351	SENS-501	Unknown	Low/High dose group (not disclosed)	Unknown	6 Months to 31 Months	[69]
Oct 30, 2024	ChiC-TR2400091517	EA0010	Unknown	Low/High dose group (not disclosed)	Unknown	1 Year to 28 Years	[70]
Dec 5, 2024	NCT06722170	EH002	Unknown	25/50/100/150μl dose-escalation groups (undisclosed concentration)	Unknown	6 Months and older	[71]

require extending research to more prevalent and genetically diverse forms of hearing loss, which in turn demands deeper mechanistic insights into underlying pathologies and inner ear physiology. Beyond biomedical challenges, social and ethical considerations, such as pediatric trial ethics, treatment affordability, and standardized diagnostic and management pathways, must also be critically addressed.

As OTOF gene therapy trials continue, effective collaboration among academic, governmental, and commercial partners will be vital to navigate these multifaceted challenges. Success in this endeavor promises to redefine the standard of care for genetic deafness, ushering in a new era of precision gene therapy for hereditary hearing loss.

Abbreviations

NSHL - Non-syndromic Hearing Loss; MET - Mechanoelectrical Transduction; LOF - Loss-of-function; GOF - Gain-of-function; DN - Dominant-negative; AAVs - Adeno-associated Viruses; RWM - Round Window Membrane; NHP - Non-human Primate; IHCs - Inner Hair Cells; hOTOF - Human OTOF; ABR - Auditory Brainstem Response; PTA - Pure-tone Average.

Author Contributions

Yu Qi: Writing - original draft, Writing - review & editing; Fangzhi Tan: Conceptualization, Writing - review & editing, Supervision; Maoli Duan: Conceptualization, Supervision; Ling Lu: Conceptualization, Supervision, Project administration, Funding acquisition, Writing - review & editing. All authors read and approved the final manuscript.

Acknowledgement

The authors would like to thank the Clinical Genome Resource (ClinGen) for generating curated content used in this review. ClinGen's curated content was obtained from www.clinicalgenome.org.

Funding Information

This work was supported by National Key R&D Program of China (2024YFC2511100/2511103) and National Natural Science Foundation of China (82471185).

Ethics Approval and Consent to Participate

Not Applicable.

Competing Interests

The authors declare that they have no existing or potential commercial or financial relationships that could create a conflict of interest at the time of conducting the study.

Data Availability

This is a review article and no new data were generated or analyzed in this study.

Reference

[1] Haile LM, Kamenov K, Briant PS, Orji AU, Steinmetz JD, Abdoli A, et al. (2021). Hearing loss prevalence and years lived with disability, 1990–2019: findings from the Global Burden of Disease Study 2019. Lancet, 397(10278), 996-1009. https://doi.org/10.1016/S0140-6736(21)00516-X

[2] Prasad K, Borre ED, Dillard LK, Ayer A, Der C, Bainbridge KE, et al. (2024). Priorities for hearing loss prevention and estimates of global cause-specific burdens of hearing loss: a systematic rapid review. Lancet Glob Health, 12(2), e217-e225. https://doi.org/10.1016/S2214-109X(23)00514-4

[3] Lieu JEC, Kenna M, Anne S, & Davidson L. (2020). Hearing Loss in Children: A Review. JAMA, 324(21), 2195-2205. https://doi.org/10.1001/jama.2020.17647

[4] Morton Cynthia C, & Nance Walter E. (2006). Newborn Hearing Screening — A Silent Revolution. N Engl J Med, 354(20), 2151-2164. https://doi.org/10.1056/NEJMra050700

[5] Walls WD, Azaiez H, & Smith RJH. Hereditary Hearing Loss Homepage. Retrieved 2025.11.3 from https://hereditaryhearingloss.org

[6] Rauschecker JP, & Shannon RV. (2002). Sending Sound to the Brain. Science, 295(5557), 1025-1029. https://doi.org/10.1126/science.1067796

[7] Kerber S, & Seeber BU. (2012). Sound localization in noise by normal-hearing listeners and cochlear implant users. Ear Hear, 33(4), 445-457. https://doi.org/10.1097/AUD.0b013e318257607b

[8] Macherey O, & Carlyon RP. (2014). Cochlear implants. Curr Biol, 24(18), R878-R884. https://doi.org/10.1016/j.cub.2014.06.053

[9] Dunbar CE, High KA, Joung JK, Kohn DB, Ozawa K, & Sadelain M. (2018). Gene therapy comes of age. Science, 359(6372), eaan4672. https://doi.org/10.1126/science.aan4672

[10] Kulkarni JA, Witzigmann D, Thomson SB, Chen S, Leavitt BR, Cullis PR, et al. (2021). The current landscape of nucleic acid therapeutics. Nat Nanotechnol, 16(6), 630-643. https://doi.org/10.1038/s41565-021-00898-0

[11] Ginn SL, Mandwie M, Alexander IE, Edelstein M, & Abedi MR. (2024). Gene therapy clinical trials worldwide to 2023—an update. J Gene Med, 26(8), e3721. https://doi.org/10.1002/jgm.3721

[12] Lv J, Wang H, Cheng X, Chen Y, Wang D, Zhang L, et al. (2024). AAV1-hOTOF gene therapy for autosomal recessive deafness 9: a single-arm trial. Lancet, 403(10441), 2317-2325. https://doi.org/10.1016/S0140-6736(23)02874-X

[13] Qi J, Tan F, Zhang L, Lu L, Zhang S, Zhai Y, et al. (2024). AAV-Mediated Gene Therapy Restores Hearing in Patients with DFNB9 Deafness. Adv Sci (Weinh), 11(11), 2306788. https://doi.org/10.1002/advs.202306788

[14] Wang H, Chen Y, Lv J, Cheng X, Cao Q, Wang D, et al. (2024). Bilateral gene therapy in children with autosomal recessive deafness 9: single-arm trial results. Nat Med, 30(7), 1898-1904. https://doi.org/10.1038/s41591-024-03023-5
[15] Qi J, Zhang L, Lu L, Tan F, Cheng C, Lu Y, et al. (2025). AAV gene therapy for autosomal recessive deafness 9: a single-arm trial. Nat Med, 31(9), 2917-2926. https://doi.org/10.1038/s41591-025-03773-w
[16] Valayannopoulos V, Bance M, Carvalho DS, Greinwald JH, Jr., Harvey SA, Ishiyama A, et al. (2025). DB-OTO Gene Therapy for Inherited Deafness. N Engl J Med, 10.1056/NEJMoa2400521. https://doi.org/10.1056/NEJMoa2400521
[17] Cheng X, Zhong J, Zhang J, Cui C, Jiang L, Liu Y-w, et al. (2025). Gene Therapy vs Cochlear Implantation in Restoring Hearing Function and Speech Perception for Individuals With Congenital Deafness. JAMA Neurol, 82(9), 941-951. https://doi.org/10.1001/jamaneurol.2025.2053
[18] Smith RJH, Bale JF, Jr., & White KR. (2005). Sensorineural hearing loss in children. Lancet, 365(9462), 879-890. https://doi.org/10.1016/S0140-6736(05)71047-3
[19] Writing Group For Practice Guidelines For Diagnosis Treatment Of Genetic Diseases Medical Genetics Branch Of Chinese Medical Association, Yuan H, Dai P, Liu Y, & Yang T. (2020). Clinical practice guidelines for hereditary non-syndromic deafness. Zhonghua Yi Xue Yi Chuan Xue Za Zhi, 37(3), 269-276. https://doi.org/10.3760/cma.j.issn.1003-9406.2020.03.008
[20] McKusick-Nathans Institute of Genetic Medicine, & Johns Hopkins University (Baltimore MD). Online Mendelian Inheritance in Man, OMIM. Retrieved 2025.11.3 from https://omim.org/
[21] Sloan-Heggen CM, Bierer AO, Shearer AE, Kolbe DL, Nishimura CJ, Frees KL, et al. (2016). Comprehensive genetic testing in the clinical evaluation of 1119 patients with hearing loss. Hum Genet, 135(4), 441-450. https://doi.org/10.1007/s00439-016-1648-8
[22] Mu Y, Han M, Li Y, Di H, Li Z, Li H, et al. (2025). Analysis of deafness gene screening results in 15771 newborn cases in Anyang city of Henan. Front Pediatr, Volume 13 - 2025. https://doi.org/10.3389/fped.2025.1645070
[23] Yan D, Xiang G, Chai X, Qing J, Shang H, Zou B, et al. (2017). Screening of deafness-causing DNA variants that are common in patients of European ancestry using a microarray-based approach. PLOS ONE, 12(3), e0169219. https://doi.org/10.1371/journal.pone.0169219
[24] Yan D, Tekin D, Bademci G, Foster J, Cengiz FB, Kannan-Sundhari A, et al. (2016). Spectrum of DNA variants for non-syndromic deafness in a large cohort from multiple continents. Hum Genet, 135(8), 953-961. https://doi.org/10.1007/s00439-016-1697-z
[25] Sheffield AM, & Smith RJH. (2019). The Epidemiology of Deafness. Cold Spring Harb Perspect Med, 9(9). https://doi.org/10.1101/cshperspect.a033258
[26] Petit C, Bonnet C, & Safieddine S. (2023). Deafness: from genetic architecture to gene therapy. Nat Rev Genet, 24(10), 665-686. https://doi.org/10.1038/s41576-023-00597-7
[27] Ma S, Chen X, Wang Y, & Guo Y. (2025). Mechanisms of congenital hearing loss caused by GJB2 gene mutations and current progress in gene therapy. Gene, 946, 149326. https://doi.org/10.1016/j.gene.2025.149326
[28] Yang T, Vidarsson H, Rodrigo-Blomqvist S, Rosengren SS, Enerbäck S, & Smith RJH. (2007). Transcriptional Control of SLC26A4 Is Involved in Pendred Syndrome and Nonsyndromic Enlargement of Vestibular Aqueduct (DFNB4). Am J Hum Genet, 80(6), 1055-1063. https://doi.org/10.1086/518314
[29] Roux I, Safieddine S, Nouvian R, Grati M, Simmler MC, Bahloul A, et al. (2006). Otoferlin, defective in a human deafness form, is essential for exocytosis at the auditory ribbon synapse. Cell, 127(2), 277-289. https://doi.org/10.1016/j.cell.2006.08.040
[30] Aldè M, Cantarella G, Zanetti D, Pignataro L, La Mantia I, Maiolino L, et al. (2023). Autosomal Dominant Non-Syndromic Hearing Loss (DFNA): A Comprehensive Narrative Review. Biomedicines, 11(6). https://doi.org/10.3390/biomedicines11061616
[31] Yasukawa R, Moteki H, Nishio SY, Ishikawa K, Abe S, Honkura Y, et al. (2019). The Prevalence and Clinical Characteristics of TECTA-Associated Autosomal Dominant Hearing Loss. Genes (Basel), 10(10). https://doi.org/10.3390/genes10100744
[32] Lee S-Y, Kim MY, Han JH, Park SS, Yun Y, Jee S-C, et al. (2023). Ramifications of POU4F3 variants associated with autosomal dominant hearing loss in various molecular aspects. Sci Rep, 13(1), 12584. https://doi.org/10.1038/s41598-023-38272-w
[33] Weegerink NJ, Huygen PL, Schraders M, Kremer H, Pennings RJ, & Kunst HP. (2011). Variable degrees of hearing impairment in a Dutch DFNX4 (DFN6) family. Hear Res, 282(1-2), 167-177. https://doi.org/10.1016/j.heares.2011.08.010
[34] Feng H, Huang S, Ma Y, Yang J, Chen Y, Wang G, et al. (2024). Genomic and phenotypic landscapes of X-linked hereditary hearing loss in the Chinese population. Orphanet J Rare Dis, 19(1), 342. https://doi.org/10.1186/s13023-024-03338-z
[35] Andersen EF, Azzariti DR, Babb L, Berg JS, Biesecker LG, Bly Z, et al. (2025). The Clinical Genome Resource (ClinGen): Advancing genomic knowledge through global curation. Genet Med, 27(1). https://doi.org/10.1016/j.gim.2024.101228
[36] Chen C, Shan W, & Guan M-X. (2024). Defective biogenesis of human mitochondrial ribosomes causes sensorineural deafness. Mitochondr Commun, 2, 114-122. https://doi.org/10.1016/j.mitoco.2024.11.001
[37] Fu X, Wan P, Li P, Wang J, Guo S, Zhang Y, et al. (2021). Mechanism and Prevention of Ototoxicity Induced by Aminoglycosides. Front Cell Neurosci, Volume 15 - 2021. https://doi.org/10.3389/fncel.2021.692762
[38] McDermott JH, Wolf J, Hoshitsuki K, Huddart R, Caudle KE, Whirl-Carrillo M, et al. (2022). Clinical Pharmacogenetics Implementation Consortium Guideline for the Use of Aminoglycosides Based on MT-RNR1 Genotype. Clin Pharmacol Ther, 111(2), 366-372. https://doi.org/10.1002/cpt.2309
[39] Giersch ABS, & Morton CC. (2025). Newborn Screening for Deafness/Hard of Hearing in the Genomic Era. Clin Chem, 71(1), 54-60. https://doi.org/10.1093/clinchem/hvae193
[40] Badonyi M, & Marsh JA. (2025). Prevalence of loss-of-function, gain-of-function and dominant-negative mecha-

nisms across genetic disease phenotypes. Nat Commun, 16(1), 8392. https://doi.org/10.1038/s41467-025-63234-3
[41] Jiang L, Wang D, He Y, & Shu Y. (2023). Advances in gene therapy hold promise for treating hereditary hearing loss. Mol Ther, 31(4), 934-950. https://doi.org/10.1016/j.ymthe.2023.02.001
[42] Izumikawa M, Minoda R, Kawamoto K, Abrashkin KA, Swiderski DL, Dolan DF, et al. (2005). Auditory hair cell replacement and hearing improvement by Atoh1 gene therapy in deaf mammals. Nat Med, 11(3), 271-276. https://doi.org/10.1038/nm1193
[43] Ishimoto S, Kawamoto K, Kanzaki S, & Raphael Y. (2002). Gene transfer into supporting cells of the organ of Corti. Hear Res, 173(1-2), 187-197. https://doi.org/10.1016/s0378-5955(02)00579-8
[44] Akil O, Seal RP, Burke K, Wang C, Alemi A, During M, et al. (2012). Restoration of hearing in the VGLUT3 knockout mouse using virally mediated gene therapy. Neuron, 75(2), 283-293. https://doi.org/10.1016/j.neuron.2012.05.019
[45] Bankoti K, Generotti C, Hwa T, Wang L, O'Malley BW, Jr., & Li D. (2021). Advances and challenges in adeno-associated viral inner-ear gene therapy for sensorineural hearing loss. Mol Ther Methods Clin Dev, 21, 209-236. https://doi.org/10.1016/j.omtm.2021.03.005
[46] Lahlou G, Calvet C, Giorgi M, Lecomte MJ, & Safieddine S. (2023). Towards the Clinical Application of Gene Therapy for Genetic Inner Ear Diseases. J Clin Med, 12(3). https://doi.org/10.3390/jcm12031046
[47] Gadenstaetter AJ, Krumpoeck PE, & Landegger LD. (2025). Inner Ear Gene Therapy: An Overview from Bench to Bedside. Mol Diagn Ther, 29(2), 161-181. https://doi.org/10.1007/s40291-024-00759-1
[48] Wu F, Sambamurti K, & Sha S. (2022). Current Advances in Adeno-Associated Virus-Mediated Gene Therapy to Prevent Acquired Hearing Loss. J Assoc Res Otolaryngol, 23(5), 569-578. https://doi.org/10.1007/s10162-022-00866-y
[49] Klimara MJ, & Smith RJH. (2023). Advances in cochlear gene therapies. Curr Opin Pediatr, 35(6), 631-640. https://doi.org/10.1097/mop.0000000000001273
[50] Yoshimura H, Shibata SB, Ranum PT, & Smith RJH. (2018). Enhanced viral-mediated cochlear gene delivery in adult mice by combining canal fenestration with round window membrane inoculation. Sci Rep, 8(1), 2980. https://doi.org/10.1038/s41598-018-21233-z
[51] Nist-Lund CA, Pan B, Patterson A, Asai Y, Chen T, Zhou W, et al. (2019). Improved TMC1 gene therapy restores hearing and balance in mice with genetic inner ear disorders. Nat Commun, 10(1), 236. https://doi.org/10.1038/s41467-018-08264-w
[52] Wu X, Zhang L, Li Y, Zhang W, Wang J, Cai C, et al. (2021). Gene therapy via canalostomy approach preserves auditory and vestibular functions in a mouse model of Jervell and Lange-Nielsen syndrome type 2. Nat Commun, 12(1), 697. https://doi.org/10.1038/s41467-020-20808-7
[53] Zhao X, Liu H, Liu H, Cai R, & Wu H. (2022). Gene Therapy Restores Auditory Functions in an Adult Vglut3 Knockout Mouse Model. Hum Gene Ther, 33(13-14), 729-739. https://doi.org/10.1089/hum.2022.062
[54] Chang M, & Kanold PO. (2021). Development of Auditory Cortex Circuits. J Assoc Res Otolaryngol, 22(3), 237-259. https://doi.org/10.1007/s10162-021-00794-3
[55] Dai C, Lehar M, Sun DQ, Rvt LS, Carey JP, MacLachlan T, et al. (2017). Rhesus Cochlear and Vestibular Functions Are Preserved After Inner Ear Injection of Saline Volume Sufficient for Gene Therapy Delivery. J Assoc Res Otolaryngol, 18(4), 601-617. https://doi.org/10.1007/s10162-017-0628-6
[56] Andres-Mateos E, Landegger LD, Unzu C, Phillips J, Lin BM, Dewyer NA, et al. (2022). Choice of vector and surgical approach enables efficient cochlear gene transfer in nonhuman primate. Nat Commun, 13(1), 1359. https://doi.org/10.1038/s41467-022-28969-3
[57] Akil O, Dyka F, Calvet C, Emptoz A, Lahlou G, Nouaille S, et al. (2019). Dual AAV-mediated gene therapy restores hearing in a DFNB9 mouse model. Proc Natl Acad Sci U S A, 116(10), 4496-4501. https://doi.org/doi:10.1073/pnas.1817537116
[58] Al-Moyed H, Cepeda AP, Jung S, Moser T, Kügler S, & Reisinger E. (2019). A dual-AAV approach restores fast exocytosis and partially rescues auditory function in deaf otoferlin knock-out mice. EMBO Mol Med, 11(1), e9396. https://doi.org/10.15252/emmm.201809396
[59] Tang H, Wang H, Wang S, Hu SW, Lv J, Xun M, et al. (2023). Hearing of Otof-deficient mice restored by trans-splicing of N- and C-terminal otoferlin. Hum Genet, 142(2), 289-304. https://doi.org/10.1007/s00439-022-02504-2
[60] Qi J, Zhang L, Tan F, Zhang Y, Zhou Y, Zhang Z, et al. (2024). Preclinical Efficacy And Safety Evaluation of AAV-OTOF in DFNB9 Mouse Model And Nonhuman Primate. Adv Sci (Weinh), 11(3), e2306201. https://doi.org/10.1002/advs.202306201
[61] Benamer N, Le Ribeuz H, Felgerolle C, Calvet C, Postal O, Plion B, et al. (2025). Cochlear gene therapy restores hearing and auditory processing in an atypical DFNB9 mouse model. Commun Med (Lond), 5(1), 229. https://doi.org/10.1038/s43856-025-00926-3
[62] Sellon JB, So KS, D'Arcangelo A, Cancelarich S, Drummond MC, Slade PG, et al. (2024). Recovery kinetics of dual AAV-mediated human otoferlin expression. Front Mol Neurosci, 17, 1376128. https://doi.org/10.3389/fnmol.2024.1376128
[63] Sanes Dan H, & Woolley Sarah MN. (2011). A Behavioral Framework to Guide Research on Central Auditory Development and Plasticity. Neuron, 72(6), 912-929. https://doi.org/10.1016/j.neuron.2011.12.005
[64] Lim R, & Brichta AM. (2016). Anatomical and physiological development of the human inner ear. Hear Res, 338, 9-21. https://doi.org/10.1016/j.heares.2016.02.004
[65] The safety, tolerability, and preliminary efficacy of RRG-003 AAV in the treatment of DFNB9 congenital deafness. (2022). https://www.chictr.org.cn/showproj.html?proj=247690.
[66] A Trial of AAVAnc80-hOTOF Gene Therapy in Individuals With Sensorineural Hearing Loss Due to Otoferlin Gene Mutations. (2023). https://clinicaltrials.gov/study/NCT05821959.
[67] A Phase 1/2, Open-Label, Multicenter Trial with a Single Ascending Dose Cohort with Unilateral Intracochlear Injection Followed by a Bilateral Injection Expansion Cohort to Evaluate the Safety, Tolerability, and Efficacy of DB-OTO in Children and Infants with Biallelic hOTOF Mutations. (2023). https://clinicaltrials.gov/study/NCT05788536.

[68] An Investigator Initiated Study Evaluating the Safety, Tolerability, and Efficacy of OTOV101N+OTOV101C Injection in Treating Patients With OTOF Mutation-related Deafness. (2023). https://clinicaltrials.gov/study/NCT05901480.
[69] A Phase I/II, Open-ended, Adaptative, Open Label Dose Escalation and Expansion Clinical Trial to Evaluate the Efficacy and Safety of Unilateral Intracochlear Injection of SENS-501 Using an Injection System in Children with Severe to Profound Hearing Loss Due to Otoferlin Gene Mutations. (2024). https://clinicaltrials.gov/study/NCT06370351.
[70] The safety, tolerability, and efficacy of EA0010 in the treatment of OTOF-deficiency hearing loss. (2024). https://www.chictr.org.cn/showproj.html?proj=247690.
[71] A Study on the Safety, Tolerability, and Preliminary Efficacy of EH002 in the Treatment of DFNB9 Congenital Deafness. (2024). https://clinicaltrials.gov/study/NCT06722170.

Research Article Head and Neck Diseases Conflux

Developmental Outcomes Following Early Cochlear Implantation in Infants and Toddlers: a Comparative Study with Normal-hearing Peers

Authors

Baodong Wu, Yi Sun, Melcol Hailu Yilala, Wei Cao

Correspondence

caowei2024@ahmu.edu.cn (W. Cao)

Graphical Abstract

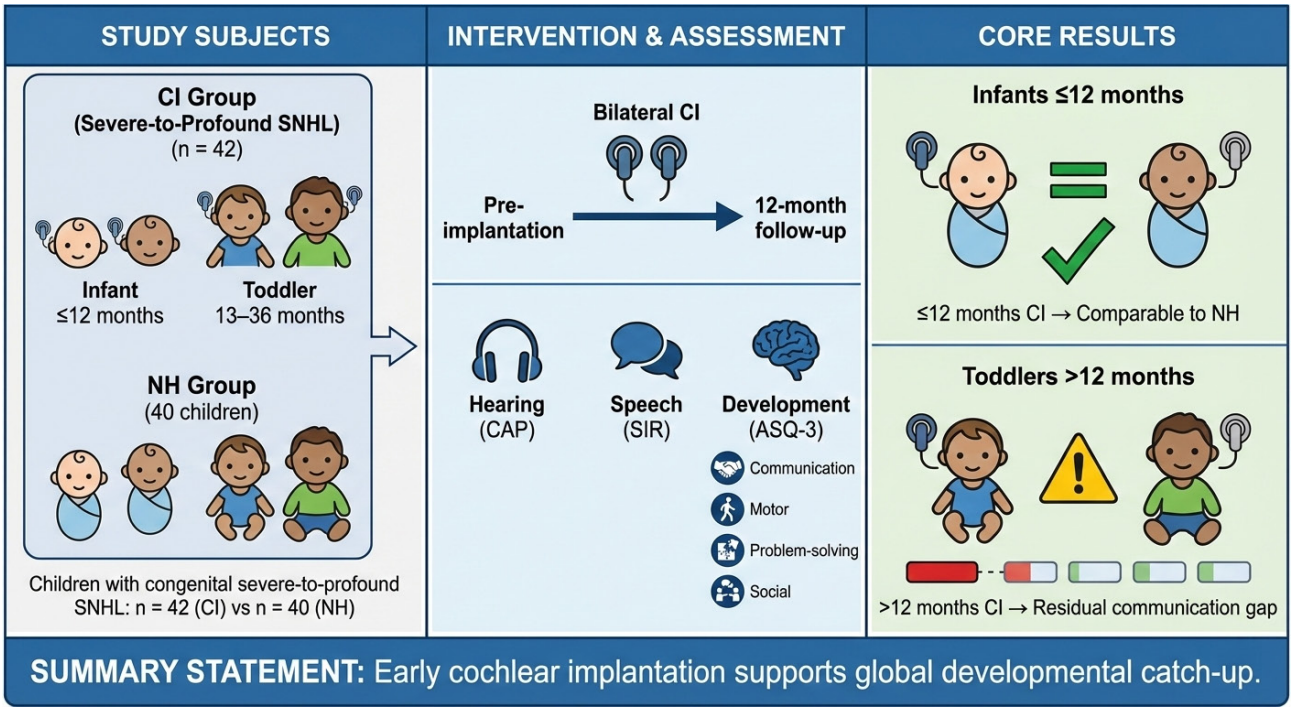

https://doi.org/10.71321/prwgkz02

Research Article Head and Neck Diseases Conflux

Developmental Outcomes Following Early Cochlear Implantation in Infants and Toddlers: a Comparative Study with Normal-hearing Peers

Baodong Wu [1] , Yi Sun [1] , Melcol Hailu Yilala [2] , Wei Cao [1*]

Received: 2026-01-12 | Accepted: 2026-02-09 | Published online: 2026-03-12

Abstract

Objective: To evaluate whether early cochlear implant (CI) use can significantly and positively change hearing and speech abilities during a child's development.

Methods: The present study included 42 children with bilateral CIs (8–36 months) and 40 age-matched children with normal hearing (NH) (6–48 months). Ages & Stages Questionnaires, Third Edition (ASQ-3); Categories of Auditory Performance (CAP); Speech Intelligibility Rate (SIR) were used.

Results: Twelve months after receiving bilateral CIs, the hearing status of the infants (1–12 months) and toddlers (13–36 months) had improved significantly. Infants using CIs were comparable to those with NH in all ASQ-3 aspects ($p > 0.05$). For toddlers, there was a post-implantation improvement in the gross motor, problem solving, and personal social domains ($p > 0.05$). However, there were still gaps in the communication domain ($p < 0.001$). Multivariate analysis revealed that pre-implantation hearing aid usage duration, schooling, SIR score, communication, and caregiver education level significantly influenced post implantation outcomes.

Conclusions: With CI use, infants and toddlers with congenital sensorineural hearing loss showed improvements in auditory perception, speech production, and developmental abilities. Infant implant recipients performed better in all areas of development than toddlers, comparable to with NH children. Hearing aid use, language rehabilitation training, caregivers' education level, and communication method were all highly correlated with the overall development of the children.

Keywords: Cochlear implants; Development; Auditory; Speech

Introduction

Hearing loss is a growing global health challenge affecting individuals across the lifespan. Recent data from the Global Burden of Disease Study highlights the increasing prevalence of hearing loss, emphasizing the need for early intervention strategies [1-3]. Hearing allows children to sense the world around them, communicate with others, acquire knowledge, and integrate into society. Auditory deprivation from birth notably hampers a child's development. Fortunately, cochlear implant (CI) use can reduce the consequences of auditory deprivation, showing how far biomedical science has progressed.

Cochlear implantation has proved to be a safe and effective treatment for children with severe-to-profound sensorineural hearing loss. CI use can help restore auditory and speech functions to varying degrees [4]. The timing of implantation is critical. Multiple lines of evidence suggest that infants who undergo implantation before 12 months exhibit better auditory performance and speech outcomes than children implanted after 12 months [5-7]. It is highly probable that the reason for this is the time sensitive window during which the auditory cortex matures, a period when the central auditory pathways exhibit maximum plasticity [8-10]. This window spans a child's first 48 months of life.

Monitoring the effects of CI use mainly focuses on tangible aspects of hearing and speech capabilities. However, cognitive development dimensions that are less directly associated with hearing are yet to be investigated [11]. The child's overall developmental status is a potential predictor of cognitive function after receiving a CI [34]. Monitoring cognitive development dimensions should be valued with equal, if not more, importance to traditional measures. The rationale lies in the fact that brain development happens in a systematic manner [12]. Hearing loss can have knock on effects on other functions, including

1 Department of Otorhinolaryngology, Head and Neck Surgery, The Second Affiliated Hospital of Anhui Medical University, Hefei, China.

2 Department of ORL-HNS, College of Health Sciences, Addis Ababa University, Addis Ababa, Ethiopia.

* Corresponding Author.

higher-order neurocognitive tasks [13]. It has been found that early deafness will hamper a child's overall development, including cognitive, motor, and social domains [14-18]. This has also been acknowledged by national guidelines for early screening; children's hearing problems should be addressed as early as possible to prevent possible developmental delays, allowing them to reach their full potential [19-22].

The present study aims to find out whether early implantation can significantly improve a child's overall development, as well as hearing and speech abilities.

Materials and Methods

Participants

The present retrospective study focused on infants (aged 1–12 months) and toddlers (aged 13–36 months) who had received bilateral CIs at the ENT department of the Second Affiliated Hospital of Anhui Medical University between 2019 and 2021. All the CI recipients were born with severe to profound hearing loss, while the control group consisted of children with normal hearing.

Data from the CI recipients were primarily collected in offline forms. The data included details such as age, gender, inner ear anomalies, cerebral lesions, hearing aid use, caregiver's education level, post-implantation communication mode (Communication modes were categorized into oral and multiple types. The 'multiple communication type' was defined as the simultaneous use of speech and sign language or a combination of oral communication with gestures.), and aural rehabilitation (Table 1). Consent was received from all the participants' parents prior to filling out the questionnaire, as well as basic information for the NH children. On top of this, the study protocol was reviewed and approved by our hospital's ethics committee.

From the preoperative brain magnetic resonance imaging (MRI) and high-resolution computed tomography (HRCT), the inner ear anomalies included enlarged vestibular aqueduct (n=5), incomplete partition II (n = 7), internal auditory canal stenosis (n = 4), and focal parenchymal lesion (n = 4). Some cases included more than one inner ear anomaly. It was noted that all the children had no congenital diseases except hearing loss before surgery. All the patients had the same doctor performing the surgery and an artificial cochlea of the same brand. The system was activated normally one month after surgery. The data were recorded 1 day before and 12 months after the surgery.

The control group included 40 children distributed across the age spectrum to match the CI cohort. Gender distribution in the NH group (21 boys and 19 girls) was not significantly different from the CI group ($p > 0.05$). Specifically, this included 11 children aged under 12 months, 11 children aged 13–24 months, 6 children aged 25–36 months and 12 children aged 36–48 months. Their ASQ-3 scores were within the normal range.

A total of 42 children with bilateral CIs and 40 children with normal hearing were initially screened. The detailed inclusion and exclusion process, as well as the final cohort composition, is illustrated in the study flowchart (Figure 1).

Table 1. Demographic characteristics of CI recipients.

Characteristic	Category	CI recipients (≤ 12 months)	CI recipients (12-36 months)
Age (months)	Mean ± SD	9.37±1.51	26.22±5.56
Sex	Female	6	13
	Male	13	10
Inner ear anomalies	None	12	12
	Anomalies	7	11
Cerebral lesions	None	18	23
	Anomalies	1	0
Hearing aids	Yes	11	10
	No	8	13
Caregiver's education level	None	1	0
	primary school	1	3
	Junior high school	8	8
	Senior high school	5	2
	University degree	4	10
Aural rehabilitation	Oral	19	21
	Sign language + Oral	0	2
	No	3	0
	Yes	16	23
Schooling status	No school	9	0
	Kindergarten	10	9
	Rehabilitation school	0	14

Figure 1. This flowchart illustrates the screening and enrollment process for children in the study. The pathway details the inclusion of children with congenital severe-to-profound sensorineural hearing loss (CI group, n = 42), stratified by age at implantation (≤12 months and >12 months). The right pathway shows the enrollment of age-matched children with normal hearing (NH group, n = 40). Excluded participants and reasons are specified. All CI recipients underwent a 12-month post-implantation assessment using the ASQ-3, and their outcomes were compared with those of the NH group. Key influencing factors analyzed included pre-implantation hearing aid use, communication mode, schooling status, aural rehabilitation, caregiver education level, CAP, and SIR scores.

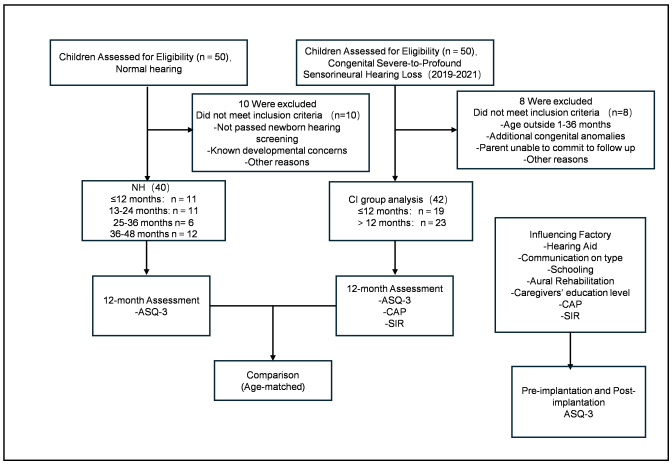

Evaluation

1) Auditory and speech evaluation

Categories of Auditory performance (CAP) is a scale used to assess the post-implantation auditory perception abilities of children who have received CIs. CAP provides 8 categories to rate hearing abilities, in order of increasing ability (Table S1) [23-24].

The Speech Intelligibility Rating (SIR) scale is used to assess the speech intelligibility of children who have received CIs. It provides 5 categories for evaluating spontaneous speech (Table S2) [25].

2) Development evaluation

The Ages & Stages Questionnaires, Third Version (ASQ-3) is an instrument completed by parents/caregivers to identify developmental delays in children aged 2–66 months [26]. It consists of 21 questionnaires for different age ranges. Each questionnaire consists of 30 items divided into 5 dimensions: 1) communication, 2) gross motor, 3) fine motor, 4) problem solving, and 5) personal-social.

The ASQ-3 has been translated into several languages, including Chinese [24]. It has excellent psychometric properties, with a test–retest reliability of 92%, a sensitivity of 87.4%, and a specificity of 95.7%, which has been tested worldwide [27-30].

The ASQ-3's easy-to-understand questions are filled out by the primary caregiver, such as the parent. Based on each section's score, the assessor determines whether the child's development is consistent with their age level, effectively identifying possible developmental delays.

Statistical Analysis

SPSS software version 26.0 was used for the data analysis. First, descriptive statistics were used to summarize the variables and calculate the frequencies and percentages of numeric variables. The Shapiro–Wilk test was used to verify the normality of numeric variables ($p < 0.05$). Due to the non-normal distribution of the data, the Wilcoxon signed-rank test was subsequently used to compare pre- and post-surgery paired scores. The Mann–Whitney U test was then used to compare overall differences between children with CIs and NH children.

Additionally, multivariate linear regression analysis was used to explore the combined effects of multiple independent variables on the baseline scores across the 5 ASQ-3 subscales before the surgery. Generalized linear regression analysis was also used to identify the factors influencing the post-implantation improvement in the five ASQ-3 subscales. All significance tests were set at a 95% confidence interval and a significance level of 0.05.

Results

pre- and post-implantation comparison among children with CIs

Table 2 shows the Wilcoxon signed-rank test results for the ASQ-3, CAP, and SIR for CI children pre- and 12 months post-implantation. The results indicated significant improvement after CI use in the communication ($p < 0.01$), gross motor, problem solving ($p < 0.01$), and personal-social domains, as well as CAP ($p < 0.01$) and SIR ($p < 0.01$) scores. However, the fine motor domain did not show a significant improvement. CI use proved to have a significant positive effect on overall development level, auditory performance, and speech intelligibility.

Table 2. Wilcoxon signed-rank test results comparing pre- and post-implantation ASQ-3, CAP, and SIR scores for children with CIs.

Instrument	Domain / Sub-scale	*z*-value	*p*-value
ASQ-3	Communication	3.83237	<.001
	Gross motor	−2.78832	0.006
	Fine motor	−1.45668	0.981
	problem-solving	3.82612	<.001
	personal-social	1.42542	0.035
CAP	-	52.04805	<.001
SIR	-	52.04805	<.001

Children with CIs and NH children, pre- and 12 months post implantation

Figure 2 and Table 3 show the significant differences in ASQ-3 scores between children with CIs and NH children pre- and 12 months post-implantation. The performance of children with CIs was below that of NH children. Before surgery, all ASQ 3 domains except for fine motor had significant differences ($p < 0.01$). After surgery, there was a noticeable improvement in the gross motor, fine motor, and personal social domains, and the mean gap had narrowed in others, indicating the positive impact of CI use.

Figure 2. Comparison of developmental outcomes before and after cochlear implantation. a (Left panel): Bar graph comparing ASQ-3 domain scores (communication, gross motor, fine motor, problem-solving, personal-social) in children with CIs before (CI Pre) and 12 months after (CI Post) implantation. Error bars represent standard deviations. Asterisks denote statistically significant improvements post-implantation (**p < 0.01, *p < 0.05). **b (Right panel):** Bar graph comparing ASQ-3 domain scores between children with CIs 12 months post-implantation (CI Post) and age-matched children with normal hearing (NH). The dashed line represents the NH group's mean score level for reference. Gaps, particularly in the communication domain, are evident between the CI Post and NH groups.

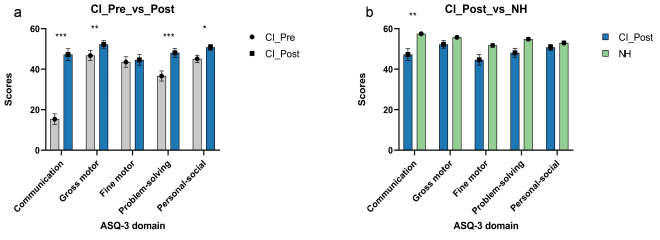

Children with CIs and NH children aged ≤ 12 months and ≥ 12 months pre- and 12 months post-implantation

Figure 3 and Table S3 show the Mann–Whitney U test results for the ASQ 3 scores of the 19 children with CIs and the 11 NH children aged ≤ 12 months. Before implantation, there was no significant difference between the two groups' fine motor domains, but the other domains were significantly different ($p < 0.05$). The scores of the children with CIs were comparable to those of the 11 NH children at the same follow-up age in all domains 24 months post-implantation ($p > 0.05$).

Figure 3 and Table S3 also show the Mann–Whitney U test

results for children ≥ 12 months. Before implantation, comparisons between children with deafness and NH children showed statistically significant differences in the communication (p < 0.01) and problem solving (p < 0.01) domains. When comparing children with CIs aged ≥ 12 months with NH children aged 24–48 months, there was an improvement in the gross motor, problem solving, and personal social domains 12 months post implantation (p > 0.05). However, there were still gaps in the communication domain (p < 0.01). The general positive effects of CI use were better in children ≤ 12 months than in children ≥ 12 months. This implies that the timing of surgical intervention is critical. In terms of the communication, fine motor, and personal-social domains, the scores decreased with age. The data demonstrate that the positive effects of CI use decrease as the recipient's age at implantation increases.

Influencing factors

Figure 4 shows the generalized linear regression analysis results examining the factors influencing the post-implantation improvement in the 5 ASQ-3 domains in children with CIs. The predictors analyzed consist of CAP, SIR, hearing aid, communication type, schooling, aural rehabilitation, and caregivers' education level and individual difference.

Caregivers' education level significantly negatively affected post-implantation communication improvement, indicating that higher caregiver education levels were associated with smaller communication improvements.

Pre-implantation hearing aid usage time and schooling status (p < .001) significantly influenced post-implantation fine motor improvement. Longer hearing aid usage was associated with greater improvement in the fine motor domain. Children without schooling showed larger improvements in the fine motor domain. The subject also significantly affected the results, highlighting variability in post-implantation improvements among children. Multiple communication types had a significant negative impact on post implantation personal-social improvement, suggesting that certain communication modes (e.g., non-verbal communication) may hinder the development of social skills. Lower SIR scores also negatively affected social improvement, indicating that children with poorer speech understanding showed smaller gains in social abilities. The detailed results can be found in Table S4.

Figure 3. Developmental outcomes stratified by age at implantation. a (Upper panel): Comparison of ASQ-3 scores between infants who received CIs at ≤ 12 months of age (CI Infants) and age-matched infants with normal hearing (NH Infants) at the 12-month follow-up. Infants with CIs achieved scores comparable to their NH peers across all developmental domains. **b (Lower panel):** Comparison of ASQ-3 scores between toddlers who received CIs at > 12 months of age (CI Toddlers) and age-matched toddlers with normal hearing (NH Toddlers). While improvements were observed in gross motor, problem-solving, and personal-social domains, a significant gap remained in the communication domain for the CI Toddlers group.

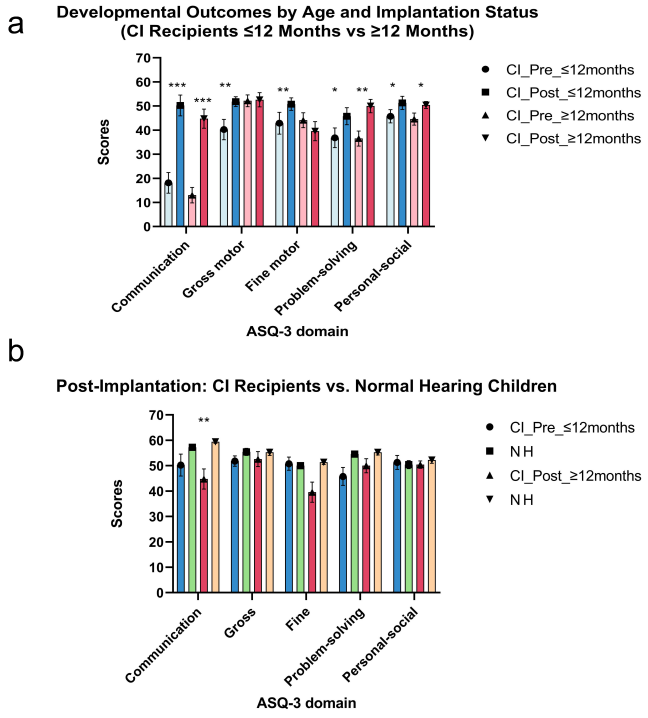

Discussion

With the development of science and technology, biomedical technology has made great progress. This includes cochlear, vestibular, and retinal implants, among which cochlear implan-

Table 3. Mann–Whitney U test results comparing pre- and post-implantation ASQ-3 scores between children with CIs and NH children.

ASQ-3 domain	Time point	CI recipients (n = 42)	NH (n = 40)	*p*-value
Communication	Pre-implantation	15.36± 2.61	57.5 ± 0.54	<0.001
	Post-implantation	47.26 ± 2.91	57.5 ± 0.54	0.004
Gross motor	Pre-implantation	46.79 ± 2.48	55.75 ± 0.68	0.011
	Post-implantation	52.26 ± 1.84	55.75 ± 0.68	0.788
Fine motor	Pre-implantation	43.57 ± 2.62	51.75 ± 0.89	0.174
	Post-implantation	44.64 ± 2.60	51.75 ± 0.89	0.339
Problem-solving	Pre-implantation	36.67 ± 2.50	54.88 ± 0.79	<0.001
	Post-implantation	48.10 ± 2.20	54.88 ± 0.79	0.085
Personal-social	Pre-implantation	45.12 ± 1.83	53.00 ± 0.96	0.004
	Post-implantation	50.83 ± 1.46	53.00 ± 0.96	0.519

tation enjoys great success [17]. Because the human cochlea begins to function between 24 and 36 weeks of gestational age, the effects on hearing may begin during intrauterine life [31], which is earlier than previously thought. Also, early deafness is often considered a connectome disease that affects the central nervous system [17], blocking the transmission of information from peripheral hearing to higher auditory centers, and affecting the interconnections between the centers and multiple cortical areas. Therefore, due to the influence of multiple factors, children will not only show different improvements in hearing and speech after CI use but may also have differences in development.

Our study showed that CI use led to improvements in auditory and speech intelligibility abilities in children with severe-to-profound deafness 12 months post-implantation. The use of CAP and SIR helped us to quickly assess each child's condition, offering the advantage of early detection and intervention for children of all ages. All children underwent bilateral cochlear implantation, which was consistent with previous evidence [33] that early bilateral cochlear implantation can significantly improve children's auditory and speech intelligibility prognoses.

As more and more children are implanted bilaterally, the post-implantation areas of focus have become more comprehensive. Previous research has found that a child's overall development status is a potential predictor of cognitive function after CI use [34]. However, it is difficult to assess the cognitive function of infants and toddlers directly, particularly when they have profound sensorineural hearing loss. This is due to them being unable to conduct the tests themselves and communicate effectively. Therefore, assessing the child's overall development status can help us solve this problem and figure out the child's cognitive status. Depending on the purpose of the test, the scales can be divided into diagnostic scales and screening scales. Although diagnostic scales are relatively accurate, they are complex and time-consuming, (e.g., the Gesell Developmental Diagnosis Scale [35] and the Bayley Scales for Infant Development, Third Edition [36]). The screening scales are simple to operate and have low medical costs, making them more suitable for regular screening and monitoring for early detection, early diagnosis, and early intervention, (e.g., the Denver Developmental Screening Test [37] and the ASQ-3 [26]).

The ASQ-3 can help to find out whether children aged 2–66 months have developmental delays [26]. It is one of the most widely used screening assessments of early childhood. Previous data from animal models and children with deafness have shown that there is a sensitive period for the maturation of the auditory cortex in the first 48 months of life [38]. CI use can alleviate auditory system deficits and promote cortical maturation in children with deafness [39]. Restoring hearing during this period can both stimulate the development of cortical function to a great extent and provide conditions in which auditory speech abilities and overall development can improve. The ASQ-3's target age group roughly coincides with the cortex's sensitive period, which covers the years from infancy to toddlerhood. The ASQ-3 can evaluate infants' and toddlers' overall developmental levels to timely discover low-level development situations, carry out appropriate interventions, reduce the risks of such diseases, and improve the population's quality of life.

Current literature shows that children with CIs experience difficulties with fine and gross motor skills, social interaction, and cognitive abilities [40]. Conversely, our study demonstrat-

Figure 4. Factors influencing post-implantation developmental improvement. Results of the generalized linear regression analysis identifying predictors of improvement in the five ASQ-3 domains 12 months after cochlear implantation. The forest plot displays estimated coefficients (β) with 95% confidence intervals for each factor: pre-implantation hearing aid use duration, communication mode (oral vs. mixed), schooling status, aural rehabilitation attendance, caregiver education level, Categories of Auditory Performance (CAP) score, and Speech Intelligibility Rating (SIR) score. Factors with confidence intervals not crossing the zero line (vertical dashed line) are considered statistically significant predictors ($p < 0.05$).

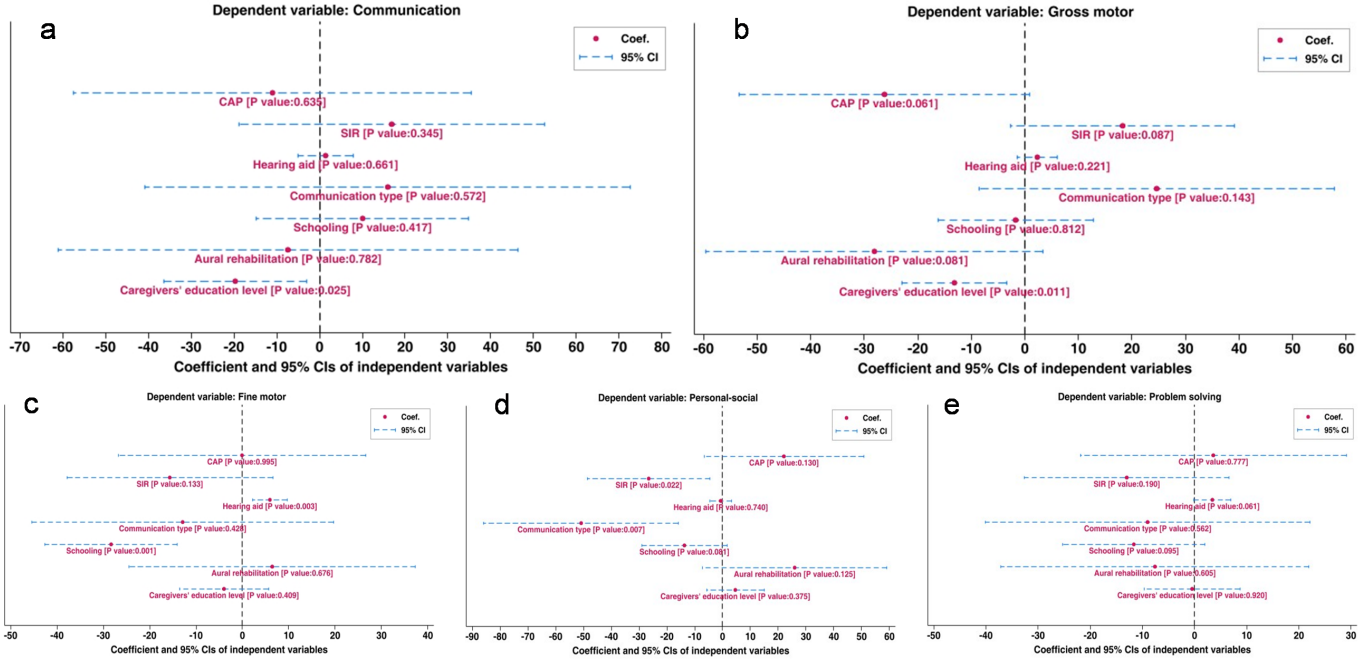

ed that CI use led to children making significant progress in the communication, gross motor, problem solving, and personal-social domains. However, a notable exception was observed in the fine motor domain, where no significant 'catch-up' occurred relative to NH peers. This specific lag warrants explanation beyond general developmental delay and is likely attributable to complex physiological constraints. Recent evidence suggests that fine motor deficits in this population are closely linked to vestibular dysfunction, which is highly prevalent (up to 60%) in children with sensorineural hearing loss [41]. The vestibular system is critical not merely for balance, but for maintaining the proximal stability and postural tone required for precise distal movements; thus, compromised vestibular input can impede the maturation of fine finger dexterity even after auditory restoration [42]. Except for the fine motor domain, children with hearing loss fall behind NH children in all other domains. Auditory deprivation in infants leads to a significant decline in fine motor function as they age [43]. Our findings suggest that CI use alleviates this downward trend: just 12 months after cochlear implantation, children with deafness showed significant improvements in gross and fine motor, problem solving, and personal-social domains, and the communication gap between children with CIs and NH children also narrowed.

Research related to the development of children with congenital deafness shows that infants who received CIs before 12 months developed better in terms of hearing and speech than those implanted after, and even reached the standards of NH children [6, 44-45]. At the same time, no significant age-related surgical complications have been reported [7, 46]. Therefore, we divided the children into two age groups: infants ≤ 12 months and toddlers ≥ 12 months. We found that, with bilateral CI use, infants with hearing loss achieve almost the same development level as NH children. However, toddlers still had communication gaps. These results indicate that CI use could help children with hearing loss develop, but this effect may decline with age. Multiple research reports showed that cochlear implantation at ≤ 12 months of age had significant advantages in long-term post implantation language skills and cognitive development outcomes [47-48]. Therefore, to allow children with deafness to develop at a better rate, we recommend that bilateral CI surgery should be performed before 12 months, if possible.

The present study found that higher levels of caregiver education are associated with poorer post-implantation communication skills in children with deafness. Previous studies have shown that parents' high level of education can improve children's developmental delays [49-50], which contradicts our research. We theorize that this may be due to caregivers with higher education levels having elevated expectations for the communication skills of their children with deafness, leading to a decrease in scores and thus affecting the ASQ-3 score. Gross motor skills involve the use of large muscle groups, while fine motor skills involve the use of smaller muscles / muscle groups. Together, they constitute components of human behavior with practical significance for day-to-day functioning [51]. Our research found a significant negative correlation between the educational level of caregivers and gross motor skills in children with deafness. We theorize that this may be because of the small sample size, which may not completely represent the entire population.

The present study found that wearing hearing aids pre-implantation has a significant positive effect on the post-implantation fine motor skills of children with deafness. This is consistent with several studies [52-54]. Other studies have also shown that exercise and language development are closely related [55-56]. Early adoption of hearing aids exposes children with deafness to verbal language at an earlier age, enabling them to adapt more quickly after implantation. This is undoubtedly beneficial for the development of motor skills in children with deafness. Additionally, there is also a significant correlation between postoperative school attendance and individual differences in fine motor skills. We found that personal-social skills correlate significantly with speech intelligibility and communication type. According to current literature, the communication style and clarity of speech of CI users affect how others understand them, which in turn affects their social functioning [57]. Using SIR to evaluate the intelligibility of children with deafness can help predict their social skills and thus plan corresponding intervention strategies.

Additionally, compared to sign language, verbal communication is more conducive to the social skills of children with deafness. This also indirectly is confirmed by the reciprocal relationship between communication and overall development, which gives us great confidence that, with CI use, infants with prelingual deafness could reach outcomes comparable to NH children in the future. Moving forward, children who receive CIs early in life should be managed in a more holistic manner to improve language skills and overall development. It seems more important than ever to individually tailor interventions to each child, to help them reach their full potential.

Clinically, integrating ASQ-3 into routine post-implantation assessments can facilitate early identification of developmental delays, enabling such tailored interventions. To maximize effectiveness in the rehabilitation plan, priority should be given to wearing hearing aids before surgery, maintaining good communication, and providing high-quality rehabilitation training (e.g., rehabilitation schools).

Despite the results mentioned above, several limitations should be mentioned. Our study was retrospective in design, which limited the availability of participants' information. Furthermore, the sample size was relatively small and the follow-up time relatively short, which may have limited the robustness of our analysis. However, data collection is still ongoing, and future analyses will benefit from an increased sample size.

Conclusion

Early cochlear implantation (≤ 12 months) significantly enhances auditory, speech, and developmental outcomes in children with congenital sensorineural hearing loss, enabling them to match NH peers in developmental milestones. Hearing aid use, language rehabilitation training, caregivers' education levels, and communication method are all highly correlated with a child's overall development. Therefore, a comprehensive evaluation of a child's overall development level using the ASQ-3 could be useful to improve the post-implantation outcomes. These findings advocate for bilateral implantation, coupled with holistic, family-centered support, to optimize developmental trajectories in children aged ≤ 12 months with

severe-to-profound sensorineural hearing loss.

Abbreviations

CI - Cochlear Implant; NH - Normal Hearing; ASQ-3 - Ages & Stages Questionnaires, Third Edition; CAP - Categories of Auditory Performance; SIR - Speech Intelligibility Rating.

Acknowledgements

We extend our gratitude to the Department of Otorhinolaryngology, Head and Neck Surgery at The Second Affiliated Hospital of Anhui Medical University for providing the clinical data and research platform. We are particularly indebted to Dr. Wei Cao for his invaluable guidance throughout the study design and manuscript preparation. Additionally, we appreciate the statistical advice provided by our colleagues and the support from all the participating children and their families.

Author Contributions

Baodong Wu: Writing - original draft, Methodology, Investigation, Data curation, Formal analysis, Conceptualization. Yi Sun: Writing - review & editing, Project administration, Methodology, Data curation. Melcol Hailu Yilala :Writing - review, Supervision. Wei Cao: Writing - review & editing, Funding acquisition, Conceptualization.

Funding Information

This research received funding from the Natural Science Foundation project of Anhui province [No. 2208085MH233] and the National Natural Science Foundation of China Incubation program [No. 2022GMFY03]

Ethics Approval and Consent to Participate

The study was conducted under the Declaration of Helsinki and approved by the Ethical Committee of the Second Affiliated Hospital of Anhui Medical University, Anhui, China.

Competing Interests

The authors declare no conflict of interest.

Data Availability

The data are available from the corresponding author on reasonable request.

Reference

[1] Li FF, Wang JP, Zhang WJ, Zhou PT, Fan M, Cai NN, et al. (2025). Trends and mechanisms of Alzheimer's disease and hearing impairment: A 20-year perspective. Ageing Res Rev, 110, 102799. https://doi.org/10.1016/j.arr.2025.102799

[2] Li FF, Fu ZY, Han K, Liang BY, Han YX, Liu YH, et al. (2025). Trends and driving factors of age-related hearing loss and severity over 30 years: a cross-sectional study. BMC Geriatr, 25(1), 387. https://doi.org/10.1186/s12877-025-06066-6

[3] Jiang CY, Han K, Yang F, Yin SY, Yin SY, Zhang L, et al. (2023). Global, regional, and national prevalence of hearing loss from 1990 to 2019: A trend and health inequality analyses based on the Global Burden of Disease Study 2019. Ageing Res Rev, 92, 102124. https://doi.org/10.1016/j.arr.2023.102124

[4] NIH Consensus Conference. (1995). Cochlear implants in adults and children. JAMA, 274(24), 1955–1961. https://doi.org/10.1001/jama.1995.03530240061037

[5] Incerti PV, Ching TYC, Hou S, Van Buynder P, Flynn C, & Cowan R. (2018). Programming characteristics of cochlear implants in children: effects of etiology and age at implantation. Int J Audiol, 57(sup2), S27-S40. https://doi.org/10.1080/14992027.2017.1370139

[6] Dettman SJ, Dowell RC, Choo D, Arnott W, Abrahams Y, Davis A, et al. (2016). Long-term communication outcomes for children receiving cochlear implants younger than 12 months: a multicenter study. Otol Neurotol, 37, e82–e95. https://doi.org/10.1097/MAO.0000000000000915

[7] Holman MA, Carlson ML, Driscoll CL, Beatles SP, Peterson AM, Sladen DP, et al. (2013). Cochlear implantation in children 12 months of age and younger. Otol Neurotol, 34, 251–258. https://doi.org/10.1097/mao.0b013e31827d0922

[8] Dorman MF, Sharma A, Gilley P, Martin K, & Roland P. (2007). Central auditory development: evidence from CAEP measurements in children fit with cochlear implants. J Commun Disord, 40, 284–294. https://doi.org/10.1016/j.jcomdis.2007.03.007

[9] Sharma A, Gilley PM, Dorman MF, & Baldwin R. (2007). Deprivation-induced cortical reorganization in children with cochlear implants. Int J Audiol, 46, 494–499. https://doi.org/10.1080/14992020701524836

[10] Sharma A, Campbell J, & Cardon G. (2009). Cortical development, plasticity and re-organization in children with cochlear implants. J Commun Disord, 42, 272–279. https://doi.org/10.1016/j.jcomdis.2009.03.003

[11] Niparko JK, Hoffman M, Tiddens E, & Quittner AL. (2018). Comparisons of visual attention in school-age children with cochlear implants versus hearing peers and normative data. Hear Res, 359, 91–100. https://doi.org/10.1016/j.heares.2018.01.002

[12] Lund E, & Dinsmoor J. (2016). Taxonomic knowledge of children with and without cochlear implants. Lang Speech Hear Serv Sch, 47, 236–245. https://doi.org/10.1044/2016_LSHSS-15-0032

[13] Harris MS, Kronenberger WG, Gao S, Hoen HM, Miyamoto RT, & Pisoni DB. (2013). Verbal short-term memory devel-

opment and spoken language outcomes in deaf children with cochlear implants. Ear Hear, 34, 179–192. https://doi.org/10.1097/AUD.0b013e318269ce50
[14] Boons T, De Raeve L, Langereis M, Peeraer L, Wouters J, & van Wieringen A. (2013). Expressive vocabulary, morphology, syntax and narrative skills in profoundly deaf children after early cochlear implantation. Res Dev Disabil, 34, 2008–2022. https://doi.org/10.1016/j.ridd.2013.03.003
[15] Conway CM, Karpicke J, Anaya EM, Henning SC, Kronenberger WG, & Pisoni DB. (2011). Nonverbal cognition in deaf children following cochlear implantation: motor sequencing disturbances mediate language delays. Dev Neuropsychol, 36, 237–254. https://doi.org/10.1080/87565641.2010.549869
[16] [Niparko JK, Tobey EA, Thal DJ, Eisenberg LS, Wang NY, Quittner AL, et al. (2010). Spoken language development in children following cochlear implantation. JAMA, 303, 1498–1506. https://doi.org/10.1001/jama.2010.451
[17] Kral A, Kronenberger WG, Pisoni DB, & O'Donoghue GM. (2016). Neurocognitive factors in sensory restoration of early deafness: a connectome model. Lancet Neurol, 15(6), 610–621. https://doi.org/10.1016/S1474-4422(16)00034-X
[18] Kronenberger WG, Beer J, Castellanos I, Pisoni DB, Miyamoto RT, Wilson BS, et al. (2014). Neurocognitive risk in children with cochlear implants. JAMA Otolaryngol Head Neck Surg, 140(7), 608-615. https://doi.org/10.1001/jamaoto.2014.757
[19] Council on Children with Disabilities, Section on Developmental Behavioral Pediatrics, & Bright Futures Steering Committee. (2006). Identifying infants and young children with developmental disorders in the medical home: an algorithm for developmental surveillance and screening. Pediatrics, 118(1), 405-420. https://doi.org/10.1542/peds.2006-1231
[20] Richter LM, Daelmans B, Lombardi J, Heymann J, Lopez Boo F, Britto PR, et al. (2017). Investing in the foundation of sustainable development: pathways to scale up for early childhood development. Lancet, 389(10064), 103–118. https://doi.org/10.1016/S0140-6736(16)31698-1
[21] Zhao J, Yu Z, Sun X, Wu S, Zhang J, Zhang D, et al. (2022). Association Between Screen Time Trajectory and Early Childhood Development in Children in China. JAMA Pediatr, 176(8), 768-775. https://doi.org/10.1001/jamapediatrics.2022.1630
[22] Filgueiras A, Pires P, Maisonette S, & Landeira-Fernandez J. (2013). Psychometric properties of the Brazilian-adapted version of the Ages and Stages Questionnaire in public child daycare centers. Early Hum Dev, 89(8), 561-576. https://doi.org/10.1016/j.earlhumdev.2013.02.005
[23] Govaerts PJ, De Beukelaer C, Daemers K, De Ceulaer G, Yperman M, Somers T, et al. (2002). Outcome of cochlear implantation at different ages from 0 to 6 years. Otol Neurotol, 23, 885-890. https://doi.org/10.1097/00129492-200211000-00013
[24] Archbold S, Lutman ME, & Marshall DH. (1995). Categories of auditory performance. Ann Otol Rhinol Laryngol Suppl, 166, 312–314.
[25] Doyle J. (1987). Reliability of audiologists' ratings of the intelligibility of hearing-impaired children's speech. Ear Hear, 8(3), 170-174. https://doi.org/10.1097/00003446-198706000-00007
[26] Squires J, Twombly E, Bricker D, & Potter L. (2009). Ages & Stages Questionnaires, (ASQ-3): User's Guide. Paul H. Brookes Publishing Co.
[27] Bian X, Yao G, Squires J, Hoselton R, Chen CI, Murphy K, et al. (2012). Translation and use of parent-completed developmental screening test in Shanghai. J Early Child Res, 10(2), 162-175.
[28] Heo KH, Squires J, & Yovanoff P. (2008). Cross-cultural adaptation of a pre-school screening instrument: comparison of Korean and US populations. J Intellect Disabil Res, 52(Pt 3), 195-206. https://doi.org/10.1111/j.1365-2788.2007.01000.x
[29] Saihong P. (2010). Use of screening instrument in Northeast Thai early childcare settings. Procedia Soc Behav Sci, 7, 97-105. https://doi.org/10.1016/j.sbspro.2010.10.015
[30] Tong L, Strong MK, Kaur T, Juiz JM, Oesterle EC, Hume CR, et al. (2015). Selective deletion of cochlear hair cells causes rapid age-dependent changes in the spiral ganglion and cochlear nucleus neurons. J Neurosci, 35, 7878–7891. https://doi.org/10.1523/JNEUROSCI.2179-14.2015
[31] Allen C, Nikolopoulos TP, Dyar D, & O'Donoghue GM. (2001). Reliability of a rating scale for measuring speech intelligibility after pediatric cochlear implantation. Otol Neurotol, 22, 631–633. https://doi.org/10.1097/00129492-200109000-00012
[32] Holt RF, & Kirk KI. (2005). Speech and language development in cognitively delayed children with cochlear implants. Ear Hear, 26, 132–148. https://doi.org/10.1097/00003446-200504000-00003
[33] Wie OB. (2010). Language development in children after receiving bilateral cochlear implants between 5 and 18 months. Int J Pediatr Otorhinolaryngol, 74, 1258–1266. https://doi.org/10.1016/j.ijporl.2010.07.026
[34] Beijing Mental Development Cooperative Group. (1985). Gesell Developmental Diagnosis Scale. Beijing Mental Development Cooperative Group.
[35] Bayley N. (2006). Bayley Scales of Infant and Toddler Development Administration Manual. Pearson.
[36] Frankenburg WK, & Dodds JB. (1967). The Denver developmental screening test. J Pediatr, 71(2), 181–191. https://doi.org/10.1016/s0022-3476(67)80070-2
[37] Kral A, Dorman MF, & Wilson BS. (2019). Neuronal development of hearing and language: Cochlear implants and critical periods. Annu Rev Neurosci, 42, 47–65. https://doi.org/10.1146/annurev-neuro-080317-061513
[38] Zanetti D, & Meli A. (2024). Congenital deafness and vestibular disorders: a systematic literature review. Acta Otorhinolaryngol Ital, 44(Supp. 1), S1-S12. https://doi.org/10.14639/0392-100X-suppl.1-44-2024-01
[39] Fallon JB, Irvine DR, & Shepherd RK. (2008). Cochlear implants and brain plasticity. Hear Res, 238, 110–117. https://doi.org/10.1016/j.heares.2007.08.004
[40] Wei QW, Zhang JX, Scherpbier RW, Zhao CX, Luo SS, Wang XL, et al. (2015). High prevalence of developmental delay among children under three years of age in poverty-stricken areas of China. Public Health, 129(12), 1610-1617. https://doi.org/10.1016/j.puhe.2015.07.036
[41] Falzone C, Guerzoni L, Ghiselli S, Franchomme L, Nicastri M, Mancini P, et al. (2025). Early Cochlear Implant Promotes Global Development in Children with Severe-to-Pro-

found Hearing Loss. Audiol Res, 15(5), 121. https://doi.org/10.3390/audiolres15050121
[42] Bruijnzeel H, Ziylan F, Stegeman I, Topsakal V, & Grolman W. (2016). A systematic review to define the speech and language benefit of early (<12 months) pediatric cochlear implantation. Audiol Neurootol, 21(2), 113–126. https://doi.org/10.1159/000443363
[43] Mitchell RM, Christianson E, Ramirez R, Onchiri FM, Horn DL, Pontis L, et al. (2020). Auditory comprehension outcomes in children who receive a cochlear implant before 12 months of age. Laryngoscope, 130(3), 776–781. https://doi.org/10.1002/lary.28061
[44] Colletti L, Mandala M, Zoccante L, Shannon RV, & Colletti V. (2011). Infants versus older children fitted with cochlear implants: performance over 10 years. Int J Pediatr Otorhinolaryngol, 75, 504–509. https://doi.org/10.1016/j.ijporl.2011.01.005
[45] Elbro C, Dalby M, & Maarbjerg S. (2011). Language-learning impairments: a 30-year follow-up of language-impaired children with and without psychiatric, neurological and cognitive difficulties. Int J Lang Commun Disord, 46, 437–448. https://doi.org/10.1111/j.1460-6984.2011.00004.x
[46] Dettman SJ, Dowell RC, Choo D, Arnott W, Abrahams Y, Davis A, et al. (2016). Long-term communication outcomes for children receiving cochlear implants younger than 12 months: a multicenter study. Otol Neurotol, 37(2), e82-95. https://doi.org/10.1097/MAO.0000000000000915
[47] Wu SS, Sbeih F, Anne S, Cohen MS, Schwartz S, Liu YC, et al. (2023). Auditory Outcomes in Children Who Undergo Cochlear Implantation Before 12 Months of Age: A Systematic Review. Otolaryngol Head Neck Surg, 169, 210–220. https://doi.org/10.1002/ohn.284
[48] Laksono AD, Wulandari RD, Amaliah N, & Wisnuwardani RW. (2022). Stunting among children under two years in Indonesia: Does maternal education matter? PLoS One, 17(7), e0271509. https://doi.org/10.1371/journal.pone.0271509
[49] Murri A, Cuda D, Guerzoni L, & Fabrizi E. (2015). Narrative abilities in early implanted children. Laryngoscope, 125(7), 1685-1690. https://doi.org/10.1002/lary.25084
[50] Nagel M, & Sharman R. (2019). The Encyclopedia of Child and Adolescent Development. Wiley.
[51] Horn DL, Pisoni DB, & Miyamoto RT. (2006). Divergence of fine and gross motor skills in prelingually deaf children: implications for cochlear implantation. Laryngoscope, 116, 1500–1506. https://doi.org/10.1097/01.mlg.0000230404.84242.4c
[52] Gheysen F, Loots G, & Van Waelvelde H. (2008). Motor development of deaf children with and without cochlear implants. J Deaf Stud Deaf Educ, 13(2), 215–224. https://doi.org/10.1093/deafed/enm053
[53] Edwards LC, Frost R, & Witham F. (2006). Developmental delay and outcomes in pediatric cochlear implantation: implications for candidacy. Int J Pediatr Otorhinolaryngol, 70(9), 1593–1600. https://doi.org/10.1016/j.ijporl.2006.04.008
[54] Xiong Y, Hu X, Cao J, Shang L, Yao Y, & Niu B. (2024). Development of gross motor skills in children under the age of 3 years: a decision tree approach. Front Public Health, 12, 1421173. https://doi.org/10.3389/fpubh.2024.1421173
[55] Iverson JM, & Goldin-Meadow S. (2005). Gesture paves the way for language development. Psychol Sci, 16, 367–371. https://doi.org/10.1111/j.0956-7976.2005.01542.x
[56] Freeman V, & Pisoni DB. (2017). Speech rate, rate-matching, and intelligibility in early-implanted cochlear implant users. J Acoust Soc Am, 142(2), 1043. https://doi.org/10.1121/1.4998590
[57] Monshizadeh L, Vameghi R, Rahimi M, Sajedi F, Hashemi SB, & Yadegari F. (2021). Is there any association between language acquisition and cognitive development in cochlear-implanted children? J Int Adv Otol, 17(3), 195-199. https://doi.org/10.5152/iao.2021.8990

Metastatic Renal Clear Cell Carcinoma First Presenting As a Head-and-Neck Mass: two case reports

Authors

Xinyao Han, Hui Huangfu

Correspondence

13934518228@163.com (H. Huangfu)

Graphical Abstract

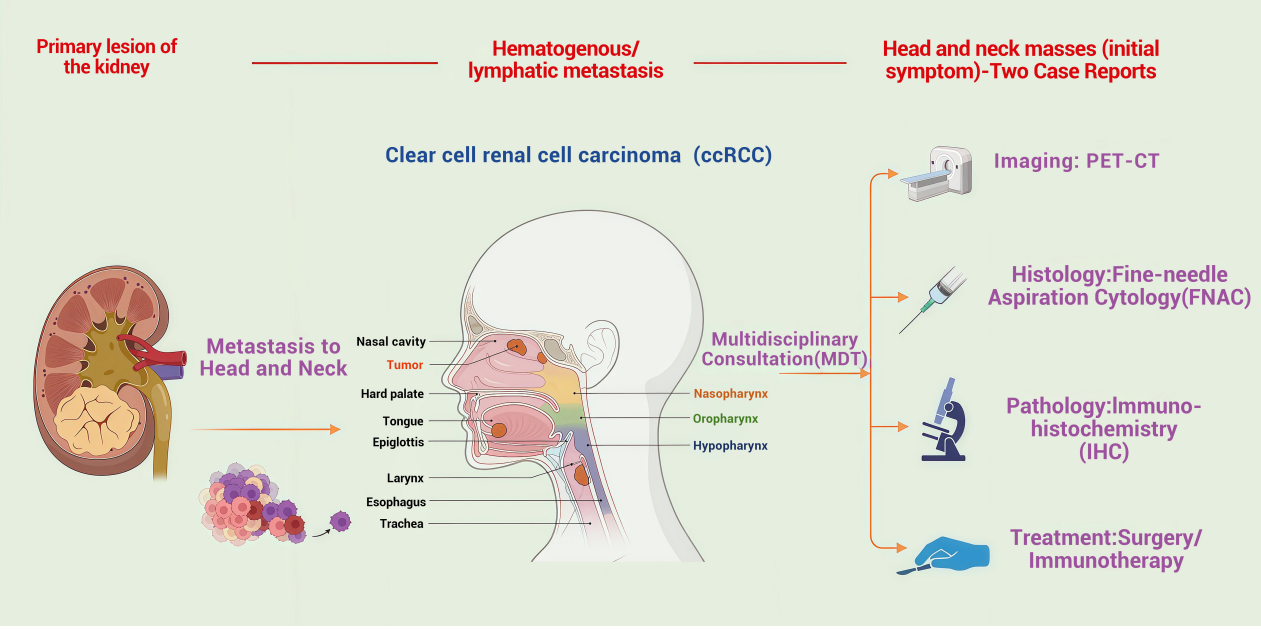

https://doi.org/10.71321/1ckasv14

Metastatic Renal Clear Cell Carcinoma First Presenting As a Head-and-Neck Mass: two case reports

Xinyao Han[1] , Hui Huangfu[2*]

Received: 2026-01-15 | Accepted: 2026-03-09 | Published online: 2026-03-22

Abstract

Background: Clear cell renal cell carcinoma (ccRCC) is a prevalent malignant tumor within the urinary system, characterized by a high metastatic potential. However, instances of ccRCC metastasizing to the head and neck are exceedingly rare.

Case presentation: This article presents two patients who were admitted to the Department of Otorhinolaryngology Head and Neck Surgery. Case 1: A 61-year-old East Asian male patient presented with a painless, progressive enlargement of the left neck. Imaging revealed a 3.6 × 2.3 cm enhancing solid lesion with cystic components in the deep lobe. After surgical resection, histopathology with immunohistochemistry ($CD10^{+}$, $vimentin^{+}$) suggested metastatic clear cell carcinoma of renal origin. Subsequent Positron Emission Tomography-Computed Tomography (PET CT) confirmed a left renal mass (11.4 × 10.1 cm, SUVmax 5.86) with ipsilateral lung nodules, establishing the diagnosis of ccRCC with parotid and pulmonary metastases. Case 2: Another 69-year-old East Asian male patient presented to the hospital with a complaint of foreign body sensation in the pharynx. This individual had previously undergone laparoscopic left nephrectomy for left renal cell carcinoma 14 years prior. Subsequent electronic laryngoscopy identified a new growth on the right side of the pharyngeal wall, leading to laryngoscopic resection of the lesion. Postoperative pathology indicated metastatic clear cell carcinoma originating from the renal site.

Conclusion: Both cases involved metastatic lesions of ccRCC in the head and neck region, underscoring the critical importance of promptly conducting PET-CT scans and relevant pathological assessments when encountering head and neck masses with unidentified primary origins to ascertain whether they represent metastatic clear cell renal cell carcinoma(mCCRCC). The vague initial clinical manifestations of mCCRCC pose significant obstacles to its early clinical detection, necessitating multidisciplinary consultations, prolonged patient monitoring, and the administration of postoperative radiotherapy, chemotherapy, immunotherapy, and other interventions to enhance patient survival rates.

Keywords: clear cell renal cell carcinoma; head and neck metastasis; parotid; oropharyngeal mass

Introduction

Renal cell carcinoma (RCC) is one of the most lethal malignancies in the urinary system and exhibiting a propensity for head and neck metastasis following breast and lung cancers [1]. Clear cell renal cell carcinoma (ccRCC), chromophobe renal cell carcinoma (chRCC), and papillary renal cell carcinoma (pRCC) are distinct subtypes of RCC. Among these subtypes, ccRCC is the predominant histological subtype, accounting for approximately 75% of all RCC diagnoses, known for its aggressive nature, high metastatic potential, and elevated recurrence rates [2]. Studies indicate that 30% of patients have metastases at diagnosis [3], and another 25–40% will develop metachronous metastases after nephrectomy [4].The most frequent sites of metastasis in RCC include the lungs (76%), bones (42%), and liver (41%). In contrast, metastasis to the head and neck is exceedingly rare, affecting regions such as cervical lymph nodes (48%), paranasal sinuses (34%), thyroid (14%), skull (10%), parotid glands (5%), tongue (5%), and facial skin (5%) [5]. In a large series of 671 RCC patients, only one case of parotid metastasis was documented [6]. This article presents two cases of ccRCC metastasizing to the head and neck, while also examining their clinical features and treatment strategies. Herein we describe two unusual presentations of ccRCC initially manifesting as head and neck masses: one in the deep lobe of the parotid gland and one in the lateral oropharyngeal wall 14 years after nephrectomy. These cases highlight the diagnostic challenges and underscore the importance of a thorough metastatic work up and long term surveillance.

1 First Clinical Medical College, Shanxi Medical University, Taiyuan, Shanxi ,China

2 Department of Otorhinolaryngology-Head and Neck Surgery, First Hospital of Shanxi Medical University, Taiyuan, Shanxi, China

* Corresponding Author.

Case presentation

Case 1: A 61-year-old East Asian male patient was admitted to the hospital following the discovery of a painless mass in the left parotid gland three weeks prior. He reported no discomfort, including pain, fever, weight loss, or facial paralysis. The patient has a 20-year history of hypertension, which is well-managed with regular treatment and effective blood pressure control. There is no family history of hereditary diseases. A specialized examination revealed a hard, painless mass approximately 4 cm in diameter in the left parotid gland region, characterized by well-defined boundaries and normal mobility. The bilateral neck appeared asymmetrical, with no palpable enlarged lymph nodes. There were no signs of inflammation or local infection on the skin, facial nerve function was intact, and the examination of the remaining cranial nerves showed no significant abnormalities.

To clarify the diagnosis, comprehensive laboratory and imaging examinations were conducted. Initial laboratory tests showed no significant abnormalities, including complete blood count, renal function tests, liver function tests, electrolyte levels, coagulation, and infectious disease screening. Ultrasound of the salivary glands and cervical lymph nodes detected a cystic and solid mass in the upper region of the left parotid gland measuring 3.2 × 2.8cm, with a clear boundary and regular shape. The solid component exhibited rich vascular distribution, indicating a potential mixed tumor (Figure 1). Plain scan and enhanced computed tomography (CT) of the soft tissue in the neck revealed a clearly demarcated lesion in the left parotid gland region, measuring approximately 3.6 × 2.3 cm, exhibiting significantly uneven enhancement. Within this lesion, multiple non-enhanced cystic cavities were identified, and a "marginal vascular sign" was noted surrounding the lesion. The enhancement degree diminished during the venous phase, demonstrating a "fast-in and fast-out" enhancement pattern. The soft tissue structures of both sides of the neck appeared symmetrical, with no evident abnormalities in size, shape, or density. Additionally, no conspicuous enlarged lymph node shadows were detected in either side of the neck, raising the possibility of adenolymphoma (Figure 2). Fine needle aspiration cytology (FNAC) was considered but not performed because the lesion was deeply situated and highly vascular (Grade 3 flow), raising concerns for both hemorrhage risk and sampling inadequacy. Furthermore, while the encapsulated appearance reduced the likelihood of tumor seeding, the potential for dissemination if malignant could not be completely ruled out. Therefore, after discussion with the patient who preferred definitive surgical management, direct excision with intraoperative frozen section was undertaken.

Differential diagnosis before surgery: Warthin tumour, pleomorphic adenoma, salivary duct carcinoma, and metastasis (especially in view of the hypervascular features). Because of the absence of known primary cancer, metastatic disease was considered less likely but not excluded. The patient underwent the necessary preoperative examinations and subsequently had surgery under general intravenous combined anesthesia on December 18, 2024. During the procedure, the tumor was identified in the deep lobe of the left parotid gland. It was solid, encapsulated, and measured approximately 4.0 × 4.0 × 3.0cm, with indistinct margins from the surrounding tissues, a brittle texture, and a tendency to bleed. The left common trunk of the facial nerve was dissected under facial nerve monitoring. After ensuring the protection of each branch of the facial nerve, the deep lobe mass of the parotid gland was excised. Intraoperative frozen section analysis suggested a low-grade malignant salivary gland tumor, prompting the resection of the surrounding glandular tissue.

Figure 1. Ultrasound: Left parotid 3.2×2.8 cm cystic-solid mass with thick walls, internal septations, and rich vascularity (Color Doppler Grade 3). Scale bar = 1 cm. Arrow indicates mass.

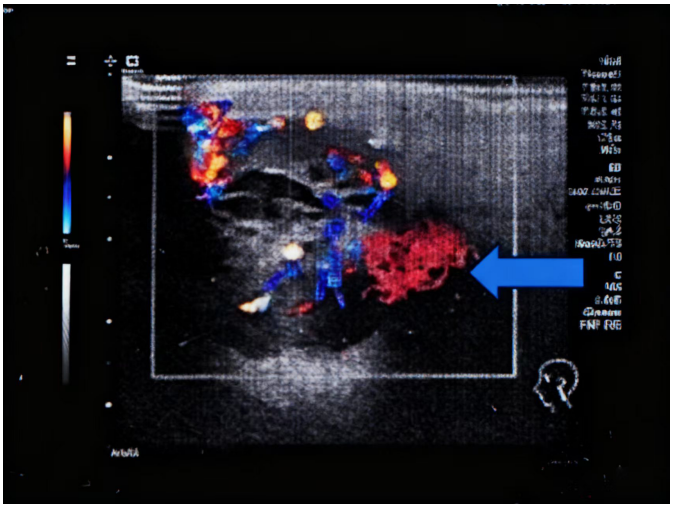

Figure 2. CT neck with contrast: Axial arterial phase showing 3.6×2.3 cm heterogeneously enhancing left deep parotid mass with "fast-in fast-out" pattern and peripheral vascular rim (arrow).

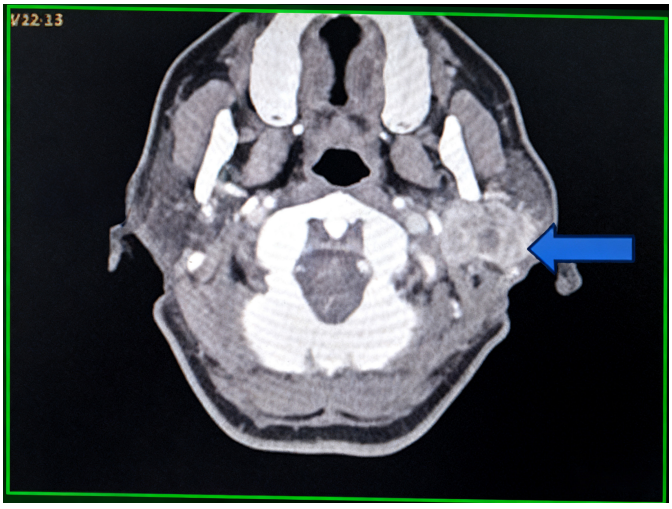

Postoperative histopathological examination, complemented by immunohistochemical (IHC) phenotyping, revealed tumor cells organized into nest-like clusters characterized by moderate cell size, clear cytoplasm, and marked hemorrhage. IHC analysis demonstrated strong positivity for PAX8, CD10, vimentin, and carbonic anhydrase IX (CAIX), while the tumor cells were negative for CK7, p63, p40, S100, SOX10, and GATA. The Ki-67 proliferation index was 10% (Figure 3 and Figure 4). A consultation with the urology department recommended a comprehensive PET-CT examination. Postoperative PET-CT revealed a left renal mass measuring 11.4 × 10.1 cm with

heterogeneous enhancement and increased FDG uptake (SUVmax 5.86), demonstrating perinephric fat invasion consistent with T3a disease. Metastatic involvement was identified in the left parotid surgical bed (SUVmax 7.39) and bilaterally in the lungs, with the largest nodule located in the posterior basal segment of the left lower lobe measuring approximately 1.2 cm (SUVmax 2.18). No bone metastases were detected, and brain imaging was not performed as the patient remained asymptomatic. Integrating the imaging findings, histopathological analysis, and the patient's medical history, a differential diagnosis was made for various benign and malignant parotid gland masses. Ultimately, the patient was diagnosed with mCCRCC to the parotid gland. Following the diagnosis, the patient was referred to urology and medical oncology for multidisciplinary management. After multidisciplinary team (MDT) discussion, a decision was made to initiate first-line systemic therapy with pembrolizumab plus axitinib, with consideration of cytoreductive nephrectomy after three cycles if a favorable response was achieved. Systemic therapy commenced with pembrolizumab 200 mg intravenously every three weeks and axitinib 5 mg orally twice daily; the axitinib dose was subsequently reduced to 3 mg twice daily after two weeks due to the development of grade 2 hypertension. The first restaging CT scan, performed approximately 8 weeks after treatment initiation and evaluated per RECIST 1.1 criteria, demonstrated a partial response (PR) in the primary renal mass, which measured 8.3 × 7.4 cm, representing a 27% reduction from baseline. The bilateral pulmonary nodules remained stable as non-target lesions, and the parotid surgical bed showed no evidence of local recurrence. The patient's renal function remained stable, with an eGFR of 45 mL/min/1.73 m². The patient is currently alive with disease 10 months after initial presentation, experiencing continuous symptomatic relief, and remains on ongoing systemic therapy with regular imaging surveillance. TNM staging (AJCC 8th edition): cT3aN0M1 (lung, parotid).

Case 2: A 69-year-old East Asian man was hospitalized for a one-week history of a foreign body sensation in the throat. He denied experiencing dry, itchy, or sore throat, or shortness of breath. An electronic laryngoscopy examination identified a new organism on the right pharyngeal lateral wall, measuring approximately 1.0 × 1.0 × 1.0cm, displaying a smooth surface with a small amount of attached pseudomembrane (Figure 5). Palpation during a specialized physical examination did not detect any lymph nodes in the neck. Initial laboratory tests revealed a significant decrease in glomerular filtration rate (47.9 ml/min/1.73 m²) with no other notable abnormalities. The patient has a history of poorly controlled hypertension spanning over two decades. Fourteen years ago, he underwent laparoscopic left nephrectomy due to ccRCC with hemorrhagic cystic changes in the left kidney (pathology: pT1b, Fuhrman grade 2, margins negative). Subsequent annual physical examinations showed no abnormalities in urine routine or renal function.

Following the completion of the necessary preoperative examinations, the patient underwent resection of a pharyngeal lesion with the assistance of a laryngoscope on May 8, 2025. During the procedure, a red solid neoplasm located on the surface of the right pharyngeal palatine arch was excised. Intraoperative cryotherapy indicated that the morphology of this mass was consistent with metastatic clear cell carcinoma of renal origin (Figure 6). The surrounding adherent tissue was also excised to ensure complete resection. Postoperative pathology confirmed the diagnosis of mCCRCC. The patient had a pathologically confirmed history of left ccRCC treated with nephrectomy 14 years earlier, and intraoperative frozen

Figure 3. H&E stain, low power (×40): Nested architecture of clear cells with delicate vascular network and focal hemorrhage. Scale bar = 500 μm.

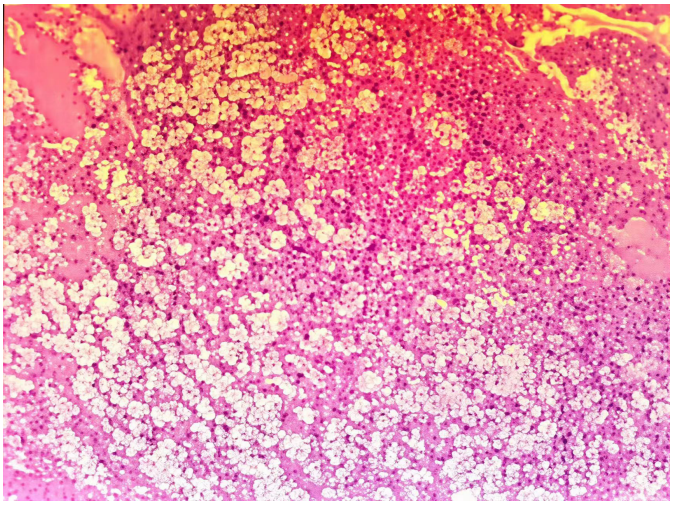

Figure 4. H&E stain, high power (×400): Clear cytoplasm with distinct cell borders, round nuclei, prominent nucleoli. Red blood cells in interstitium. Scale bar = 50 μm.

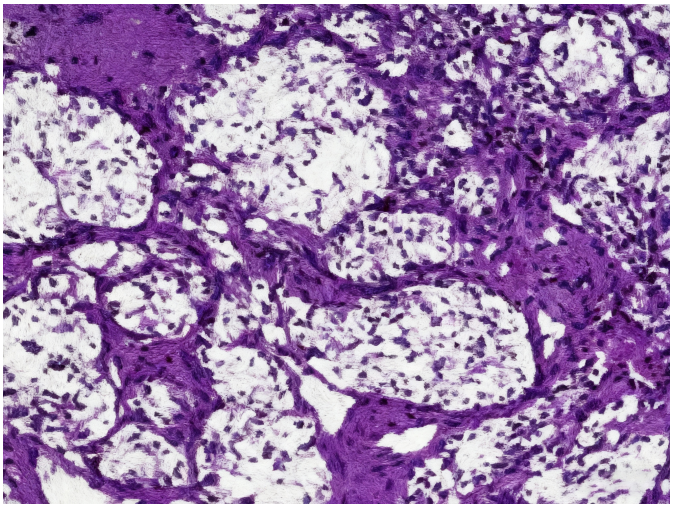

Figure 5. Laryngoscopic view: Smooth, reddish, submucosal mass on right lateral oropharyngeal wall, measuring 1.0×1.0 cm, with small pseudomembrane.

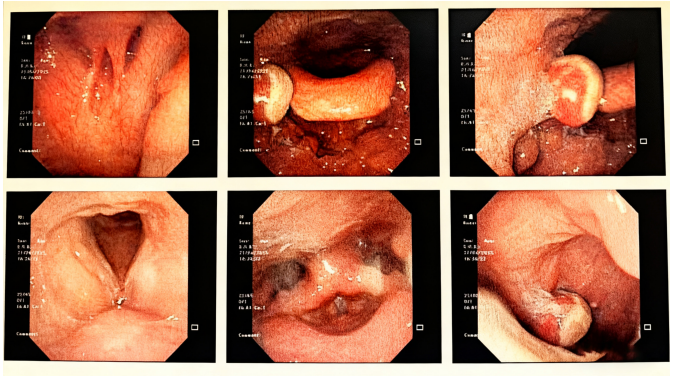

section of the oropharyngeal lesion revealed classic clear cell morphology, which was subsequently confirmed on routine histopathology. Given the definitive history of ccRCC and the characteristic pathological features, the diagnosis was considered sufficiently established at that time. Furthermore, due to the patient's advanced age (69 years) and pre-existing chronic kidney disease stage 3 (eGFR 47.9 mL/min/1.73 m²), the clinical team had concerns about the potential nephrotoxicity of iodinated contrast agents required for PET-CT or contrast-enhanced CT. After thorough discussion with the patient and his family, a decision was made to proceed with close surveillance following complete local excision rather than immediate extensive staging investigations. Additional immunohistochemical markers—such as PAX8, CK7, p63, p40, S100, and SOX10—were not pursued at that time due to resource considerations and the perceived diagnostic certainty based on the strong clinical and pathological correlation.

Following MDT consultation, the patient was staged as pTx-N0M1 (solitary oropharyngeal metastasis) according to the AJCC 8th edition, with the current recurrence classified as distant metastasis (M1) given the 14-year interval since the original nephrectomy. After discussion at a MDT board, the medical oncology team recommended adjuvant systemic therapy with nivolumab plus cabozantinib as the preferred option for intermediate-risk recurrence, versus observation, acknowledging that the prolonged latency might suggest an aggressive clone with high metastatic potential. The patient elected active treatment and initiated therapy with nivolumab 240 mg intravenously every two weeks plus cabozantinib 40 mg orally daily; the cabozantinib dose was reduced to 20 mg daily due to baseline chronic kidney disease. The first restaging evaluation, performed approximately 8 weeks after treatment initiation and assessed per RECIST 1.1 criteria, demonstrated no measurable disease (status post-surgical resection) and no new lesions. Treatment was continued as an adjuvant approach. As of the most recent follow-up, the patient remains stable with no evidence of disease progression and continues on regular imaging surveillance. Additionally, we have created detailed clinical timelines for both cases (Table 1 and Table 2), which include all key events from initial presentation through diagnosis, treatment, and follow-up. The timelines are presented in a clear chronological format with approximate dates and corresponding clinical events.

Discussion

We report two exceptional cases of ccRCC presenting initially as head and neck masses: one in the parotid deep lobe and one isolated oropharyngeal metastasis 14 years after nephrectomy. Both presentations are extraordinarily rare; only a handful of similar cases have been reported. A summary of the most relevant published cases is presented in Table 3.

mCCRCC presenting with head and neck space-occupying lesions as the initial manifestation is exceptionally uncommon in clinical practice, representing only 13% of distant metastasies of RCC [6]. Most head and neck metastatic tumors stem from primary lesions in the upper digestive or respiratory tracts, with metastases from distant primary sites, such as renal tumors, being infrequent. Due to the kidney receives 25% of the circulating blood volume, RCC, a hypervascular tumor

Figure 6. H&E stain (×200): mCCRCC with clear cell morphology, rich vasculature, and hemorrhage. Scale bar = 100 μm.

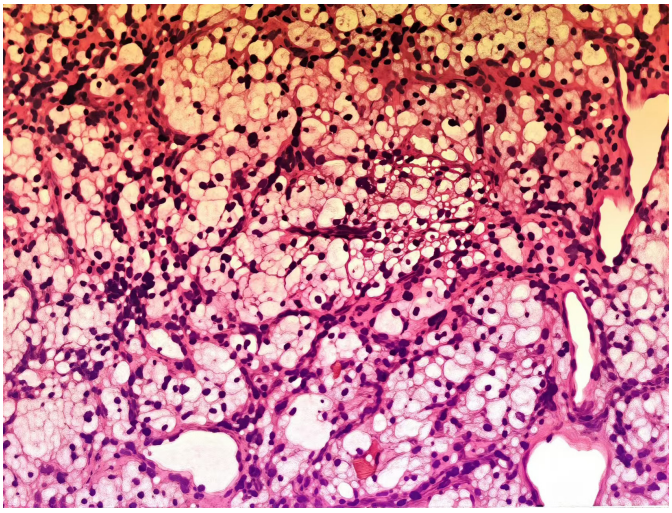

with numerous arteriovenous shunts, can disseminate to the head and neck via the paravertebral venous plexus (Batson's plexus) [7]. This mechanism underscores its significance as a rare cause of head and neck metastases unrelated to the upper digestive or respiratory tracts. Despite its relatively low overall incidence, priority should be given to considering it in the differential diagnosis of head and neck space-occupying lesions. In the absence of any other identified primary tumors, the clinical differential diagnosis for a patient presenting with a mass in the head and neck encompasses both benign lesions and malignant tumors, the latter including primary tumors and metastases. Benign tumors in this region typically exhibit slow growth and are often discovered incidentally. Their duration can range from several years to several decades [8]. In some patients, head and neck metastases may arise following radical nephrectomy for RCC, with time intervals varying from several months to several years. mCCRCC is associated with a poor prognosis, characterized by a 5-year survival rate of less than 10% and an average life expectancy of 5.8 months [1]. Research indicates that complete surgical resection of isolated metastases can significantly enhance the long-term survival rates of affected patients. O'Dea et al. investigated patients who underwent radical nephrectomy for RCC and had isolated metastatic sites completely excised. Their findings indicated that patients with metastases identified within a specific timeframe following nephrectomy exhibited a more favorable prognosis compared to those whose primary tumors and metastatic sites were diagnosed and treated concurrently. The 5-year survival rate for the former group was 50% [9]. Although RCC is characterized as a radioresistant tumor, it demonstrates a notable response to chemotherapy and radiotherapy. Moreover, the implementation of targeted therapy and immunotherapy can substantially enhance survival outcomes for patients [5]. The first case is notable for the deep lobe location and the synchronous lung metastases, underscoring the need for complete staging even when a head and neck mass appears isolated. The hypervascular imaging features (fast wash in/wash out on CT) mimicked a primary salivary gland tumour, but should raise suspicion for metastasis from a highly vascular primary such as RCC. The second case illustrates that ccRCC can recur after more than a decade, and isolated

head and neck metastases may be the first sign. Therefore, lifelong surveillance is mandatory after nephrectomy.

Most patients with mCCRCC initially present with clinical symptoms related to metastatic sites. Risk factors for this condition include older age, male gender, hypertension, smoking, and obesity. The absence of specific indicators in imaging studies and routine biological examinations complicates the differentiation of mCCRCC from the primary disease at the metastatic site, thereby hindering the development of an accurate treatment plan. Typical symptoms associated with tumors originating in the kidneys include hematuria, low back pain, and abdominal masses. However, in the case discussed in this article, the patient did not exhibit these characteristic symptoms during the initial visit; instead, the primary complaint was a painless mass in the head and neck. Postoperative pathological analysis confirmed the presence of a malignant tumor with renal metastasis. mCCRCC typically has a relatively insidious onset, and its clinical symptoms are often subtle. It is frequently diagnosed when patients undergo evaluation for various non-specific symptoms or other medical conditions. Determining whether a head and neck mass is primary or metastatic cancer can be challenging. Yu reported that the accuracy rate of ultrasound diagnosis for parotid gland tumors is only 78.6% [10]. The ultrasound characteristics of Case 1 in this article resemble those of benign tumors, suggesting a potential risk of misdiagnosis. To minimize the likelihood of misdiagnosis, a thorough medical history inquiry, careful consideration of the relationship between systemic and local factors, and a meticulous physical examination, including necessary general assessments, are essential for accurately determining the tu-

Table 1. The detailed clinical timelines for Case 1.

Date	Event	Clinical/Pathological Details
November 20, 2024	Symptom onset	Patient notices painless left preauricular mass
December 5, 2024	Initial presentation	ENT clinic visit; physical exam confirms 4 cm firm, mobile left parotid mass
December 6, 2024	Ultrasound	Left parotid: 3.2×2.8 cm cystic-solid lesion, well-circumscribed, rich vascularity (Grade 3 flow on color Doppler). **No FNA performed** due to high vascularity and differential including Warthin tumor
December 8, 2024	CT neck (contrast-enhanced)	Left deep parotid lobe: 3.6×2.3 cm heterogeneously enhancing mass with "fast-in fast-out" enhancement pattern, central cystic areas, peripheral vascular rim sign. **Differential:** Warthin tumor vs. salivary malignancy vs. metastatic hypervascular lesion
December 10, 2024	Preoperative labs	Normal renal function, no hematuria
December 18, 2024	Surgery	Left deep lobe parotidectomy with facial nerve preservation (monitored with NIM-Response 3.0). Intraoperative findings: 4.0×4.0×3.0 cm encapsulated, friable, highly vascular mass
December 18, 2024	Intraoperative frozen section	"Low-grade malignant salivary gland tumor" → prompted complete deep lobe resection with margin clearance
December 22, 2024	Final pathology	**Metastatic ccRCC:** Nested architecture, clear cytoplasm, delicate vasculature. Immunohistochemistry: PAX8(+), CAIX(+), CD10(+), Vimentin(+), CK7(-), p63(-), SOX10(-), Ki-67 10%
December 24, 2024	PET-CT staging	**Primary:** Left kidney lower pole cystic-solid mass 11.4×10.1 cm, SUVmax 5.86, perinephric fat invasion (T3a). **Metastases:** Left parotid (post-surgical bed, SUVmax 7.39), bilateral pulmonary nodules (The larger one is located in the posterior basal segment of the lower lobe of the left lung, approximately 1.2 cm, SUVmax 2.18), no bone or brain metastases
December 28, 2024	MDT consultation	Urology, oncology, radiation oncology. Decision: Systemic therapy first-line (pembrolizumab/axitinib), consider cytoreductive nephrectomy after 3 cycles if response
January 5, 2025	Treatment initiation	Pembrolizumab 200mg IV q3weeks + Axitinib 5mg PO BID (dose reduced to 3mg BID after 2 weeks due to grade 2 hypertension)
February 20, 2025	First restaging CT (8 weeks)	**RECIST 1.1:** Primary renal mass 8.3×7.4 cm (27% reduction, PR), pulmonary nodules stable (non-target). Parotid surgical bed clear. eGFR stable at 45 mL/min/1.73m²
April 2025	Ongoing	Continuous relief; alive

Note: Detailed clinical timeline for Case 1, illustrating the diagnostic trajectory from presentation with a left parotid mass through staging, surgical resection, and systemic therapy initiation. Key findings include characteristic hypervascular imaging features, definitive pathology confirming metastatic ccRCC with supportive immunohistochemistry (PAX8+, CAIX+), and favorable early response to pembrolizumab/axitinib combination therapy.

mor's nature.

The most prevalent histological type of RCC is ccRCC, which typically presents as nest-like transparent cells abundant in glycogen when examined under light microscopy. Its characteristic histological feature includes a rich network of interstitial blood vessels, with red blood cells often visible within the vascular lumen or between the nests of clear cells [11]. In histochemical analyses, RCC typically exhibits positive staining for glycogen and lipids. Immunohistochemical findings reveal a high expression rate of CD10 and Vimentin, which supports the diagnosis of RCC. Vimentin is predominantly expressed in mesenchymal tissue cells and tumor cells derived from mesenchymal tissue, while it is absent in normal epithelial cells. Historically, Vimentin served as a marker to differentiate mesenchymal tissue components from those of other origins. Recent literature has demonstrated that Vimentin is aberrantly expressed in the epithelial tumor cells of poorly differentiated carcinomas, indicating that this abnormal expression is closely associated with the invasive and metastatic potential of tumor cells [12-13]. CD10 exhibits strong positive expression primarily in normal renal balloon epithelial cells and proximal convoluted tubular epithelial cells, predominantly localized in the cell membrane with potential positivity in the cytoplasm below. Its positive presence in mCCRCC correlates with advanced

Table 2. The detailed clinical timelines for Case 2.

Date	Event	Clinical/Pathological Details
May 2011	Initial diagnosis	Left nephrectomy for pT2aN0M0 ccRCC, Fuhrman grade 2, clear cell type
2011-2024	Surveillance	Annual abdominal CT and chest X-ray, no recurrence detected
April 1, 2025	Symptom onset	Foreign body sensation right oropharynx
May 6, 2025	ENT evaluation	Laryngoscopy: 1.0×1.0 cm smooth reddish mass, right lateral pharyngeal wall
May 8, 2025	Surgery	Laryngoscopic transoral resection of right oropharyngeal mass with 5mm margins. Intraoperative findings: Highly vascular, friable red mass
May 8, 2025	Intraoperative frozen	Consistent with metastatic ccRCC (clear cells, rich vasculature)
May 12, 2025	Final pathology	ccRCC metastasis, negative margins (R0), lymphovascular invasion present
May 15, 2025	MDT consultation	Medical oncology recommendation: Adjuvant systemic therapy with nivolumab/cabozantinib (preferred for intermediate-risk recurrence) vs. observation (high-risk for further metastasis given 14-year latency suggesting aggressive clone)
May 20, 2025	Treatment decision	Patient elected active treatment. Initiated Nivolumab 240mg IV q2weeks + Cabozantinib 40mg PO daily (dose reduced to 20mg due to baseline CKD)
July 2025	First restaging (8 weeks)	**RECIST 1.1:** No measurable disease (post-surgical), no new lesions. Treatment continued as adjuvant approach
September 2025	Ongoing	Stable, no progression

Note: Detailed clinical timeline for Case 2, illustrating an ultra-late recurrence (14 years post-nephrectomy) of ccRCC manifesting as isolated oropharyngeal metastasis. The timeline encompasses the 14-year disease-free interval, diagnostic workup, complete surgical resection, and initiation of adjuvant immunotherapy-based systemic treatment, highlighting the importance of prolonged surveillance in ccRCC survivors.

Table 3. A summary of the most relevant published cases.

Reference	Age/Sex	Site	Time from nephrectomy	Other metastases	Outcome (follow up)
Owens et al. 1989 [9]	55/M	Parotid	0 (synchronous)	Lung, brain, bone	Alive at 2 years
Owens et al. 1989 [9]	75/F	Parotid	8 years	None	recurrence (6 months after parotid resection)
Spreafico et al. 2008 [7]	67/M	Parotid	1 years	neck lymph nodes	Alive, radiotherapy
Ahmed et al. 2023 [5]	66/M	Larynx	0 (synchronous)	None	Alive, NED at 4 months
Present Case 1	61/M	Parotid (deep lobe)	0 (synchronous)	Lung	Alive, on IT at 10 months
Present Case 2	69/M	Oropharynx	14 years	None	Alive, NED at 8 months

Note: Comparative summary of published ccRCC head and neck metastasis cases, highlighting the rarity of deep parotid involvement (Case 1) and the unprecedented 14-year latency for oropharyngeal recurrence (Case 2) among reported series.

tumor stage, suggesting involvement in invasion and progression. Notably, poorly differentiated mCCRCC tumors display a significantly lower CD10 expression rate compared to moderately and well-differentiated tumors, indicating a link between CD10 expression and mCCRCC cell differentiation [14]. From a pathological perspective, a definitive diagnosis of mCCRCC requires a panel of IHC markers. PAX8 is the most sensitive and specific marker for renal origin. CD10, and vimentin are supportive but not entirely specific. Exclusion of salivary gland tumours (p63, p40, S100, SOX10) and other clear cell neoplasms (e.g., from thyroid, adrenal, or female genital tract) is essential [14]. Ki 67 provides prognostic information. In our cases, the IHC profile was classic for ccRCC and ruled out mimics.

Our report has limitations. First, we lack long term follow up for both patients, especially regarding treatment response beyond 10 and 8 months. Second, the decision not to perform FNAC in two cases might be debated; however, in many centres, surgical excision is preferred for deep parotid lesions when malignancy is suspected, because FNAC can be non diagnostic or misleading. Despite these limitations, these cases contribute valuable observations: (1) ccRCC can present as a parotid deep lobe mass, which has not been specifically highlighted before; (2) a latency of 14 years before oropharyngeal metastasis is one of the longest reported; (3) hypervascular imaging features should prompt consideration of ccRCC; (4) a comprehensive IHC panel is crucial for accurate diagnosis.

Conclusion

In summary, instances of mCCRCC spreading to the head and neck are exceedingly uncommon, representing only approximately 6% of cases [15]. mCCRCC should be included in the differential diagnosis of hypervascular head and neck masses, even in patients without known renal cancer or with a remote history of nephrectomy. The diagnosis relies significantly on identifying the distinct pathological characteristics of metastatic cancer through meticulous IHC analysis. The presence of CD10 and Vimentin positivity aids in confirming the diagnosis of mCCRCC. When encountering clear cell carcinoma in pathological samples, consideration must be given to the potential metastasis of RCC. Timely PET-CT and a thorough immunohistochemical work up are essential for correct diagnosis and staging. Patients typically do not exhibit evident symptoms like hematuria or lumbar pain. Merely excising the metastatic cancer lesions does not result in complete remission. Prompt initiation of MDT consultations is essential, with a comprehensive treatment approach primarily centered on radical surgical excision. Regular and lifelong monitoring should also be implemented. The primary lesions associated with head and neck metastatic cancer predominantly arise from the upper digestive and respiratory tracts, with a minority originating from distant organs. Specifically, 45% of metastatic cancers are classified as malignant melanoma, while 37% are identified as squamous cell carcinoma. Distant metastatic cancers may also originate from sites such as the breast, kidneys, and prostate [16]. For the majority of these patients, a definitive diagnosis is achievable only through postoperative pathological examination. Consequently, in clinical practice, it is advisable to extend the follow-up period for patients with mCCRCC as much as possible. In cases where patients present with head and neck masses without identifiable tumors in that region, primary tumors located below the clavicle should be considered, prompting the initiation of appropriate staging examinations. For isolated metastatic lesions, surgical intervention may be indicated. Additionally, postoperative immunotherapy or molecular targeted therapies can be employed to extend patient survival and enhance quality of life.

Abbreviations

chromophobe renal cell carcinoma : chRCC; metastatic clear cell renal cell carcinoma : mCCRCC; papillary renal cell carcinoma : pRCC; Renal cell carcinoma: RCC; Clear cell renal cell carcinoma: ccRCC; FNAC: fine needle aspiration cytology; IHC: immunohistochemistry; PET-CT: Positron Emission Tomography-Computed Tomography; CAIX: carbonic anhydrase IX; MDT: multidisciplinary team; RECIST: Response Evaluation Criteria in Solid Tumours; TNM: tumour node metastasis.

Author Contributions

Xinyao Han drafted the manuscript and collected clinical cases. Hui Huangfu performed the operation on the patient and participated in revising this manuscript. All authors read and approved the final manuscript.

Acknowledgements

I am grateful for the assistance provided by my mentor. We acknowledge the patient's contributions to the study.

Funding Information

Not Applicable

Ethics Approval and Consent to Participate

This study was reviewed and approved by the Research Ethics Committee of First Hospital of Shanxi Medical University with the ethical code KYLL-2025-429 on 24 November 2025.

Competing Interests

The authors declare that they have no existing or potential commercial or financial relationships that could create a conflict of interest at the time of conducting this study.

Data availability

Not Applicable

References

[1] KWEON H T, YOO J S, HONG Y T. Tongue Metastasis From Renal Cell Carcinoma: A Rare Case Presentation[J/OL]. Ear, Nose, & Throat Journal, 2024: 1455613231226038. https://doi.org/10.1177/01455613231226038

[2] Linehan, W. M., & Ricketts, C. J. (2019). The Cancer Genome Atlas of renal cell carcinoma: findings and clinical implications. Nature reviews. Urology, 16(9), 539–552. https://doi.org/10.1038/s41585-019-0211-5

[3] Gao, S., Yan, L., Zhang, H., Fan, X., Jiao, X., & Shao, F. (2021). Identification of a Metastasis-Associated Gene Signature of Clear Cell Renal Cell Carcinoma. Frontiers in genetics, 11, 603455. https://doi.org/10.3389/fgene.2020.603455

[4] Lalani, A. A., McGregor, B. A., Albiges, L., Choueiri, T. K., Motzer, R., Powles, T., Wood, C., et al. (2019). Systemic Treatment of Metastatic Clear Cell Renal Cell Carcinoma in 2018: Current Paradigms, Use of Immunotherapy, and Future Directions. European urology, 75(1), 100–110. https://doi.org/10.1016/j.eururo.2018.10.010

[5] Ahmed, S. S., Barik, S. K., Adhya, A. K., Das, D. K., Parida, A. V., Mukherjee, P., Das Majumdar, et al. (2023). Metastatic Renal Cell Carcinoma Masquerading as a Laryngeal Tumor: A Case Report. Cureus, 15(5), e39229. https://doi.org/10.7759/cureus.39229

[6] Lieder, A., Guenzel, T., Lebentrau, S., Schneider, C., & Franzen, A. (2017). Diagnostic relevance of metastatic renal cell carcinoma in the head and neck: An evaluation of 22 cases in 671 patients. International braz j urol : official journal of the Brazilian Society of Urology, 43(2), 202–208. https://doi.org/10.1590/S1677-5538.IBJU.2015.0665

[7] Spreafico, R., Nicoletti, G., Ferrario, F., Scanziani, R., & Grasso, M. (2008). Parotid metastasis from renal cell carcinoma: a case report and review of the literature. Acta otorhinolaryngologica Italica : organo ufficiale della Societa italiana di otorinolaringologia e chirurgia cervico-facciale, 28(5), 266–268.

[8] Wang Jibao, Kong Weijia, Huang Xuanzhao. Practice Of Otorhinolaryngology Head and Neck Surgery [M]. 2nd ed. Beijing: People's Medical Publishing House, 2008: 653

[9] Owens, R. M., Friedman, C. D., & Becker, S. P. (1989). Renal cell carcinoma with metastasis to the parotid gland: case reports and review of the literature. Head & neck, 11(2), 174–178. https://doi.org/10.1002/hed.2880110212

[10] Yu GY (ed): Salivary Gland Diseases. Beijing Medical University Press, Beijing, 1994.

[11] Majewska, H., Skálová, A., Radecka, K., Stodulski, D., Hyrcza, M., Stankiewicz, C., et al. (2016). Renal clear cell carcinoma metastasis to salivary glands - a series of 9 cases: clinico-pathological study. Polish journal of pathology : official journal of the Polish Society of Pathologists, 67(1), 39–45. https://doi.org/10.5114/pjp.2016.59475

[12] Singh, S., Sadacharan, S., Su, S., Belldegrun, A., Persad, S., & Singh, G. (2003). Overexpression of vimentin: role in the invasive phenotype in an androgen-independent model of prostate cancer. Cancer research, 63(9), 2306–2311.

[13] Lang, S. H., Hyde, C., Reid, I. N., Hitchcock, I. S., Hart, C. A., Bryden, A. A., et al. (2002). Enhanced expression of vimentin in motile prostate cell lines and in poorly differentiated and metastatic prostate carcinoma. The Prostate, 52(4), 253–263. https://doi.org/10.1002/pros.10088

[14] Shaoxiong Ming. (2014). Expression and Clinical Significance of CD10 in Renal Cell Carcinoma [Master's thesis, Nankai University]. http://dx.chinadoi.cn/10.7666/d.Y2699723.

[15] F Higuera, L A Boccalatte, M J Labanca, A Jaén del Valle, J J Larrañaga, M F Figari, Renal clear cell carcinoma metastasis to submandibular gland: case report and review of the literature, Journal of Surgical Case Reports, Volume 2018, Issue 10, October 2018, rjy261, https://doi.org/10.1093/jscr/rjy261

[16] Hongchi Xue, Jinhua Yu, Yan Gao, & Minxian Huang. (2000). Renal clear cell carcinoma metastasis to the parotid gland: A case report. Journal of Modern Stomatology. 14(1), 38. http://dx.chinadoi.cn/10.3969/j.issn.1003-7632.2000.01.043.

A Predictive Model for Lateral Cervical Lymph Node Metastasis in Thyroid Cancer

Authors

Shu Wang, Yanqiang Zhang, Ziyue Fu, Chuanlu Shen, Siyu Jia, Shugang Zhao, Kaile Wu

Correspondence

960092599@qq.com (S. Zhao), wukaile@fy.ahmu.edu.cn (K. Wu)

Graphical Abstract

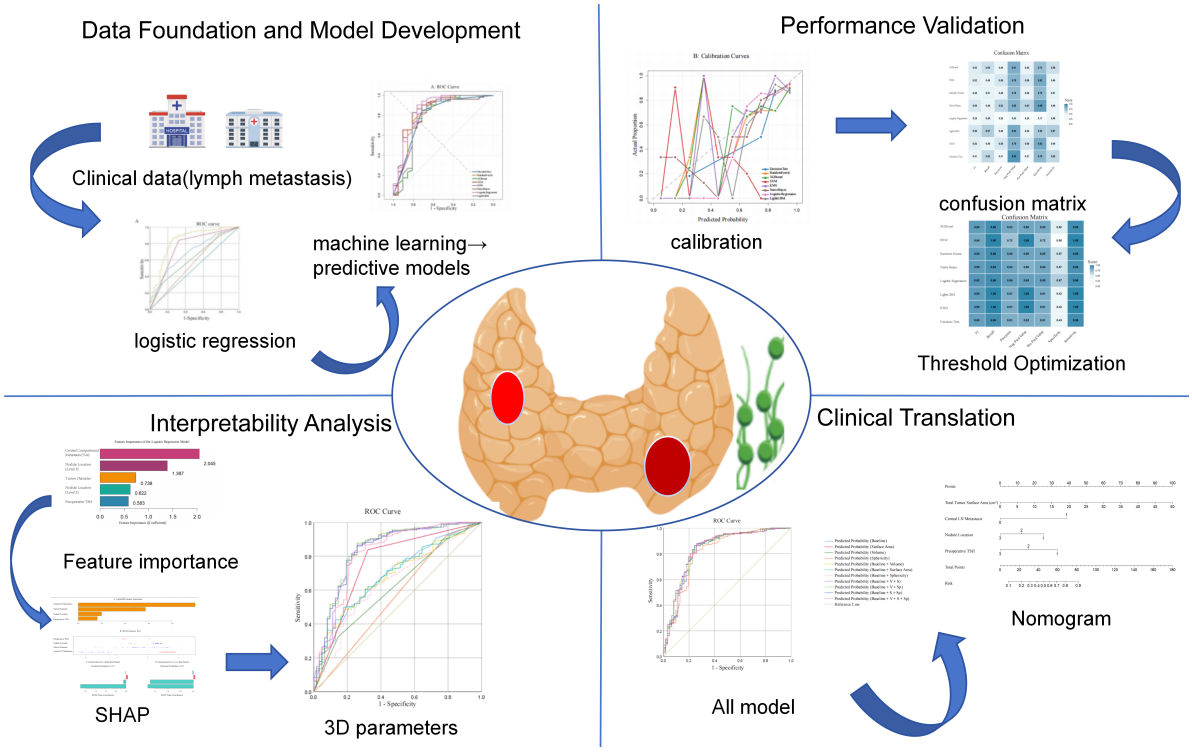

https://doi.org/10.71321/5r3ppj45

Research Article Head and Neck Diseases Conflux

A Predictive Model for Lateral Cervical Lymph Node Metastasis in Thyroid Cancer

Shu Wang [1] , Yanqiang Zhang [1] , Ziyue Fu [1] , Chuanlu Shen [1] , Siyu Jia [2] , Shugang Zhao [2*] , Kaile Wu [1*]

Received: 2026-03-20 | Accepted: 2026-03-26 | Published online: 2026-04-03

Abstract

Objective: To investigate the predictive factors for lateral lymph node metastasis (LLNM) in patients with papillary thyroid carcinoma (PTC) and to develop an individualized prediction model.

Methods: Clinical data from 241 PTC patients who underwent lateral neck dissection were analyzed. Logistic regression and machine learning methods were employed to identify predictive factors and construct a model. The predictive value of three-dimensional morphological parameters (total tumor surface area and total tumor volume) was also evaluated.

Results: Maximum tumor diameter, central lymph node metastasis, preoperative Thyroid-Stimulating Hormone (TSH), and tumor location were identified as independent predictors of LLNM. A baseline combined model based on maximum tumor diameter showed good predictive performance (AUC 0.832). Furthermore, three-dimensional parameters (total surface area and total volume) demonstrated complementary predictive potential compared to the baseline model.

Conclusion: An effective clinical prediction model for assessing LLNM risk was successfully developed. Three-dimensional morphological parameters represent promising predictive indicators with potential complementary value.

Keywords: Papillary thyroid carcinoma; Lateral lymph node metastasis; Machine learning; Clinical prediction model; SHapley Additive exPlanations (SHAP)

Introduction

Thyroid cancer is a common malignant tumor of the endocrine system, with its global incidence continuing to rise [1-4]. Papillary thyroid carcinoma (PTC) is the most common pathological type. Patients with cervical lymph node metastasis have a higher risk of recurrence and distant metastasis, leading to a poorer prognosis [5-10]. Relevant guidelines recommend that PTC patients assessed preoperatively with lymph node metastasis should undergo surgical treatment [11]. Cervical lymph node dissection is a critical step in surgery, and the extent of dissection needs to balance complete tumor removal with postoperative quality of life. For lateral cervical lymph nodes, current guidelines recommend therapeutic dissection only when preoperative imaging suggests metastasis [3, 12]. However, existing imaging modalities have limitations in assessing lymph node metastasis [13-14]. Therefore, accurately predicting lateral cervical lymph node metastasis is of great significance for formulating individualized surgical strategies. Current preoperative assessment primarily relies on ultrasound, CT, etc., but their sensitivity and specificity are limited [2, 15-18]. Preoperative lymph node biopsy is the standard method for evaluating LLNM [3]. However, ultrasound-guided fine-needle aspiration (FNA) has limitations in accuracy and carries the potential for sampling error [3, 19]. Constructing prediction models by combining clinicopathological features has become an important approach to improving preoperative assessment accuracy. This study aims to develop an individualized prediction model for lateral cervical lymph node metastasis using routine clinical indicators and to validate its performance through various statistical methods and machine learning algorithms, thereby providing a tool for clinical decision-making.

1 The First Affiliated Hospital of Anhui Medical University, Hefei, Anhui, 230022, China

2 Hefei Cancer Hospital, Chinese Academy of Sciences, Hefei, Anhui, 230031, China

* Corresponding Author.

Methods

Clinical Study and Design

Study Design

This study included patients with PTC who were admitted to the First Affiliated Hospital of Anhui Medical University from March 2021 to September 2025 and to the Hefei Cancer Hospital of the Chinese Academy of Sciences from March 2019 to September 2025. All surgeries were performed by surgeons from the same treatment team, and postoperative pathological examination confirmed the diagnosis of PTC. Patients who underwent concurrent central and lateral neck lymph node dissection during surgery were selected. Inclusion criteria were: 1) preoperative conventional ultrasound examination; 2) no history of thyroid surgery. Exclusion criteria were: 1) history of head and neck radiotherapy; 2) concurrent other head and neck malignancies; 3) incomplete clinical, pathological, or ultrasound data (see Figure 1). The study protocol was approved by the Ethics Committees of The First Affiliated Hospital of Anhui Medical University and Hefei Cancer Hospital of Chinese Academy of Sciences.

Figure 1. Study flow chart.

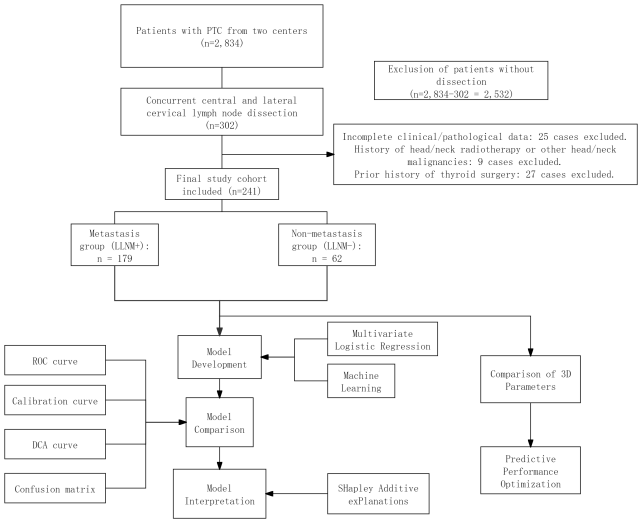

Data Collection

Data were retrieved from inpatient medical records. Based on guidelines and previous studies [20-23], 14 variables were selected as candidate predictors: age, sex, maximum tumor diameter, central compartment lymph node metastasis (assessed based on preoperative imaging and intraoperative frozen section pathology), number of metastatic central lymph nodes, number of tumor foci, capsular invasion, calcification, aspect ratio, punctate-strip blood flow signal, nodule margin, nodule location, preoperative TSH, and preoperative Parathyroid Hormone (PTH). Additionally, the three-dimensional measurements (long, intermediate, and short axes) of all tumor foci were collected.

Statistical Analysis

SPSS software (version 26.0) was used for statistical analysis. Categorical data are presented as n (%), and comparisons between groups were performed using the χ^2 test. + Variables with a P value < 0.1 in univariate analysis were included in a subsequent multivariate logistic regression analysis to identify independent predictors. The predictive performance of individual factors and combined indicators was evaluated using Receiver Operating Characteristic (ROC) curves. A P value < 0.05 was considered statistically significant.

Further modeling was conducted using R software (version 4.5.1). The analysis was performed in two stages. Stage 1: Development and internal validation of the logistic regression model using the full dataset. A prediction model and a corresponding nomogram were constructed based on the independent predictors. Model performance was evaluated in terms of: 1) Discrimination ability (Receiver Operating Characteristic [ROC] curve and Area Under the Curve, AUC); 2) Calibration (calibration curve and Hosmer-Lemeshow test); 3) Clinical utility (Decision Curve Analysis and Clinical Impact Curve). Internal validation was performed using the bootstrap method with 1000 resamples. Stage 2: Comparative analysis using a training-test set split (70%/30%). The data were split into training and validation sets in a 7:3 ratio. Applied machine learning algorithms included: Decision Tree, Random Forest, XGBoost, Support Vector Machine, K-Nearest Neighbors, LightGBM, and Naïve Bayes. These algorithms were selected to represent a diverse range of machine learning paradigms, thereby enabling a comprehensive comparison with the traditional logistic regression model. Specifically, Decision Tree provides an intuitive, rule-based approach for risk classification; Random Forest and XGBoost (extreme gradient boosting) are ensemble methods that handle non-linear relationships and feature interactions effectively, with XGBoost known for its robust performance in structured data; LightGBM (light gradient boosting machine) offers high efficiency and accuracy in gradient boosting frameworks; Support Vector Machine (SVM) is suitable for high-dimensional feature spaces through kernel transformation; K-Nearest Neighbors (KNN) serves as a non-parametric, instance-based learning method; and Naïve Bayes provides a probabilistic approach based on conditional independence assumptions. Collectively, this set of algorithms covers key categories—including tree-based models, ensemble methods, kernel-based methods, distance-based methods, and probabilistic classifiers—allowing for a rigorous evaluation of model performance across different analytical frameworks. Models were comprehensively assessed using the Area Under the ROC Curve, calibration curves, and decision curves. The SHAP (SHapley Additive exPlanations) method was used to interpret the model decision mechanisms.

Using an ellipsoid geometric model, we calculated three refined metrics beyond the "maximum tumor diameter" for each patient: total volume sum of all tumor foci ($V=(\pi/6)abc$), total surface area sum ($S\approx\pi(((ab)^p+(ac)^p+(bc)^p)/3)^{1/p}$, $p=1.6075$), and sphericity of the largest tumor focus ($\Psi=3a/(a+b+c)$) (see Figure 1).

*The ellipsoid model was selected because it is the most commonly used geometric approximation for thyroid nodules in clinical ultrasound practice. In this setting, tumors are typically measured along three orthogonal axes (long, intermediate, and short). In our study population, the majority of tumor foci exhibited a shape consistent with the ellipsoid assumption (i.e., well-defined, roughly ovoid contours), as confirmed by preoperative ultrasound imaging. While more sophisticated three-di-

mensional reconstruction techniques exist, the ellipsoid model offers a practical and reproducible method for routine clinical application.

Results

Development of a Prediction Model Based on Logistic Regression

Univariate and Multivariate Analysis

Among the 241 patients, significant differences (P < 0.1) were found between the metastasis and non-metastasis groups regarding the following variables: age, sex, maximum tumor diameter (>1 cm), central compartment lymph node metastasis, number of metastatic central lymph nodes, ill-defined nodule margin, aspect ratio (>1), nodule location, preoperative TSH, and preoperative PTH. These variables were included in a multivariate logistic regression analysis. The results identified the following as independent risk factors for predicting lateral lymph node metastasis (LLNM): maximum tumor diameter, central compartment lymph node metastasis status, nodule location, and preoperative TSH level (see Tables 1, 2, and 3).

Development and Predictive Performance of Model

Using the full dataset (241 patients), ROC curves were plotted for each independent predictor to evaluate their individual predictive value (see Figure 2). The prediction model was converted into a nomogram for direct clinical application (see Figure 3). The model exhibited good discriminatory ability with an AUC of 0.832. Internal validation using the bootstrap method (1000 repetitions) showed a high consistency between predicted and actual probabilities on the calibration curve (mean

Table 1. Univariate analysis of clinical characteristics in patients with PTC.

Factor	Non-metastasis Group (n=62), n (%)	Metastasis Group (n=179), n (%)	χ^2 Value	P Value
Age			44.780	0.000
≤35 years	52 (83.9%)	62 (34.6%)		
>35 years	10 (16.1%)	117 (65.4%)		
Sex			7.340	0.007
Male	9 (14.5%)	58 (32.4%)		
Female	53 (85.5%)	121 (67.6%)		
Maximum Tumor Diameter			13.686	0.000
≤1 cm	40 (64.5%)	67 (37.4%)		
>1 cm	22 (35.5%)	112 (62.6%)		
Central LN Metastasis			58.865	0.000
Yes	20 (32.3%)	150 (83.8%)		
No	42 (67.7%)	29 (16.2%)		
No. of Central LNs			30.920	0.000
≤3	56 (90.3%)	90 (50.3%)		
>3	6 (9.7%)	89 (49.7%)		
No. of Tumor Foci			2.442	0.295
Single	34 (54.8%)	81 (45.3%)		
Double	15 (24.2%)	43 (24.0%)		
Multiple	13 (21.0%)	55 (30.7%)		

Table 2. Multivariate logistic regression analysis of factors associated with lateral cervical lymph node metastasis.

Factor	β	SE	Wald χ^2	P Value	OR (95% CI)
Factor	-0.761	0.478	2.532	0.112	0.467 (0.183–1.191)
Sex (Male vs. Female)	-0.010	0.015	0.440	0.507	0.990 (0.961–1.020)
Age	0.689	0.259	7.062	0.008	1.992 (1.199–3.310)
Maximum Tumor Diameter	1.727	0.419	17.008	0.000	5.623 (2.471–12.794)
Central LN Metastasis	1.058	0.554	3.644	0.056	2.882 (0.973–8.534)
No. of Central LNs	0.085	0.495	0.030	0.864	1.089 (0.413–2.873)
Ill-defined Nodule Margin	-0.739	0.315	5.490	0.019	0.478 (0.258–0.885)
Nodule Location	0.055	0.420	0.017	0.896	1.056 (0.463–2.409)
Aspect Ratio (>1)	-1.056	0.448	5.562	0.018	0.348 (0.145–0.837)
Preoperative TSH	0.664	0.560	1.406	0.236	1.943 (0.648–5.823)
Preoperative PTH	1.762	2.123	0.689	0.406	5.827

Note: Statistically significant factors (P < 0.05) are highlighted in bold.

absolute deviation [MAD] = 0.023). The Hosmer-Lemeshow test yielded a P-value of 0.137, suggesting good model calibration. Decision curve analysis demonstrated that within the threshold probability range of 0.1 to 0.5, the net benefit of applying this model was higher than both the "intervention for all" and "intervention for none" strategies, indicating its potential clinical utility.

Construction and Comparison

To compare the performance of different modeling approaches, a training-test set split strategy (70%/30%) was employed. Based on the preliminary analysis, four predictive variables were included: central compartment lymph node metastasis status, maximum tumor diameter, nodule location, and preoperative TSH. All models were developed on the training set (70% of the data) and evaluated on the validation set (30% of the data). Multivariate logistic regression was used as the primary method to construct the prediction model. For supplementary comparison, seven machine learning algorithms were also applied, resulting in a total of eight prediction models. The confusion matrices for each model in the validation set are shown in Figure 4. The LightGBM model achieved the highest F1 score (0.56), indicating the best balance between sensitivity and specificity. However, the logistic regression model outperformed all other models in terms of discriminative ability (highest AUC), calibration (lowest Brier score [a measure of calibration accuracy], 0.124), and clinical utility (broadest range of net benefit on the decision curve analysis), suggesting it holds the greatest potential for broad clinical applicability (see Figure 5).

Figure 2. ROC curve, calibration curve, and decision curve analysis of the prediction model.

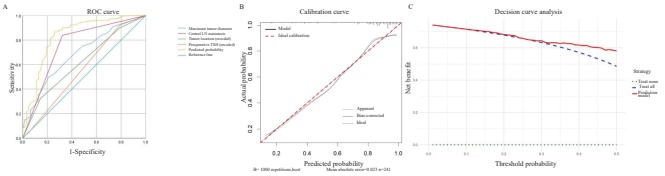

Figure 3. Nomogram model constructed based on multivariate variables.

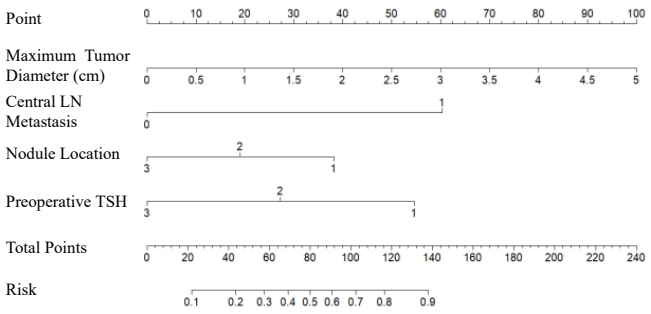

Table 3. Univariate analysis of ultrasound characteristics and serological indicators in patients with PTC.

Factor	Non-metastasis Group (n=62), n (%)	Metastasis Group (n=179), n (%)	χ^2 Value	P Value
Capsular Invasion			1.773	0.183
Yes	12 (19.4%)	50 (27.9%)		
No	50 (80.6%)	129 (72.1%)		
Ultrasound Calcification			0.417	0.518
Yes	31 (50.0%)	98 (54.7%)		
No	31 (50.0%)	81 (45.3%)		
Aspect Ratio (>1)			3.436	0.064
Yes	24 (38.7%)	47 (26.3%)		
No	38 (61.3%)	132 (73.7%)		
Punctate-Strip Blood Flow			0.039	0.843
Yes	32 (51.6%)	95 (53.1%)		
No	30 (48.4%)	84 (46.9%)		
Ill-defined Nodule Margin			25.513	0.000
Yes	32 (51.6%)	148 (82.7%)		
No	30 (48.4%)	31 (17.3%)		
Nodule Location			9.9	0.007
Upper	9 (14.5%)	58 (32.4%)		
Middle	40 (64.5%)	103 (57.5%)		
Lower	13 (21.0%)	18 (10.1%)		
Preoperative TSH			8.116	0.017
Low	3 (4.8%)	8 (4.5%)		
Normal	46 (74.2%)	157 (87.7%)		
High	13 (21.0%)	14 (7.8%)		
Preoperative PTH			5.218	0.074
Low	1 (1.6%)	7 (3.9%)		
Normal	59 (95.2%)	150 (83.8%)		
High	2 (3.2%)	22 (12.3%)		

Figure 4. Ensemble of confusion matrices for each model.

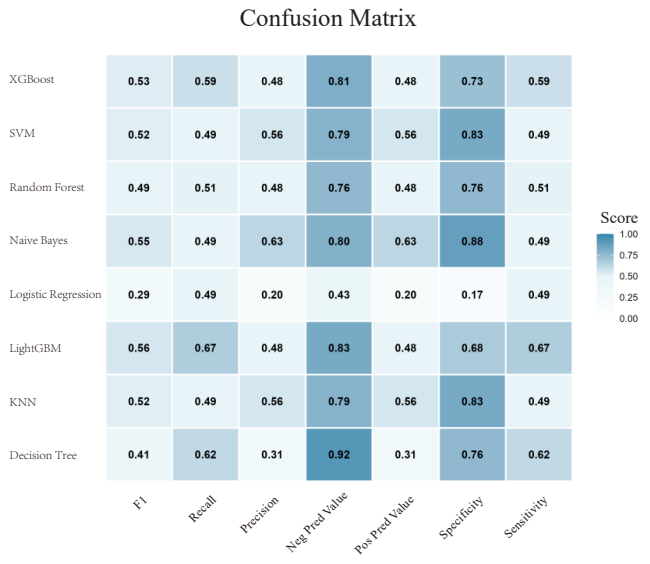

Figure 5. Comparison of discrimination, calibration, and clinical utility among the models.

A. The Logistic Regression model achieved the highest area under the curve (AUC) among all models, demonstrating the best overall discriminative ability for lateral cervical lymph node metastasis status. **B.** This model also had the lowest Brier score (0.124), and its calibration curve was closest to the ideal diagonal, indicating the best agreement between predicted probabilities and actual risk. **C.** In the decision curve analysis, the Logistic Regression model provided a net clinical benefit across the threshold probability range of 0.05–0.75, with a wider effective range than other models, suggesting broader clinical applicability.

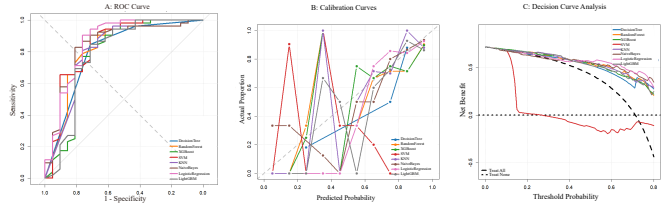

Threshold Optimization

Systematic optimization of classification thresholds revealed that the default threshold (0.5) was not optimal. Logistic Regression achieved its best F1 score (0.917) at a threshold of 0.6, making it suitable for scenarios emphasizing specificity. LightGBM reached its optimal F1 score (0.889) at a threshold of 0.3, rendering it more appropriate for screening contexts requiring high sensitivity (see Table 4). After threshold optimization, Logistic Regression, with the highest AUC and the optimal F1 score, emerged as the prediction model with the best overall performance (see Figure 6).

Figure 6. Ensemble of confusion matrices for each model under the optimal threshold range.

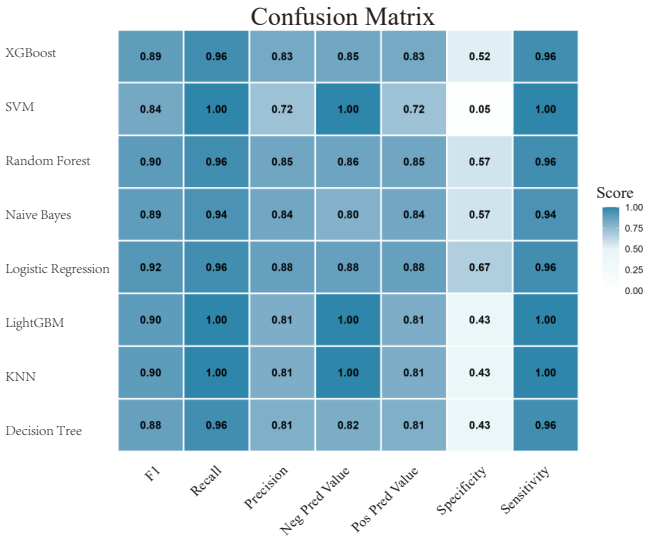

Comprehensive Evaluation and Discussion of Algorithmic Models

Based on the comprehensive performance evaluation, the Logistic Regression model demonstrated the best performance in terms of predictive accuracy and clinical utility. This model exhibited the highest discriminative ability (AUC=0.859), the most accurate predicted probabilities (Brier score=0.124), and its calibration curve aligned most closely with the ideal diagonal line. Within the clinical decision threshold range of 0.05 to 0.75, this model could provide the greatest net benefit (0.579). It ranked first across all three core evaluation dimensions: the ROC curve, calibration curve, and decision curve analysis. Its performance improved significantly after optimizing the classification threshold to 0.6. This model was thus identified as the optimal prediction model in this study.

Model Interpretability Analysis Based on SHAP

Model interpretability analysis was conducted using the SHAP (SHapley Additive exPlanations) method. In the Logistic Regression model, the order of variable importance was as follows: Central Compartment Metastasis > Nodule Location > Maximum Tumor Diameter > Preoperative TSH (see Figure 7). In the LightGBM model, the order of feature importance was: Central Compartment Metastasis > Maximum Tumor Diameter > Nodule Location > Preoperative TSH (see Figure 8). The SHAP summary plot illustrates the contribution of each feature's value to the model's predictive output, visually explaining the process of transforming feature inputs into predicted probabilities.

Table 4. Comparison of model performance after threshold optimization.

Model	Optimal Threshold	AUC	F1 Score	Accuracy	Sensitivity	Specificity
Logistic Regression	0.6	0.859	0.917	0.877	0.877	0.875
LightGBM	0.3	0.782	0.889	0.822	0.800	1.000

Figure 7. Feature importance analysis of the Logistic Regression model.

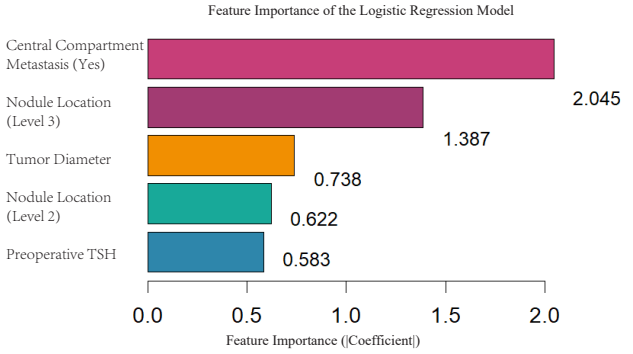

Figure 8: SHAP plot for the LightGBM model.

A. Feature Importance: The mean absolute SHAP value was used to evaluate each feature's contribution to the model's predictions. In the LightGBM model, the order of feature importance (highest to lowest) was: central compartment metastasis, tumor diameter, nodule location, preoperative TSH. **B.** SHAP Summary Plot: This plot visualizes the relationship between individual feature values and their corresponding SHAP values, providing a visual representation of each feature's contribution to the final predicted probability. **C.** High-Risk Case Example: For a patient with actual lateral lymph node metastasis, both the Logistic Regression and LightGBM models attributed increased risk prediction to features such as larger tumor diameter (and preoperative TSH in LightGBM). The final predicted probability was 0.609, correctly identifying this high-risk individual. **D.** Low-Risk Case Example: For a patient without metastasis, protective features like preoperative TSH (in Logistic Regression) and the absence of central metastasis/smaller tumor diameter (in both models) contributed negatively to the risk score. The final predicted probability was 0.194, correctly classifying this low-risk individual.

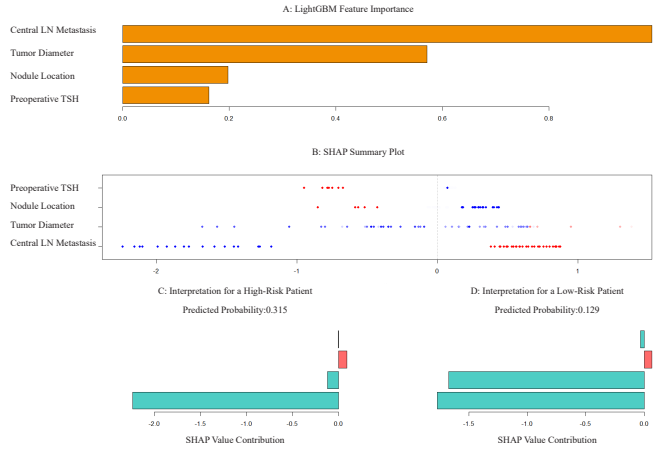

Exploration of Multivariate Prediction Models Using Alternatives to Maximum Tumor Diameter

Consistent with the comparative analysis described above, the training-test set split strategy (70%/30%) was used in this section as well. The variable "maximum tumor diameter" in the original model was sequentially replaced with the total tumor volume, total tumor surface area, and sphericity, following the same modeling process. The results showed that the AUCs for models based on total tumor volume, total tumor surface area, and sphericity were 0.835, 0.839, and 0.816, respectively. Notably, the AUCs for models using total tumor volume and total surface area were 0.835 and 0.839, respectively, which were slightly higher compared to that of the original model (AUC=0.832) (see Table 5).

ROC curves and nomograms were plotted for each alternative indicator (see Figures 9 and 10). The optimal cut-off value of total tumor surface area for predicting LLNM was 4.6295 cm², yielding a sensitivity of 49.7% and a specificity of 82.3%, with an AUC of 0.689 (95% CI: 0.616-0.762). Patients with a total tumor surface area exceeding this threshold should be alerted to a higher risk of LLNM.

Figure 9. ROC curves of individual factors and the prediction model for predicting lateral cervical lymph node metastasis.

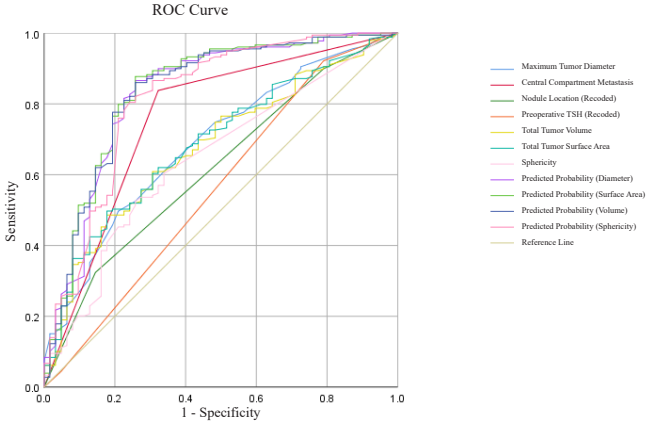

Figure 10: Nomogram model constructed based on significant new variables in the multivariate analysis.

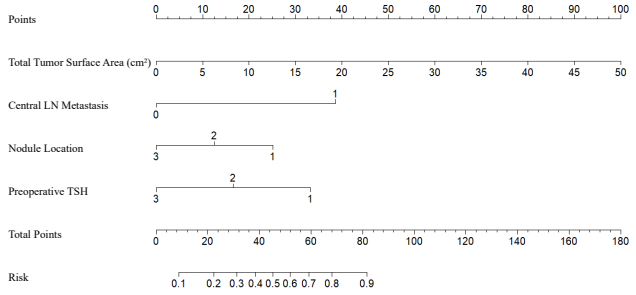

Note: The coding for categorical variables is as follows: Central Compartment Metastasis (0 = No, 1 = Yes); Nodule Location (1 = Upper, 2 = Middle, 3 = Lower); Preoperative TSH (1 = Low, 2 = Normal, 3 = High).

Maximum tumor diameter, total tumor volume, total tumor surface area, and sphericity provide complementary multidimensional information: maximum diameter serves as the classic one-dimensional indicator of linear growth; total tumor volume quantifies the overall tumor burden, which may be more directly related to metastatic potential; total tumor surface area characterizes the contact interface between the tumor and its microenvironment (blood vessels, lymphatic vessels) and is theoretically more closely associated with invasion and metastasis; sphericity reflects the morphological irregularity of the dominant tumor focus, potentially indicating more aggressive growth. Although these metrics are computationally related, they individually characterize the tumor's size, burden, interface, and shape features, holding independent biological significance. We regard them as a set of geometric candidate predictors to verify their incremental predictive value relative to maximum diameter indicators.

A baseline model was constructed based on maximum tumor diameter, central compartment metastasis, nodule location, and preoperative TSH, with each three-dimensional parameter subsequently added for comparison. The results revealed that the AUC of all combined models did not exceed that of the "Predicted probability (surface area sum)" model (AUC=0.839) (Figure 11, Table 6). This model incorporated only the core three-dimensional parameter. This model achieved the highest sensitivity (87.7%) and accuracy (84.0%) while maintaining stable specificity (74.2%), and its AUC was also superior to that of the baseline model (0.839 vs. 0.832). The performance of other models containing three-dimensional parameters was comparable but did not surpass it, suggesting that three-dimensional parameters—especially surface area sum—already possess promising independent predictive potential.

Figure 11. ROC Curves of the New Predictive Model for Lateral Lymph Node Metastasis.

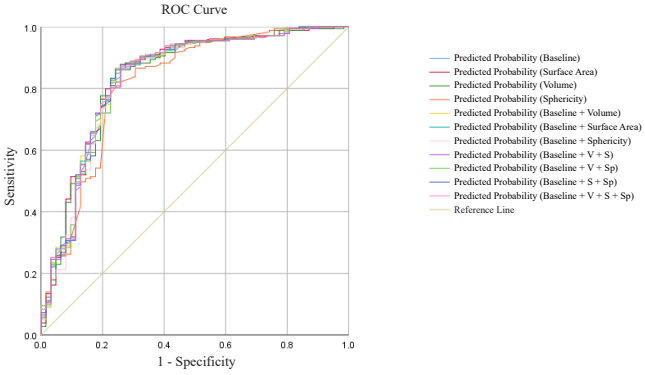

To further validate the incremental predictive value of three-dimensional geometric parameters, this study adopted a training-test set split strategy (70%/30%) to redevelop and systematically compare 11 prediction models. It should be noted that while the specific numerical results obtained from this validation approach differ from those derived from the Stage 1 full-dataset analysis, the core conclusions remain consistent, reflecting the generalization performance of the models in an independent test set.

In the test set, the model with the highest AUC was the "Basic + Volume" model (AUC = 0.8475, 95% CI: 0.7521–0.9428). Although its point estimate of AUC was marginally higher than that of the basic model (AUC = 0.8455), the difference was not statistically significant (Delong test, adjusted P = 1.000) (Table 7). This finding suggests that adding total tumor volume to the maximum diameter may provide modest complementary information in quantifying tumor burden, thereby achieving favorable discriminative performance within this dataset.

From a clinical perspective, the lack of statistical significance indicates that the basic model—which relies on the more readily available maximum tumor diameter—achieves predictive performance comparable to the more complex model incorporating total tumor volume. However, the slightly higher AUC of the "Basic + Volume" model suggests that total tumor volume may capture additional information related to overall tumor burden in multifocal cases, which could be clinically valuable when preoperative assessment aims to maximize predictive accuracy. Thus, model selection can be tailored to clinical priorities: the basic model offers simplicity and ease of use, making it a more practical alternative for general application, while the "Basic + Volume" model may be considered when a marginally higher discriminative performance is desired, particularly in patients with multifocal disease. By incorporating only four routine variables, the basic model achieves nearly equivalent discriminative efficacy (AUC difference: 0.002) while substantially enhancing generalizability and operational feasibility.

Discussion

Surgery is the primary treatment for papillary thyroid carci-

Table 5. Predictive value of individual factors and combined model indicators for lateral cervical lymph node metastasis.

Factor / Model Indicator	Sensitivity (%)	Specificity (%)	Accuracy (%)	AUC	95% CI	P Value
Maximum Tumor Diameter	83.8	67.7	79.6	0.687	0.613–0.761	<0.001
Central LN Metastasis	49.7	79.0	63.0	0.758	0.682–0.833	<0.001
Nodule Location (Recoded)	32.4	85.4	46.0	0.617	0.538–0.697	0.006
Preoperative TSH (Recoded)	92.2	21.0	73.8	0.561	0.474–0.648	0.152
Total Tumor Volume	48.6	82.3	58.3	0.678	0.604–0.752	<0.001
Total Tumor Surface Area	49.7	82.3	58.9	0.689	0.616–0.762	<0.001
Sphericity	52.5	74.2	58.8	0.646	0.567–0.724	0.001
Model (Based on Diameter)	86.6	74.2	83.4	0.832	0.766–0.898	<0.001
Model (Based on Surface Area)	87.7	74.2	81.0	0.839	0.774–0.903	<0.001
Model (Based on Volume)	86.0	74.2	83.0	0.835	0.770–0.899	<0.001
Model (Based on Sphericity)	82.1	74.2	80.1	0.816	0.748–0.884	<0.001

Note: Key indicators are highlighted in bold for emphasis.

noma (PTC). Accurate preoperative assessment of lateral cervical lymph node metastasis (LLNM) status is crucial for determining the extent of lymph node dissection, which directly impacts surgical complications (such as recurrent laryngeal nerve injury [24], hypoparathyroidism [25], chylous leakage [26], etc.) and patients' quality of life.

This study collected data from PTC patients across two centers. Based on three indicators—maximum tumor diameter, central compartment lymph node metastasis status, and nodule location—an individualized prediction model for LLNM was developed. The model demonstrated good predictive performance (AUC=0.832) and calibration. Decision curve analysis confirmed its clinical utility.

To further enhance and compare performance, this study constructed multiple models, including multivariate logistic regression and seven machine learning algorithms. A comprehensive comparison revealed that after threshold optimization, the Logistic Regression model performed optimally at a threshold of 0.6, making it suitable for decision-making scenarios emphasizing specificity. The LightGBM model performed best at a threshold of 0.3, rendering it more appropriate for high-sensitivity screening. Considering all evaluation metrics, Logistic Regression was identified as the optimal prediction model.

Furthermore, this study innovatively introduced three-dimensional morphological parameters. For multifocal PTC, the total tumor volume and total tumor surface area were calculated.

Table 6. Predictive value of various prediction model indicators for lateral cervical lymph node metastasis.

Model Indicator	Sensitivity (%)	Specificity (%)	Accuracy (%)	AUC	95% CI	P Value
Predicted Probability (Baseline)	86.6	74.2	83.3	0.832	0.766–0.898	<0.001
Predicted Probability (Surface Area)	87.7	74.2	84.0	0.839	0.774–0.903	<0.001
Predicted Probability (Volume)	86.0	74.2	82.9	0.835	0.770–0.899	<0.001
Predicted Probability (Sphericity)	82.1	74.2	80.4	0.816	0.748–0.884	<0.001
Predicted Probability (Baseline + Volume)	87.7	74.2	84.0	0.833	0.768–0.899	<0.001
Predicted Probability (Baseline + Surface Area)	86.6	74.2	83.3	0.835	0.769–0.901	<0.001
Predicted Probability (Baseline + Sphericity)	86.0	75.8	83.5	0.829	0.762–0.896	<0.001
Predicted Probability (Baseline + V + S)	86.6	74.2	83.3	0.834	0.768–0.900	<0.001
Predicted Probability (Baseline + V + Sp)	86.6	75.8	83.9	0.833	0.767–0.899	<0.001
Predicted Probability (Baseline + S + Sp)	87.7	74.2	84.0	0.835	0.769–0.900	<0.001
Predicted Probability (Baseline + V + S + Sp)	87.2	74.2	84.0	0.835	0.769–0.900	<0.001

Notes: Baseline model predictors: Maximum tumor diameter, central compartment metastasis, nodule location, preoperative TSH.

Table 7. Delong Test Results for Key Model Comparisons.

Comparison Group	Model A AUC	Model B AUC	AUC Difference	Raw P-value	Adjusted P-value	Conclusion
Basic model vs. Surface area substitution	0.8455	0.8426	0.0029	0.807	1.000	No significant difference
Basic model vs. Volume substitution	0.8455	0.8397	0.0058	0.622	1.000	No significant difference
Basic model vs. Basic + Volume	0.8455	0.8475	0.0019	0.818	1.000	No significant difference
Basic model vs. Basic + Surface area	0.8455	0.8397	0.0058	0.714	1.000	No significant difference
Surface area substitution vs. Volume substitution	0.8426	0.8397	0.0029	0.478	1.000	No significant difference
Surface area substitution vs. Basic + All 3D parameters	0.8426	0.8124	0.0302	0.305	1.000	No significant difference
Basic model vs. Basic + All 3D parameters	0.8455	0.8124	0.0331	0.297	1.000	No significant difference

*Note: Adjusted P-values were calculated using the Bonferroni correction for multiple comparisons; the significance threshold was set at $P < 0.05$.

Models based on total tumor surface area (AUC=0.839) or total tumor volume (AUC=0.835) showed slightly higher predictive performance than the model based on maximum diameter (AUC=0.832). When the total tumor surface area exceeds 4.6295 cm², a high risk of LLNM should be strongly suspected. This finding validates the hypothesis that three-dimensional morphological parameters possess complementary discriminatory power, providing a new basis for clinical assessment.

Maximum tumor diameter reflects only unidimensional linear growth and does not accurately quantify total tumor burden or the true spatial configuration of multifocal lesions. Total tumor volume directly represents the overall tumor cell load, and its association with metastatic potential may be stronger than that of maximum diameter alone in multifocal PTC. Total surface area more closely approximates the interface between the tumor and surrounding lymphatic and vascular pathways. A larger surface area may provide greater opportunity for tumor cells to breach the basement membrane and invade the vasculature, thus serving as a more direct indicator of invasive potential. Sphericity, as a morphological descriptor, offers a novel perspective for evaluating tumor growth patterns, with irregular morphology often suggesting enhanced proliferative activity and aggressive behavior.

Although the inclusion of three-dimensional parameters did not significantly improve the AUC of the basic model, both the "Surface area substitution" and "Volume substitution" models demonstrated predictive performance comparable to that of the basic model, with no statistically significant differences. These findings indicate that the predictive information embedded in three-dimensional parameters—particularly total surface area—largely encompasses that conveyed by unidimensional maximum diameter, conferring independent and equivalent discriminative capacity. Accordingly, total surface area derived from 3D imaging reconstruction holds promise as a preoperative predictive biomarker. It is at least equivalent to, and potentially provides more information than, maximum tumor diameter. It may facilitate risk assessment and guide individualized surgical decision-making, underscoring its clear potential for clinical translation.

In summary, this study advances the exploration from "unidimensional metrics" to the refinement of "three-dimensional geometric characterization." The results demonstrate that three-dimensional geometric parameters—especially total surface area—more comprehensively elucidate metastatic risk across dimensions such as tumor burden, interfacial effects, and growth morphology. These findings establish them as valuable complementary predictors of lateral cervical lymph node metastasis in PTC. Future research should validate their robustness in prospective, multicenter cohorts and investigate their integrated application with radiomic features and molecular markers.

Analysis of Predictive Factors

This study confirms that the maximum tumor diameter is an independent predictive factor for LLNM, consistent with previous research [27-30]. Larger tumor diameters are typically associated with greater invasiveness and a higher risk of metastasis. Central compartment lymph node metastasis was also confirmed as a robust predictive indicator [31-32]. As the primary lymphatic drainage site, its status effectively reflects the tumor's metastatic propensity. However, in some cases, patients may exhibit skip metastasis: negative central lymph nodes with positive lateral lymph nodes [33-34], which can be easily missed during preoperative evaluation and surgery [35]. The influence of tumor location on metastasis risk may be related to anatomical differences in lymphatic drainage [27, 36-37]. The results of this study indicate that when the total tumor surface area exceeds 4.6295 cm², patients face a significantly increased risk of LLNM. This threshold can serve as an effective early-warning indicator.

Model Comparison and Strengths

Compared to previous studies, the strengths of our model include: 1) It integrates multiple independent predictive factors to provide individualized risk assessment; 2) Visualization through a nomogram facilitates direct clinical application; 3) Comprehensive validation of model performance using various statistical methods; and 4) Systematic comparison of multiple machine learning algorithms, revealing their respective application potentials.

Clinical Significance and Application

The prediction model and nomogram tool developed herein can assist clinicians in more accurately assessing the risk of lateral cervical lymph node metastasis preoperatively, thereby facilitating the formulation of individualized surgical plans. For patients identified as high-risk by the model, therapeutic or prophylactic lateral neck dissection may be considered. For low-risk patients, overtreatment can be potentially avoided.

Study Limitations and Future Directions

This study is a dual-center investigation with a limited sample size; therefore, its conclusions require further validation through multicenter, prospective studies with larger cohorts. Future research could integrate multi-dimensional information such as radiomics and circulating tumor markers [29, 38-40] to enhance predictive accuracy. Despite these limitations, this study successfully developed and validated a prediction model based on readily available clinical indicators. It demonstrates good predictive performance and clinical utility, providing a valuable reference for individualized preoperative lymph node assessment in PTC patients.

Conclusion

In this study, an effective clinical prediction model for assessing lateral lymph node metastasis risk was successfully developed using readily available clinical indicators, demonstrating good predictive performance and clinical utility. This model, based on four routine variables (maximum tumor diameter, central lymph node metastasis, nodule location, and preoperative TSH), is well-suited for widespread application across various clinical settings—from primary hospitals where advanced imaging resources may be limited to tertiary referral centers seeking rapid, standardized risk stratification. The incorporation of three-dimensional morphological parameters—particularly total tumor surface area and total tumor volume—shows promising potential for enhancing risk assessment in multifocal papillary thyroid carcinoma. However, these findings require further validation in prospective, multicenter cohorts before clinical implementation. Additionally, the relatively com-

plex measurement procedures and the need for automated tools currently limit the widespread applicability of three-dimensional parameters. Future efforts should focus on developing efficient, automated measurement tools to facilitate clinical translation.

Abbreviations

AUC: Area Under the Curve; CI: Confidence Interval; CT: Computed Tomography; FNA: Fine-Needle Aspiration; LightGBM: Light Gradient Boosting Machine; LLNM: Lateral Lymph Node Metastasis; MAD: Mean Absolute Deviation; PTC: Papillary Thyroid Carcinoma; PTH: Parathyroid Hormone; ROC: Receiver Operating Characteristic; SHAP: SHapley Additive exPlanations; TSH: Thyroid-Stimulating Hormone; SVM: Support Vector Machine; KNN: K-Nearest Neighbors; XGBoost: Extreme Gradient Boosting.

Acknowledgements

Not applicable.

Author Contributions

The manuscript was conceived by all authors. WS,ZYQ and WKL designed the article, WS drafted the manuscript which was subsequently edited by FZY,SCL,JSY,ZSG,WKL. All authors reviewed the manuscript.

Funding Information

Not applicable.

Ethical Approval and Consent to Participate

This study was conducted in accordance with the principles of the Declaration of Helsinki. With approval from the Ethics Committees of The First Affiliated Hospital of Anhui Medical University (Approval No. PJ 2024-12-91) and Hefei Cancer Hospital of Chinese Academy of Sciences (Approval No. PJ-KY2025-008), the need for informed consent was waived due to the non-interventional, retrospective study design.

Competing Interests

The authors declare no competing interests.

Data Availability

The datasets obtained and/or analyzed during the current study are available from the corresponding author on reasonable request.

References

[1] Miranda-Filho A, Lortet-Tieulent J, Bray F, Cao B, Franceschi S, Vaccarella S, et al. Thyroid cancer incidence trends by histology in 25 countries: a population-based study. Lancet Diabetes Endocrinol. 2021;9:225–34. https://doi.org/10.1016/S2213-8587(21)00027-9.

[2] Bray F, Laversanne M, Sung H, Ferlay J, Siegel RL, Soerjomataram I, et al. Global cancer statistics 2022: GLOBOCAN estimates of incidence and mortality worldwide for 36 cancers in 185 countries. CA Cancer J Clin. 2024;74:229–63. https://doi.org/10.3322/caac.21834.

[3] Haugen BR, Alexander EK, Bible KC, Doherty GM, Mandel SJ, Nikiforov YE, et al. 2015 American Thyroid Association Management Guidelines for Adult Patients with Thyroid Nodules and Differentiated Thyroid Cancer: The American Thyroid Association Guidelines Task Force on Thyroid Nodules and Differentiated Thyroid Cancer. Thyroid Off J Am Thyroid Assoc. 2016;26:1–133. https://doi.org/10.1089/thy.2015.0020.

[4] Siegel RL, Miller KD, Wagle NS, Jemal A. Cancer statistics, 2023. CA Cancer J Clin. 2023;73:17–48. https://doi.org/10.3322/caac.21763.

[5] Zaydfudim V, Feurer ID, Griffin MR, Phay JE. The impact of lymph node involvement on survival in patients with papillary and follicular thyroid carcinoma. Surgery. 2008;144:1070–7; discussion 1077-1078. https://doi.org/10.1016/j.surg.2008.08.034.

[6] Basolo F, Macerola E, Poma AM, Torregrossa L. The 5th edition of WHO classification of tumors of endocrine organs: changes in the diagnosis of follicular-derived thyroid carcinoma. Endocrine. 2023;80:470–6. https://doi.org/10.1007/s12020-023-03336-4.

[7] Shen G, Ma H, Huang R, Kuang A. Predicting large-volume lymph node metastasis in the clinically node-negative papillary thyroid microcarcinoma: a retrospective study. Nucl Med Commun. 2020;41:5–10. https://doi.org/10.1097/MNM.0000000000001119.

[8] Smith VA, Sessions RB, Lentsch EJ. Cervical lymph node metastasis and papillary thyroid carcinoma: does the compartment involved affect survival? Experience from the SEER database. J Surg Oncol. 2012;106:357–62. https://doi.org/10.1002/jso.23090.

[9] de Meer SGA, Dauwan M, de Keizer B, Valk GD, Borel Rinkes IHM, Vriens MR. Not the number but the location of lymph nodes matters for recurrence rate and disease-free survival in patients with differentiated thyroid cancer. World J Surg. 2012;36:1262–7. https://doi.org/10.1007/s00268-012-1427-1.

[10] Ruan J, Chen Z, Chen S, Xu Z, Wen L, Mao Z, et al. Lateral lymph node metastasis in papillary thyroid microcarcinoma: a study of 5241 follow-up patients. Endocrine. 2024;83:414–21. https://doi.org/10.1007/s12020-023-03486-5.

[11] Haddad RI, Bischoff L, Ball D, Bernet V, Blomain E, Busaidy NL, et al. Thyroid Carcinoma, Version 2.2022, NCCN Clinical Practice Guidelines in Oncology. J Natl Compr Cancer Netw JNCCN. 2022;20:925–51. https://doi.org/10.6004/jnccn.2022.0040.

[12] Fei Y, Wang B, Yao X, Wu J. Factors associated with

occult lateral lymph node metastases in patients with clinically lymph node negative papillary thyroid carcinoma: a systematic review and meta-analysis. Front Endocrinol. 2024;15:1353923. https://doi.org/10.3389/fendo.2024.1353923.
[13] Zhang S, Liu R, Wang Y, Zhang Y, Li M, Wang Y, et al. Ultrasound-Base Radiomics for Discerning Lymph Node Metastasis in Thyroid Cancer: A Systematic Review and Meta-analysis. Acad Radiol. 2024;31:3118–30. https://doi.org/10.1016/j.acra.2024.03.012.
[14] Mulla MG, Knoefel WT, Gilbert J, McGregor A, Schulte K-M. Lateral cervical lymph node metastases in papillary thyroid cancer: a systematic review of imaging-guided and prophylactic removal of the lateral compartment. Clin Endocrinol (Oxf). 2012;77:126–31. https://doi.org/10.1111/j.1365-2265.2012.04336.x.
[15] Alabousi M, Alabousi A, Adham S, Pozdnyakov A, Ramadan S, Chaudhari H, et al. Diagnostic Test Accuracy of Ultrasonography vs Computed Tomography for Papillary Thyroid Cancer Cervical Lymph Node Metastasis: A Systematic Review and Meta-analysis. JAMA Otolaryngol-- Head Neck Surg. 2022;148:107–18. https://doi.org/10.1001/jamaoto.2021.3387.
[16] Zhang Y, Lu Y-Y, Li W, Zhao J-H, Zhang Y, He H-Y, et al. Lymphatic Contrast-enhanced US to Improve the Diagnosis of Cervical Lymph Node Metastasis from Thyroid Cancer. Radiology. 2023;307:e221265. https://doi.org/10.1148/radiol.221265.
[17] Lin S, Zhong Y, Lin Y, Liu G. Prediction model for lateral lymph node metastasis of papillary thyroid carcinoma in children and adolescents based on ultrasound imaging and clinical features: a retrospective study. BMC Med Imaging. 2024;24:228. https://doi.org/10.1186/s12880-024-01384-4.
[18] Yang Z, Wang X, Tao T, Zou J, Qiu Z, Wang L, et al. Diagnostic value of contrast-enhanced ultrasonography in the preoperative evaluation of lymph node metastasis in papillary thyroid carcinoma: a single-center retrospective study. BMC Surg. 2023;23:325. https://doi.org/10.1186/s12893-023-02199-w.
[19] Tee YY, Lowe AJ, Brand CA, Judson RT. Fine-needle aspiration may miss a third of all malignancy in palpable thyroid nodules: a comprehensive literature review. Ann Surg. 2007;246:714–20. https://doi.org/10.1097/SLA.0b013e3180f61adc.
[20] Shao L, Wang Z, Dong W, Sun W, Zhang H. Risk factors associated with preferential lateral lymph node metastasis in papillary thyroid carcinoma. Cancer Med. 2023;12:20670–6. https://doi.org/10.1002/cam4.6567.
[21] So YK, Kim M-J, Kim S, Son Y-I. Lateral lymph node metastasis in papillary thyroid carcinoma: A systematic review and meta-analysis for prevalence, risk factors, and location. Int J Surg Lond Engl. 2018;50:94–103. https://doi.org/10.1016/j.ijsu.2017.12.029.
[22] Zhao L, Wu F, Zhou T, Lu K, Jiang K, Zhang Y, et al. Risk factors of skip lateral cervical lymph node metastasis in papillary thyroid carcinoma: a systematic review and meta-analysis. Endocrine. 2022;75:351–9. https://doi.org/10.1007/s12020-021-02967-9.
[23] Zhao H, Huang T, Li H. Risk factors for skip metastasis and lateral lymph node metastasis of papillary thyroid cancer. Surgery. 2019;166:55–60. https://doi.org/10.1016/j.surg.2019.01.025.
[24] Mizuno K, Takeuchi M, Kanazawa Y, Kitamura M, Ide K, Omori K, et al. Recurrent laryngeal nerve paralysis after thyroid cancer surgery and intraoperative nerve monitoring. The Laryngoscope. 2019;129:1954–60. https://doi.org/10.1002/lary.27698.
[25] Yazıcıoğlu MÖ, Yılmaz A, Kocaöz S, Özçağlayan R, Parlak Ö. Risks and prediction of postoperative hypoparathyroidism due to thyroid surgery. Sci Rep. 2021;11:11876. https://doi.org/10.1038/s41598-021-91277-1.
[26] Hassan I, Hassan L, Bacha F, Alsalameh M, Qatee O, Hassan W. Clinico-pathological initial outcome of a newly adopted novel surgical technique for nodal metastatic thyroid cancer at a large-volume centre in a high-income developing country. Front Surg. 2023;10:1204230. https://doi.org/10.3389/fsurg.2023.1204230.
[27] Zhang X, Chen W, Fang Q, Fan J, Feng L, Guo L, et al. Lateral Lymph Node Metastases in T1a Papillary Thyroid Carcinoma: Stratification by Tumor Location and Size. Front Endocrinol. 2021;12:716082. https://doi.org/10.3389/fendo.2021.716082.
[28] Bae SY, Jung SP, Choe J-H, Kim JS, Kim JH. Prediction of lateral neck lymph node metastasis according to preoperative calcitonin level and tumor size for medullary thyroid carcinoma. Kaohsiung J Med Sci. 2019;35:772–7. https://doi.org/10.1002/kjm2.12122.
[29] Yu Q, Hao W, He Y, Ruan X, Liu L, Yun X, et al. Multi-omics analysis unveils dysregulation of the tumor immune microenvironment and development of a machine learning-based multi-gene classifier for predicting lateral lymph node metastasis in papillary thyroid carcinoma. Endocrine. 2025;90:172–87. https://doi.org/10.1007/s12020-025-04308-6.
[30] Ywata de Carvalho A, Kohler HF, Gomes CC, Vartanian JG, Kowalski LP. Predictive factors for recurrence of papillary thyroid carcinoma: analysis of 4,085 patients. Acta Otorhinolaryngol Ital Organo Uff Della Soc Ital Otorinolaringol E Chir Cerv-facc. 2021;41:236–42. https://doi.org/10.14639/0392-100X-N1412.
[31] Wada N, Duh Q-Y, Sugino K, Iwasaki H, Kameyama K, Mimura T, et al. Lymph Node Metastasis From 259 Papillary Thyroid Microcarcinomas. Ann Surg. 2003;237:399–407. https://doi.org/10.1097/01.SLA.0000055273.58908.19.
[32] Zhan S, Luo D, Ge W, Zhang B, Wang T. Clinicopathological predictors of occult lateral neck lymph node metastasis in papillary thyroid cancer: A meta-analysis. Head Neck. 2019;41:2441–9. https://doi.org/10.1002/hed.25762.
[33] Hu D, Lin H, Zeng X, Wang T, Deng J, Su X. Risk Factors for and Prediction Model of Skip Metastasis to Lateral Lymph Nodes in Papillary Thyroid Carcinoma. World J Surg. 2020;44:1498–505. https://doi.org/10.1007/s00268-019-05332-0.
[34] Feng J-W, Qin A-C, Ye J, Pan H, Jiang Y, Qu Z. Predictive Factors for Lateral Lymph Node Metastasis and Skip Metastasis in Papillary Thyroid Carcinoma. Endocr Pathol. 2020;31:67–76. https://doi.org/10.1007/s12022-019-09599-w.
[35] Wu X, Li B, Zheng C, He X. Risk factors for skip metastasis in patients with papillary thyroid microcarcinoma. Cancer Med. 2023;12:7560–6. https://doi.org/10.1002/

cam4.5507.
[36] Qubain SW, Nakano S, Baba M, Takao S, Aikou T. Distribution of lymph node micrometastasis in pN0 well-differentiated thyroid carcinoma. Surgery. 2002;131:249–56. https://doi.org/10.1067/msy.2002.120657.
[37] Back K, Kim JS, Kim J-H, Choe J-H. Superior Located Papillary Thyroid Microcarcinoma is a Risk Factor for Lateral Lymph Node Metastasis. Ann Surg Oncol. 2019;26:3992–4001. https://doi.org/10.1245/s10434-019-07587-2.
[38] Yu Y, Ouyang W, Huang Y, Huang H, Wang Z, Jia X, et al. Artificial intelligence-based multi-modal multi-tasks analysis reveals tumor molecular heterogeneity, predicts preoperative lymph node metastasis and prognosis in papillary thyroid carcinoma: a retrospective study. Int J Surg Lond Engl. 2025;111:839–56. https://doi.org/10.1097/JS9.0000000000001875.
[39] Yu S, Liu C, Hou Y, Li J, Guo Z, Chen X, et al. Integrative metabolomic characterization identifies plasma metabolomic signature in the diagnosis of papillary thyroid cancer. Oncogene. 2022;41:2422–30. https://doi.org/10.1038/s41388-022-02254-5.
[40] Zhang L, Zhang J, Fan S, Zhong Y, Li J, Zhao Y, et al. A case-control study of urinary concentrations of bisphenol A, bisphenol F, and bisphenol S and the risk of papillary thyroid cancer. Chemosphere. 2023;312 Pt 1:137162. https://doi.org/10.1016/j.chemosphere.2022.137162.

Management of Difficulty in Decannulation for Patients with Long-Term Tracheostomy Tubes Following Brain Diseases

Authors

Quanhui Guo, Wenying Zhu , Ying Shen, Hening Sun, Mengya Du, Lirong Liu, Haiwen Hu

Correspondence

huhaiwen@999brain.com (H. Hu)

Graphical Abstract

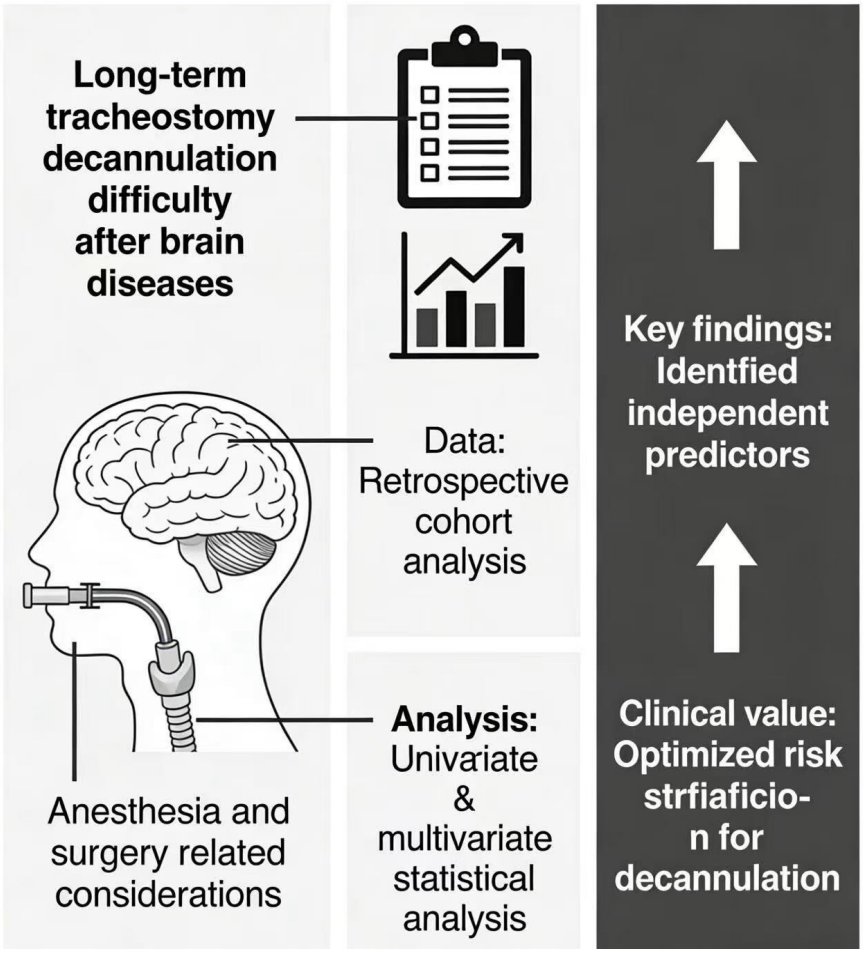

https://doi.org/10.71321/eakbax42

Research Article Head and Neck Diseases Conflux

Management of Difficulty in Decannulation for Patients with Long-Term Tracheostomy Tubes Following Brain Diseases

Quanhui Guo [1†], Wenying Zhu [1†], Ying Shen [1], Hening Sun [1], Mengya Du [1], Lirong Liu [2], Haiwen Hu [1*]

Received: 2026-01-22 | Accepted: 2026-03-25 | Published online: 2026-04-03

Abstract

Objective: To investigate the etiology of difficult decannulation in patients with long-term tracheostomy following brain-related diseases, and to explore the preoperative examination and assessment, selection of surgical indications, surgical and postoperative management methods. This aims to provide a scientific basis for facilitating successful decannulation, improving patients' quality of life, and guiding clinical practitioners in the management of such cases.

Methods: A retrospective analysis was conducted on 27 patients who were hospitalized in our department from May to December 2025 and had experienced failed decannulation after long-term tracheostomy. Preoperative examination and assessment included electronic laryngoscopy and laryngotracheal CT three-dimensional reconstruction. Electronic laryngoscopy was simultaneously used to assess swallowing function, including the Penetration-Aspiration Scale score, Murray Secretion Scale score, vallecula and pyriform sinus residue grading, and swallowing disability grading and classification. The surgical procedure involved endoscopic-assisted resection of laryngeal and tracheal granulation tissue via a supporting laryngoscope under general anesthesia.

Results: The primary cause of laryngotracheal stenosis leading to decannulation failure in patients with long-term tracheostomy due to brain diseases was obstruction from granulation tissue hyperplasia within the larynx and trachea, followed by restricted bilateral vocal cord abduction. Based on detailed preoperative examinations and assessments, all 27 patients in this group were deemed suitable candidates for surgery. They successfully underwent endoscopic-assisted resection of laryngeal and tracheal granulation tissue via a supporting laryngoscope under general anesthesia without any complications. Decannulation was successfully achieved in all patients within 7 to 10 days postoperatively.

Conclusions: 1) Electronic fiberoptic laryngoscopy and laryngotracheal CT three-dimensional reconstruction are effective methods for preoperative examination and evaluation. 2) Appropriate surgical candidates can be selected based on these two examinations. 3) Endoscopic-assisted resection of laryngotracheal granulation lesions via a supporting laryngoscope under general anesthesia is a safe and effective method to resolve decannulation difficulties in such patients.

Keywords: Brain; Diseases tracheotomy; Laryngotracheal stenosis; Difficult decannulation

Introduction

Brain-related diseases such as cerebral hemorrhage, brain tumor postoperative states, and traumatic brain injury often lead to weakened respiratory function or difficulty breathing, necessitating tracheotomy. Since these brain conditions frequently result in prolonged coma or impaired consciousness, treatment and rehabilitation periods are extended, requiring long-term cannulation to maintain airway patency. When patients' brain conditions stabilize and they enter the rehabilitation phase, long-term cannulation inevitably poses significant challenges to recovery and nursing care, severely impacting the quality of life for both patients and their families. Decannulation becomes essential. However, due to prolonged cannulation, some patients cannot undergo decannulation smoothly. This article aims to investigate the causes of decannulation difficulties, preoperative examination and assessment, selection of surgical indications, and surgical and postoperative management strategies for patients with long-term tracheostomy cannulation following brain-related diseases, through a retrospective analysis of 27 cases admitted to our department between May and December 2025. The goal is to facilitate successful decannulation, improve patients' quality of life, and provide scientific evidence for clinicians managing such cases.

1 Department of Otolaryngology, Head and Neck Surgery, Guangdong Sanjiu Brain Hospital, Guangzhou, Guangdong, China.

2 Department of Rehabilitation Medicine, Guangdong Sanjiu Brain Hospital, Guangzhou, Guangdong, China.

† These authors contributed equally to this work.

* Corresponding Author.

Materials and Methods

Patients

From May to December 2025, our department treated 27 patients who failed decannulation after tracheotomy due to brain-related diseases. Among them, 18 were male and 9 were female, aged ranging from 17 to 84 years, with a mean age of 47.52 ± 17.20 years. In our study cohort, obstructions were primarily localized at the previous tracheostomy stoma site. The duration of cannulation ranged from 1 to 15 months, with a mean duration of 5.19 ± 4.08 months. The primary brain diseases included cerebral hemorrhage (16 cases), brain tumor (2 cases), cerebral infarction (1 case), and severe traumatic brain injury (8 cases), as shown in Table 1.

Decannulation

We defined successful extubation as the lack of need for reintubation within 24 hours of successful tracheostomy tube withdrawal.

Occlusion protocol: The patient needs to switch to an airless catheter (or with the airbag completely deflated) and undergo a 24-hour full occlusion test throughout the day.

Objective respiratory indicators: During the occlusion period, the patient must maintain a resting blood oxygen saturation (SpO_2) of >90% without oxygen inhalation, and there should be no symptoms such as breathing difficulty, wheezing, or excessive sweating.

Failure criteria: If the patient experiences a sustained SpO_2 below 90% after occlusion or tube removal, develops respiratory distress, severe wheezing sounds, requires reopening of the airway, or reinsertion of the tracheal tube, it is considered a failed tube removal.

Long-term tracheostomy: tube dependency for over 30 days.

Surgical Intervention

All surgical interventions were performed under general anesthesia. The airway lesions were exposed utilizing a suspension laryngoscope. Granulation tissue excision was performed using low-temperature plasma coblation, and precise hemostasis was achieved intraoperatively via plasma radiofrequency ablation. Regarding the ventilation strategy, standard positive pressure ventilation was maintained through the pre-existing tracheostomy tube or via an endotracheal tube placed directly through the stoma, without the need for high-frequency jet ventilation.

For the postoperative decannulation pathway, routine endoscopic re-evaluation was not performed. Instead, decannulation decisions were guided by a strict clinical protocol. Once postoperative reactive edema was clinically determined to

Table 1. Baseline Characteristics of Patients with Laryngotracheal Stenosis.

Baseline Data	Sex	Age	Mean Age ("x" ±s)	Primary Disease	Tube indwelling time(month)	Average Tube Indwelling Time ("x" ±s)
Zeng**	male	51		Cerebral Artery Stenosis	3 +	
Tang*	male	45		Brainstem Hemorrhage	12 +	
Li**	female	51		Brainstem Hemorrhage	3 +	
Lai**	male	26		Intracerebral Hemorrhage	2 +	
Lin**	male	71		Intracerebral Hemorrhage	3 +	
Xie**	male	61		Cerebral Infarction	3 +	
Yu**	male	37		Traumatic Brain Injury	2 +	
Huang**	male	27		Intracerebral Hemorrhage	5 +	
Chen**	female	61		Intracerebral Hemorrhage	3 +	
Jin**	female	55		Intracerebral Hemorrhage	3 +	
Chen**	female	17		Brainstem tumor	10 +	
Lai**	male	69		Intracerebral Hemorrhage	2 +	
Ye**	male	62		Intracerebral Hemorrhage	2 +	
Zhang**	male	43	47.52±17.20	Intracerebral Hemorrhage	5 +	5.19±4.08
Zeng**	female	58		Traumatic Brain Injury	11 +	
Xie*	male	65		Traumatic Brain Injury	11 +	
Hu**	female	19		Intracerebral Hemorrhage	1 +	
Liu**	male	19		Traumatic Brain Injury	5 +	
Feng**	male	46		Intracerebral Hemorrhage	10 +	
Luo**	female	43		Intracerebral Hemorrhage	5 +	
Wu**	male	56		Traumatic Brain Injury	3 +	
Su**	male	44		Traumatic Brain Injury	1 +	
Ran**	male	42		Intracerebral Hemorrhage	1 +	
Li*	male	37		Brainstem Hemorrhage	8 +	
Deng**	female	32		Traumatic Brain Injury	10 +	
Lu**	female	84		Intracerebral Hemorrhage	1 +	
Kang**	male	62		postoperative brain tumor	15 +	

have subsided (typically 2 days post-surgery), patients underwent a continuous capping trial. Successful decannulation was strictly based on objective clinical criteria (stable SpO_2 >90%, and absence of stridor or distress during the occlusion trial), rather than anatomic visualization via post-operative endoscopy.

Fiberoptic Endoscopic Evaluation of Swallowing (FEES)

Evaluation Method: Fiberoptic Endoscopic Evaluation of Swallowing (FEES) was performed for all participants in this study. Test Boluses and Procedure: Three bolus consistencies were utilized during the assessment: low-viscosity (thin liquid), medium-viscosity (thick liquid), and high-viscosity (paste). All boluses were tinted with green additives (e.g., natural spinach juice) to enhance visualization and contrast during the endoscopic procedure.

Preoperative Examination and Assessment

The results of electronic laryngoscopy and swallowing function assessment are presented in Table 2. Three-dimensional reconstruction images of the laryngotracheal CT are shown in Figure 1. Preoperative and postoperative images of laryngoscopy are shown in Figure 2 and Figure 3.

Table 2. Electronic Laryngoscopy Assessment Form for Patients with Laryngotracheal Stenosis

Baseline Data	Swallowing Impairment Score (Residue Rating) - Adduction	Swallowing Impairment Score (Residue Rating) - Abduction	Swallowing Impairment Score (Residue Rating)	Penetration-Aspiration Scale (PAS)	Percentage of Airway Occlusion (%)
Zeng * *	left: normal right: normal	left: normal right: normal	Dysphagia (not have) valleculae: TracePyriform Sinus: Trace	1	80
Tang * *	left: reduce right: reduce	left: normal right: normal	Dysphagia (Oropharyngeal Phase) valleculae: MildPyriform Sinus: Mild	5	70
Li * *	left: reduce right: reduce	left: reduce right: reduce	Dysphagia (Oropharyngeal Phase) valleculae: TracePyriform Sinus: Mild	5	80
Lai * *	left: normal right: normal	left: normal right: normal	Dysphagia (Oropharyngeal Phase) valleculae: TracePyriform Sinus: Trace	4	100
Lin * *	left: normal right: fixed	left: normal right: fixed	Dysphagia (Oropharyngeal Phase) valleculae: MildPyriform Sinus: Trace	6	70
Xie * *	left: reduce right: reduce	left: reduce right: reduce	Dysphagia (Oropharyngeal Phase) valleculae: MildPyriform Sinus: Moderate	4	50
Yu * *	left: reduce right: reduce	left: reduce right: reduce	Dysphagia (Oropharyngeal Phase) valleculae: ModeratePyriform Sinus: Moderate	4	100
Huang * *	left: reduce right: normal	left: reduce right: normal	Dysphagia (Oropharyngeal Phase) valleculae: ModeratePyriform Sinus: Moderate	6	90
Chen * *	left: reduce right: reduce	left: reduce right: reduce	Dysphagia (Oropharyngeal Phase) valleculae: TracePyriform Sinus: Trace	5	90
Jing * *	left: reduce right: reduce	left: reduce right: reduce	Dysphagia (Oropharyngeal Phase) valleculae: MildPyriform Sinus: Mild	4	80
Chen * *	left: reduce right: reduce	left: reduce right: reduce	Dysphagia (Oropharyngeal Phase) valleculae: MildPyriform Sinus: Moderate	4	95
Lai * *	left: fixed right: reduce	left: fixed right: reduce	Dysphagia (Not assessed) valleculae: MildPyriform Sinus: Mild	/	60
Ye * *	left: fixed right: normal	left: fixed right: normal	Dysphagia (Oropharyngeal Phase) valleculae: MildPyriform Sinus: Mild	4	60
Zhang * *	left: reduce right: reduce	left: reduce right: reduce	Dysphagia (Oropharyngeal Phase) valleculae: MildPyriform Sinus: Mild	2	50-55

Zeng * *	left: reduce right: reduce	left: normal right: normal	Dysphagia (Oropharyngeal Phase) valleculae: MildPyriform Sinus: Mild	5	98
Xie * *	left: reduce right: reduce	left: normal right: normal	Dysphagia (Oropharyngeal Phase) valleculae: MildPyriform Sinus: Mild	5	50
Hu * *	left: reduce right: reduce	left: normal right: normal	Dysphagia (Oropharyngeal Phase) valleculae: MildPyriform Sinus: Mild	4	70
Liu * *	left: reduce right: reduce	left: normal right: normal	Dysphagia (Oropharyngeal Phase) valleculae: MildPyriform Sinus: Mild	5	40
Feng * *	left: reduce right: reduce	left: normal right: normal	Dysphagia (Oropharyngeal Phase) valleculae: SeverePyriform Sinus: Severe	7	70-75
Luo * *	left: normal right: normal	left: normal right: normal	Dysphagia (Oropharyngeal Phase) valleculae: ModeratePyriform Sinus: Moderate	4	55-60
Wu * *	left: reduce right: reduce	left: reduce right: reduce	Dysphagia (Oropharyngeal Phase) valleculae: ModeratePyriform Sinus: Moderate	6	100
Su * *	left: normal right: normal	left: normal right: normal	Dysphagia (Oropharyngeal Phase) valleculae: MildPyriform Sinus: Mild	4	40
Ran * *	left: reduce right: reduce	left: normal right: normal	Dysphagia (Oropharyngeal Phase) valleculae: MildPyriform Sinus: Mild	4	/
Li *	left: reduce right: reduce	left: normal right: normal	Dysphagia (Oropharyngeal Phase) valleculae: ModeratePyriform Sinus: Moderate	6	60-65
Deng * *	left: reduce right: reduce	left: normal right: normal	Dysphagia (Oropharyngeal Phase) valleculae: MildPyriform Sinus: Mild	5	100
Lu * *	left: reduce right: reduce	left: normal right: normal	Dysphagia (Oropharyngeal Phase) valleculae: MildPyriform Sinus: Mild	4	90
Kang * *	left: reduce right: reduce	Unable to abduct, fixed in the para-median position	Dysphagia (Oropharyngeal Phase) valleculae: MildPyriform Sinus: Mild	3	/

Figure 1. Laryngotracheal CT Image.

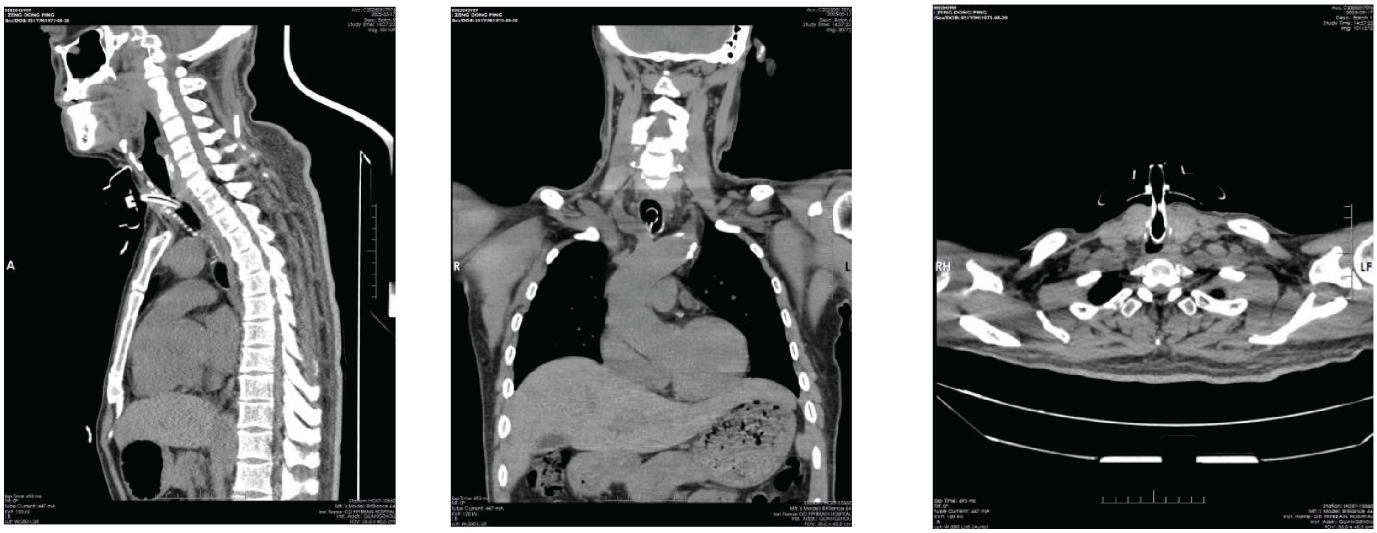

Figure 2. Preoperative images of laryngoscopy.

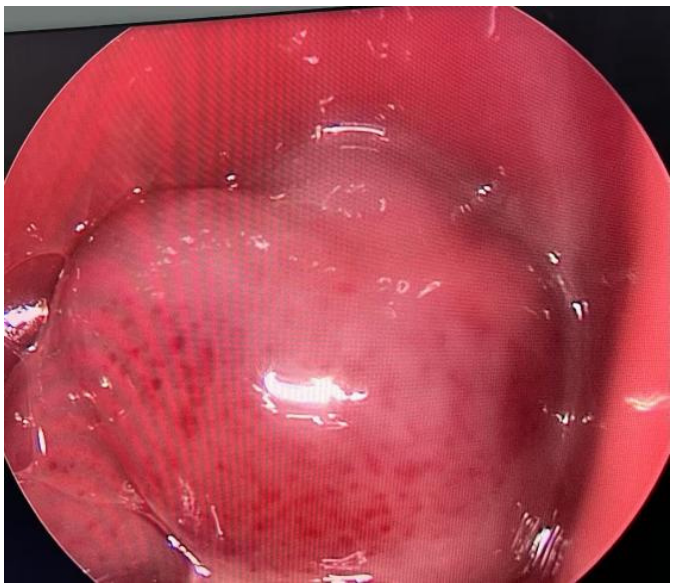

Figure 3. Postoperative images of laryngoscopy.

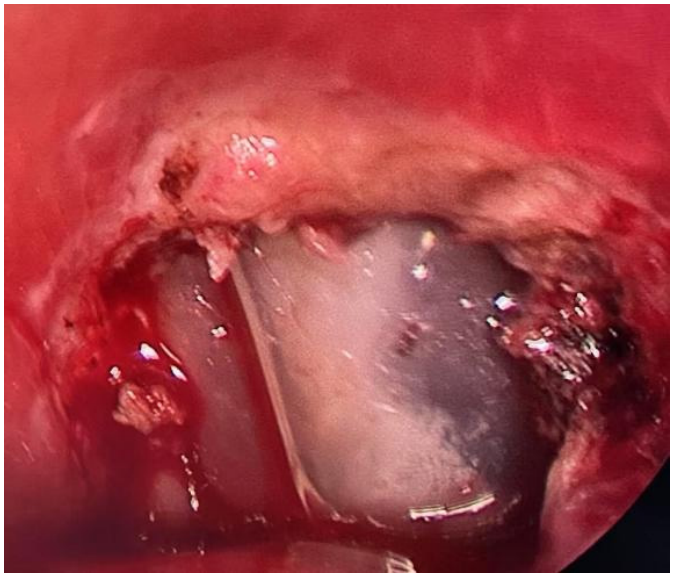

Surgical Indication Selection

Patients with long-term tracheostomy tube dependence after tracheotomy, whose primary disease does not cause dyspnea, but who have failed multiple tube occlusion attempts or attempted extubation.

1) Electronic laryngoscopy reveals good mobility of both or at least one vocal cord, with laryngeal or tracheal granulation tissue obstructing > 50% of the tracheal lumen, and normal mouth opening.
2) Electronic laryngoscopy indicates a penetration-aspiration score ≤ 4 points and a swallowing impairment assessment score < 3 points.
3) Three-dimensional reconstruction of laryngotracheal CT shows soft tissue.
4) Obstruction above the tracheostomy site.
5) The patient or their family strongly requests extubation.
6) Other surgical contraindications are excluded.

All patients underwent endoscopic-assisted laryngotracheal granuloma resection under general anesthesia with suspension laryngoscopy. The procedures were successfully completed without complications. All patients achieved successful tube occlusion and decannulation within 7 to 10 days postoperatively.

Result

Causes of Laryngotracheal Stenosis in Patients with Long-Term Tracheostomy Tube Dependence After Brain Disease

Laryngotracheal Granulation Tissue Hyperplasia Obstructing the Trachea

In this cohort of 27 patients, 26 cases (96.3%) were attributed to laryngotracheal granulation tissue hyperplasia obstructing the trachea, leading to extubation failure. All these patients achieved successful decannulation after surgical intervention.

Impaired Bilateral Vocal Cord Abduction

Only 1 patient (3.7%) in the cohort experienced extubation failure due to bilateral vocal cord fixation with impaired abduction.

Endoscopic-Assisted Laryngotracheal Granuloma Resection Under General Anesthesia: A Safe and Effective Approach

Endoscopic-assisted laryngotracheal granuloma resection under general anesthesia with suspension laryngoscopy proved to be a safe and effective method for resolving extubation difficulties in such patients. The procedures were completed successfully without complications.

Discussion

Impact of Long-Term Tracheostomy Tube Dependence on Patients' Quality of Life

Tracheostomy tubes significantly impair fundamental life functions, including respiration, swallowing, and nutritional intake. Prolonged tube retention can lead to excessive secretions or complications such as tracheal obstruction, exacerbating patient discomfort [1]. Multiple studies indicate a substantial decline in quality of life among patients with long-term tracheostomy tube dependence [2-3]. This phenomenon, described as "severely compromised quality of life," is particularly evident in patients with extended tube dependence (e.g.3-12 months), showing a significant gap compared to non-tracheostomy patients [5]. The detrimental effects manifest across multiple dimensions, as summarized below:

Swallowing and Respiratory Functions

After tracheostomy tube placement, patients frequently experience dysphagia (reported in 44% of cases), dyspnea, pain, and restricted mobility [4]. Pediatric patients may face developmental delays and neurocognitive impairments [5].In terms of respiratory mechanics, long-term tube dependence alters breathing function. For instance, tracheostomy reduces airway resistance, decreasing respiratory work but potentially leading to respiratory muscle atrophy due to disuse. In patients requiring prolonged mechanical ventilation, the tube's persistent presence can cause structural damage to the trachea, such as scar formation, tracheal stenosis, or malacia [6]. Complications like tube displacement or blockage may precipitate acute

respiratory failure [7], while tube malposition or barotrauma can cause pneumomediastinum as air leaks into surrounding tissues, compressing the airway [8].Studies also indicate weakened pharyngeal reflexes and increased gastroesophageal reflux ($p < 0.05$) in long-term tube-dependent patients, elevating aspiration risks and secondary pneumonia [9]. Difficult decannulation is common: one study found that although 57% of patients achieved short-term decannulation, 32% required reinsertion within two years due to respiratory issues, suggesting incomplete functional recovery. These factors contribute to sustained reliance on mechanical ventilation support [10].

Respiratory Infections

From a physiological perspective, tracheostomy alters the normal anatomy and function of the respiratory tract, compromising the warming, humidifying, and filtering capabilities of the upper airways. This allows inhaled air to directly enter the lower respiratory tract, leading to dryness of the airway mucosa and thickened secretions. Long-term tube retention can induce chronic inflammation in the respiratory tract, thereby increasing the risk of pulmonary infections. A retrospective cohort study demonstrated that among patients with severe traumatic brain injury, the incidence of pulmonary infections following tracheostomy reached as high as 26.85% [11]. Frequent respiratory infections not only cause physical discomfort but may also lead to increased hospitalizations and healthcare costs, further impairing patients' quality of life.

Impact of Long-Term Tracheostomy Tube Dependence on Patients' Psychological and Social Functioning

Long-term tracheostomy tube dependence frequently leads to psychological disturbances, including diminished self-esteem, anxiety, stress, and depression. Communication barriers-particularly the inability to speak normally-directly undermine self-image and social adaptability. Anxiety and depression are the most prevalent psychological issues in this population. A study of 89 patients recorded pre-intervention scores of SAS: 56.78 ± 6.42 and SDS: 57.62 ± 7.12, both significantly exceeding normal thresholds, indicating widespread moderate-to-severe anxiety and depressive symptoms. The visible tracheostomy tube on the neck acts as a social stigma, further inhibiting social interaction [12]. Due to the need for frequent stoma care, infection concerns, fear of negative social perceptions, and general functional decline, patients often progressively reduce social activities.

Impact of Long-Term Tracheostomy Tube Dependence on Family and Economic Burden

For patients with long-term tracheostomy tube dependence, the challenges extend beyond health issues to significant family and economic burdens. In addition to direct medical costs, prolonged tube retention often leads to reduced or complete loss of labor capacity, resulting in decreased household income. Simultaneously, caregivers may be forced to leave their jobs to provide full-time care, further exacerbating financial strain. The uncertainty of the patient's condition, potential complications (e.g., tube blockage or infection), and concerns about long-term quality of life contribute to chronic psychological stress among family members, manifesting as anxiety, depression, and emotional exhaustion. This psychological burden not only affects caregivers' well-being but may also indirectly hinder the patient's recovery process by compromising the quality of home care.

Reasons for Difficult Decannulation in Patients with Brain Diseases After Long-Term Tracheostomy

Laryngotracheal stenosis (LTS) is a major cause of decannulation failure. It can result from iatrogenic injury, trauma, infection, autoimmune diseases, or congenital anomalies, with prolonged endotracheal intubation or tracheostomy being the most common predisposing factors. Stenosis typically occurs in the subglottic region or cervical trachea, primarily due to abnormal mucosal repair and fibrosis following mechanical injury. In the present case series, granulation tissue hyperplasia obstructing the tracheal lumen was the leading cause of decannulation failure in 26 patients (96.3%), while only 1 case (6.7%) resulted from bilateral vocal fold immobility.

Clinical Management

1.Detailed history taking to assess whether the primary brain disease is stable and whether the patient or family members have a strong desire for decannulation.

2.Preoperative electronic laryngoscopy to comprehensively evaluate swallowing function, including grading of penetration and aspiration, secretions scale scoring, and documentation with photos and videos. Simultaneously, laryngotracheal CT three-dimensional reconstruction is performed to quantify the degree of stenosis or obstruction.

3.Strict adherence to indication criteria for surgical intervention. All patients underwent endoscopic-assisted laryngotracheal granuloma resection under general anesthesia with suspension laryngoscopy. The procedures were completed successfully without complications. Decannulation was achieved within 7-10 days postoperatively in all cases.

Finally, due to the retrospective nature of this study, specific details regarding baseline airway management-such as precise tracheostomy tube sizes, cuff management protocols, and the exact duration of prior endotracheal intubation were inconsistently documented in the historical medical records and could not be analyzed. Future prospective studies are warranted to evaluate the impact of these specific variables on decannulation outcomes.

Conclusion

In conclusion, electronic fiberoptic laryngoscopy and laryngotracheal CT three-dimensional reconstruction serve as reliable preoperative modalities for examination and evaluation. These complementary techniques enable precise selection of suitable surgical candidates. Furthermore, endoscopic-assisted resection of laryngotracheal granulation lesions via a supporting laryngoscope under general anesthesia is demonstrated to be a safe and effective approach for addressing decannulation difficulties in this patient population.

Abbreviations

ABI: Acquired Brain Injury; CT: Computed Tomography; FEES: Fiberoptic Endoscopic Evaluation of Swallowing; LTS: Laryngotracheal Stenosis; PAS: Penetration-Aspiration Scale; QOL:

Quality of Life; SAS: Self-Rating Anxiety Scale; SDS: Self-Rating Depression Scale; SpO_2: Resting Blood Oxygen Saturation; WHO-QOL BREF: World Health Organization Quality of Life BREF Questionnaire.

Acknowledgments

We would like to thank the anonymous reviewers and the editors for their constructive comments.

Author Contributions

Haiwen Hu designed the study, performed the experiments and data analysis.Quanhui Guo wrote the manuscript. All authors read and approved the final manuscript. The author(s) report no conflicts of interest in this work.

Funding Information

This research received no external funding.

Ethical Approval and Consent to Participate

Not applicable.

Competing Interests

The authors declare no competing interests.

Data Availability

All data generated or analyzed during this study are included in this published article.

References

[1] Marcet-Gonzalez J, Barton G, Lambert E. Severity of sialorrhea and tracheal secretions in infants and toddlers with a tracheostomy with a focus on quality of life. American Journal of Otolaryngology. 2021;42(6):103074. https://doi.org/10.1016/j.amjoto.2021.103074

[2] Kumar V, Malhotra V, Sinha V. Evaluation of individual quality of life (QOL) among patients with tracheostomy using WHO-QOL BREF questionnaire. Indian Journal of Otolaryngology and Head & Neck Surgery. 2022;74(Suppl 3):5207-5216. https://doi.org/10.1007/s12070-020-02298-0

[3] Lakshmanan S, Manimaran V, Mohanraj L. Quality of life in non-ventilated tracheostomised patients. Indian Journal of Otolaryngology and Head & Neck Surgery. 2023;75(2):282-286. https://doi.org/10.1007/s12070-022-03310-7

[4] Freeman-Sanderson AL, Togher L, Elkins MR, Phipps PR. Quality of life improves for tracheostomy patients with return of voice: a mixed methods evaluation of the patient experience across the care continuum. Intensive and Critical Care Nursing. 2018;46:10-16. https://doi.org/10.1016/j.iccn.2018.02.004

[5] Mizuno K, Takeuchi M, Kishimoto Y, et al. Indications and outcomes of paediatric tracheotomy: a descriptive study using a Japanese claims database. BMJ open. 2019;9(12):e031816. https://doi.org/10.1136/bmjopen-2019-0318166.

[6] Morimoto N, Maekawa T, Kubota M, et al. Challenge for management without tracheostomy tube after laryngo-tracheal separation in children with neurological disorders. Laryngoscope Investigative Otolaryngology. 2021;6(2):332-339. https://doi.org/10.1002/lio2.534

[7] Kadasah SK, Alshammari AM, Alharbi NS, et al. Fractured tracheostomy tube as a foreign body in a pediatric patient: a case report and review of literature. Journal of Surgical Case Reports. 2025;2025(4):rjaf194. https://doi.org/10.1093/jscr/rjaf194

[8] Elkholy KO, Akhtar H, Landa E, et al. A case of pneumomediastinum and pneumoperitoneum with concurrent massive subcutaneous emphysema due to repositioning of a tracheostomy tube. Cureus. 2019;11(1):e3869. https://doi.org/10.7759/cureus.3881

[9] Wang T, Tai J, Hu R, et al. Impacts of long-term nasogastric tube feeding and tracheostomy on pharyngeal and laryngeal structure in ABI patients: an FEES study. European Journal of Medical Research. 2025;30(1):109. https://doi.org/10.1186/s40001-025-02375-z

[10] Kumar VA, Reddy BU, Kumar VAK, et al. Speech and swallowing function outcome following early tracheostomy in patients who underwent neurosurgical intervention. Indian Journal of Critical Care Medicine. 2018;22(6):427-431. https://doi.org/10.4103/ijccm.IJCCM_31_18

[11] Zhang X, Zhou H, Shen H, et al. Pulmonary infection in traumatic brain injury patients undergoing tracheostomy: predicators and nursing care. BMC pulmonary medicine. 2022;22(1):130. https://doi.org/10.1186/s12890-022-01928-w

[12] Phookan J, Talukdar R. A study on quality of life in post-tracheostomised patients. Indian Journal of Otolaryngology and Head & Neck Surgery. 2023;75(2):848-856. https://doi.org/10.1007/s12070-022-03311-6